UNIVERSITY OF CALIFORNIA,
IRVINE

Performance Enhancing Mechanisms for Human Manipulation

DISSERTATION

submitted in partial satisfaction of the requirements
for the degree of

DOCTOR OF PHILOSOPHY

in Mechanical and Aerospace Engineering

by

Julius Klein

Dissertation Committee:
Professor David J. Reinkensmeyer, Chair
Professor James E. Bobrow
Professor Steven C. Cramer

2009

The dissertation of Julius Klein
is approved and is acceptable in quality and form for
publication on microfilm and in digital formats:

_____

_____

_____
Committee Chair

University of California, Irvine
2009

DEDICATION

To Kelly for her love, energy and patience.

To my parents for their unconditional love, and for understanding
that birds have to spread their wings and leave the nest.

To my homeland, Catalunya, which I've missed deeply throughout these years.

Quan surts per fer el viatge cap a Itaca,
has de pregar que el camí sigui llarg,
ple d'aventures, ple de coneixences.
Has de pregar que el camí sigui llarg,
que siguin moltes les matinades
que entraràs en un port que els teus ulls ignoraven,
i vagis a ciutats per aprendre dels que saben.
Tingues sempre al cor la idea d'Itaca.
Has d'arribar-hi, és el teu destí,
però no forcis gens la travessia.
És preferible que duri molts anys,
que siguis vell quan fondegis l'illa,
ric de tot el que hauràs guanyat fent el camí,
sense esperar que et doni més riqueses.
Itaca t'ha donat el bell viatge,
sense ella no hauries sortit.
I si la trobes pobra, no és que Itaca
t'hagi enganyat. Savi, com bé t'has fet,
sabràs el que volen dir les Itaques.

(Constantinos Kavafis / Lluís Llach)

TABLE OF CONTENTS

LIST OF FIGURES

LIST OF TABLES

ACKNOWLEDGMENTS

I would like to express the deepest gratitude and admiration towards my mentor, professor, and Chair of the Committee, David Reinkensmeyer, for his guidance throughout this journey. His encouragement, support, and advice since my arrival in the Biomechatronics Lab, have made these years the most enjoyable period in my life. Dave, may your passion never decay.

I would like to thank Professor James Bobrow for being my advisor during Professor Reinkensmeyer's sabbatical year abroad. I will always have fond memories of the "Bobrow-proof" concept, a measure of structural endurance of a mechanism subject to your brutal, yet effective force tests.

I would like to show my most sincere gratitude to Steven Spencer for all his invaluable work on BONES. Without all you have done for this project, BONES would be just a beautiful metal sculpture in a museum. Your work has been one of the main pillars of the success of the project, and my research as well.

I would like to thank James Allington for being my machine shop partner and sharing with me his wisdom and tricks (I would have never imagined power tapping could be so much fun). It's because of you that I am a better machinist.

I would also like to thank my current and former colleagues and friends for making the Biomechatronics and Robotics Laboratory more than just a lab: Eric Wolbrecht, Koyiro Minakata, Robert Smith, Gim Song Soh, Nina Robson, Luís Rodríguez , Robert Sánchez, John Clanton, Laura Marchal, Mine Akoner and Sergi Pérez.

Last, but not least, I would like to thank the Balsells Fellowship community, in particular Pete Balsells and Roger Rangel for making this dream become true. You built a bridge between California and Catalunya, a bridge of prosperity, community and friendship.

Work presented in this dissertation was supported under contract N01-HD-3-3352 with the National Institute of Health and by grant M01RR00827 from the U.C. Irvine General Clinical Research Centers Program of the National Center for Research Resources, National Institutes of Health.

CURRICULUM VITAE

Julius Klein

EDUCATION

Ph.D. in Mechanical and Aerospace Engineering, 2009
Department of Mechanical and Aerospace Engineering, University of California, Irvine

M.S. in Mechanical Engineering, 2005
Department of Mechanical and Aerospace E080ngineering, University of California, Irvine

B.S. in Industrial Engineering, 2003
Escola Politècnica Superior, Universitat de Girona (Spain)

EXPERIENCE

Graduate Research Assistant, September 2005 – March 2009
Biomechatronics Laboratory, Department of Mechanical and Aerospace Engineering, University of California, Irvine

Main research project is the analysis and design of performance enhancement mechanisms for human manipulation.

Graduate Research Assistant, September 2003 – May 2005
Robotics and Automation Laboratory, Department of Mechanical and Aerospace Engineering, University of California, Irvine

Main research project is the implementation of a SolidWorks Add-in interface for the synthesis of an RSSR function generator.

Graduate Teaching Assistant, January 2005 - March 2005
Dept. of Mechanical and Aerospace Engineering, University of California Irvine

Served as lecturer for laboratory session in Mechanical Systems Laboratory course. Provided grading and review sessions.

Graduate Teaching Assistant, March 2005 - June 2005
Dept. of Mechanical and Aerospace Engineering, University of California Irvine

Served as lecturer for laboratory sessions in Computer Aided Design course. Provided grading and review sessions.

Graduate Teaching Assistant, March 2006 - June 2006
Dept. of Mechanical and Aerospace Engineering, University of California Irvine
Served as discussion sessions leader for Dynamics course. Provided grading and review sessions for Mechanics-Dynamics.

Graduate Teaching Assistant, June 2006 - August 2006
Dept. of Mechanical and Aerospace Engineering, University of California Irvine
Served as lecturer for laboratory sessions in Computer Aided Design course. Provided grading and review sessions.

Junior Engineer, June 2002 - September 2002
Instal·lacions Valentí, Torroella de Montgrí, Catalunya, Spain
Served as junior programmer of automated industrial processes.

Sound Engineer, January 1996 – April 2002
La Carota Teatre, Torroella de Montgrí, Catalunya, Spain
Served as studio and live sound engineer.

Swimming Instructor, June 1993 - September 2001
Ajuntament de Torroella de Montgrí, Catalunya, Spain
Served as swimming instructor for kids and summer camp activities coordinator.

HONORS AND AWARDS

Balsells Fellowship, August 2003 – 2005
Department of Mechanical and Aerospace Engineering, University of California, Irvine

California-Catalunya Innovation Program, September 2005 –2006
Department of Mechanical and Aerospace Engineering, University of California, Irvine

GAAN Fellowship, September 2006 – 2007
Department of Mechanical and Aerospace Engineering, University of California, Irvine

PROFESSIONAL AFFILITIATIONS

Member of the Institute of Electrical and Electronic Engineers (IEEE)

PUBLICATIONS

J. Klein, M. Obrador, N. Gascons, and D. J. Reinkensmeyer, "The effect of dynamic arm support on grip forces and steering errors during simulated driving," Int. J. Heavy Vehicle Systems, vol. 15, pp.449-459, 2008.

J. Klein, S. J. Spencer, J. Allington, K. Minakata, W. Wolbrecht, R. F. Smith, J. Bobrow, and D. J. Reinkensmeyer, "Biomimetic Orthosis for the Neurorehabilitation of the Elbow and Shoulder (BONES)," in Conference on Biomedical Robotics and Biomechatronics, IEEE, Ed. Scottsdale, Arizona, U.S.A, 2008, pp. 535-541.

S. J. Spencer, J. Klein, K. Minakata, V. Le, J. E. Bobrow, and D. J. Reinkensmeyer, "A Low Cost Parallel Robot and Trajectory Optimization Method for Wrist and Forearm Rehabilitation using the Wii," in Conference on Biomedical Robotics and Biomechatronics, IEEE, Ed. Scottsdale, AZ, USA, 2008, pp. 869-874.

ABSTRACT OF THE DISSERTATION

Performance Enhancing Mechanisms for Human Manipulation

By

Julius Klein

Doctor of Philosophy in Mechanical and Aerospace Engineering

University of California, Irvine, 2009

Professor David Reinkensmeyer, Chair

The goal of this dissertation project was to develop and evaluate three novel mechanisms for assisting people in moving the upper extremity for three functionally important tasks.

The objective of the first mechanism was to improve steering of an automobile. This task is commonly affected in old age, but there currently exist few devices to assist in driving. We developed a novel passive, moving arm rest that can provide support to the arms when the hands are in the recommended grip positions behind a vehicle's steering wheel. We provide experimental evidence that this simple gravity-balancing mechanism can improve human performance and ergonomics in steering a car.

The second mechanism aimed at assisting movement exercise of the forearm and wrist, an important task for rehabilitation after stroke. Existing mechanisms are cumbersome and expensive or achieve lighter weight by using a reduced number of degrees-of-freedom. A novel parallel mechanism was designed that is capable of

moving a person's wrist along most of its natural workspace. The design of the device was inspired by the kinematics of the bones in the human forearm itself. The prototype device was used in preliminary experiments for a novel movement training application with the Nintendo Wii.

The objective of the third mechanism was to assist in naturalistic movement exercise of the human arm, again an important task for rehabilitation after stroke. Existing arm exoskeletons suffer from limited backdriveability, high weight, reduced number of degrees-of-freedom and/or limited force generation capability. The novel parallel mechanism developed here is a modified version of the wrist/forearm mechanism. The device incorporates lightweight, high-force, mechanically grounded pneumatic actuators, along with a spring-based counterbalancing system to balance the weight of the robot. The resulting exoskeleton can apply substantial forces to the human arm across a wide range of joint movement, while remaining lightweight, matching or exceeding capabilities of existing arm exoskeletons. The orthosis was used in an experiment with unimpaired subjects to test the hypothesis that practicing integrated, multi-joint movement will improve naturalistic movement ability more than practicing a matched amount of the isolated components of the integrated movement.

Chapter 1 Introduction

Arm weakness is a key factor that limits human motor function for a large number of people. For example, as people age, they often become weaker (Lord et al. 2007), and this, combined with other aging-related functional deficits (such as reduced peripheral sensation, reduced control precision and poor reaction times) may affect their ability to perform important tasks such as driving (Anstey et al. 2005; Bryan and Luszcz 2000; Llaneras et al. 1998). Following a stroke or spinal cord injury, weakness can be particularly severe, limiting a person's ability to achieve many activities of daily living (Brenneman 2000; Chiou and Burnett 1985; Gosman-Hedström et al. 2008). Unsuccessful attempts to move the impaired arm during recovery may also lead to frustration, decreasing a person's willingness to exercise the arm, resulting in a downward spiral of disuse-related atrophy (Seligman and Maier 1967; Wolf et al. 1989).

A promising approach to addressing the arm movement problems induced by weakness is to develop mechanical devices or orthoses that provide assistive forces for moving the arm. Such devices can be used as exercise machines to help people in rehabilitating impaired limbs after suffering an accident (Emken et al. 2007; Frisoli et al. 2007; Gopura and Kiguchi 2007; Jackson et al. 2007; Kikuchi et al. 2007; Krebs et

al. 2007; Li-Qun et al. 2007; Loureiro et al. 2003; Lum et al. 2005; Mayr et al. 2008; Mihelj et al. 2007; Mistry et al. 2005; Perry et al. 2007; Rosati et al. 2007; Sanchez et al. 2006; Takahashi et al. 2005; Zhang et al. 2007), or for assisting humans in activities of daily living in order to improve their quality of life (Chakrabarti and Abel 1994; Herder 2005; Herder et al. 2006; Kramer et al. 2007; Mastenbroek et al. 2007; Odell et al. 2007; Rodriguez 1972).

The goal of this dissertation project is to develop and evaluate three novel mechanisms for assisting people in moving the upper extremity. Three target movement tasks were selected:

1) Steering an automobile (a 1 DOF task). This task is commonly affected in old age, but there currently exist no performance-enhancing mechanisms to assist in driving, to our knowledge.

2) Unconstrained movement of the forearm and wrist (a 3 DOF task). This is an important task for rehabilitation exercise after stroke, but existing mechanisms are cumbersome and expensive or achieve lighter weight by using a reduced number of DOF.

3) Unconstrained movement of the shoulder and elbow (a 4 DOF task). This again is an important task for rehabilitation after stroke, but existing mechanisms suffer from limited backdriveability, high weight, reduced number of DOF and/or limited force generation capability.

1.1 Contributions and Goals

The primary novel contributions of this dissertation are:

1. Development of a novel passive arm rest that can provide support to the arms when the hands are in the recommended grip positions behind a vehicle's steering wheel. Additionally, we provide experimental evidence that this simple gravity-balancing mechanism can improve human performance and ergonomics in steering a car (Chapter 2).
2. Design and implementation of a novel parallel mechanism suited to assist the three degrees-of-freedom of human wrist/forearm movement (Chapter 3). This low-cost wrist robot is capable of moving a person's wrist along most of its natural workspace. The design of the device was inspired by the kinematics of the bones in the human forearm itself. The prototype device was used in preliminary experiments by a colleague for a novel movement training application with the Nintendo Wii (Spencer et al. 2008).
3. Design and implementation of a novel active arm exoskeleton that provides human-like range of motion for four degrees of freedom of elbow and shoulder movement (Chapter 4). The mechanism is a modified version of the wrist/forearm mechanism. The device incorporates lightweight, high-force, mechanically grounded pneumatic actuators, along with a spring-based counterbalancing system to balance the weight of the robot (Chapter 5). The resulting exoskeleton can apply substantial forces to the human arm across a wide range of joint movement, while remaining lightweight, matching or exceeding capabilities of existing arm exoskeletons.

4. Design and implementation of a motor learning experiment to validate the design of the BONES device. Important design goals for BONES were that it be capable of quantifying recovery of human movement ability of the four main joints of the human arm following rehabilitation exercise, and that it maximize motor learning during rehabilitation exercise by allowing functional movement practice. The experiment tests whether BONES meets these goals. In this experiment we used BONES in order to assess whether motor learning of functional movement is improved by allowing practice of more functional movement (Chapter 6). The hypothesis is that practicing an integrated, multi-joint movement will improve movement ability more than practicing a matched amount of the isolated components of the integrated movement.

Chapter 2 The effect of dynamic arm support on grip forces and steering errors during simulated driving

2.1 Introduction

The goal of this project was to develop a moving arm rest that can provide support to the arms when the hands are in the recommended grip positions. A literature search did not reveal previous research on dynamic arm rests for automobiles, so we based our research on mobile arm supports for neuromuscular rehabilitation (Rahman et al. 2000; Sanchez et al. 2006) in order to develop an arm support appropriate for driving. Once this prototype had been built, we assessed its performance by monitoring the hand gripping forces and steering errors for 23 young adult subjects as they steered - using a driving simulator - through three virtual tracks of varying difficulty with and without the dynamic arm rest. The results indicate that a dynamic arm rest can reduce grip forces and reduce steering errors.

2.2 Background and Motivation

Loss of control of an automobile is the second largest factor contributing to motor vehicle accidents (Land Transport Safety Authority 2005). A key factor in maintaining control of an automobile is the driver's manual grip of the steering wheel. Securely gripping the steering wheel with both hands requires significant force generation to support the weight of the arms. The goal of this project was to develop a simple arm support mechanism that could help relieve the weight of the arm during driving, and test whether it improved driving performance and ergonomics.

The traditional recommendation is to keep the hands at "ten o'clock two o'clock", with the rationale being that control with two hands is more stable and allows the driver to make turns without releasing the wheel (State Compensation Insurance Fund 2007). It is unclear, however, whether this recommendation has been rigorously validated. Recently, some driving organizations have recommended a lowering of the hands to between seven and nine o'clock for the left hand and between three and five o'clock for the right hand (Lehrer 2007; Long 2004; Minnesota Department of Public Safety 2007; Pennsylvania Department of Transportation 2007). This lower hand position may make a person less likely to overcorrect in an emergency situation, reduce arm fatigue, and prevent the arms from being damaged in case the airbag deploys (Manitoba Public Insurance 2007). Race car drivers, who presumably optimize their hand position to improve control and reduce fatigue, typically drive with their hands at three and nine o'clock (Grinstead 2007).

Drivers often do not drive with the hands in the recommended positions, as recently quantified in a study that observed the hand positions of 4804 drivers as they

drove through eight road situations, including large multi-lane, freeways, tunnels, and arterial roads (Walton and Thomas 2005). Only 25% of the drivers had both hands in the recommended positions, while 25% of the drivers kept both hands on the bottom half of the steering wheel, and 50% had one hand in recommended position. About 40% of 229 drivers who were tracked between two sites 10 km apart had shifted hand positions by the time they reached the second site, indicating that hand grip position selection is dynamic. Drivers adopted the recommended position more frequently at faster speeds and on the six-lane freeway, suggesting that they believed that the recommended position provided better control in these conditions.

For most cars, keeping the hands in the recommended position requires supporting the arms against gravity. Conventional arm rests are typically too low to provide support for the arms with the hands at the top half of the steering wheel. Drivers can support the weight of the arms by contracting shoulder and elbow muscles, or, alternately, they can relax the shoulder and elbow muscles and suspend the arm between the two points defined by the steering wheel and the shoulder. This second strategy requires the driver to grasp the steering wheel with a sufficient grip force as to resist the weight of the arm. The relative contribution of these two strategies to normal driving has not been clearly defined. However, what is clear is that either technique requires tonic muscle force generation of the arm or hand muscles respectively, which can lead to muscle fatigue and discomfort. Drivers may minimize such fatigue by shifting each arm to and from the car's arm rests, as was observed by (Walton and Thomas 2005). Essentially, it seems that drivers may choose to temporarily rest one arm on the car's arm rest, adopting a non-

recommended grip position, in order to recover from fatigue, and then re-adopt the recommended position as driving conditions or perceived comfort change.

2.3 Methodology

2.3.1 Dynamic arm rest

The dynamic arm rest that we have developed has three degrees of freedom (DoF, Figure 2.1). The main component of this arm support consists of a four bar mechanism that provides weight support to the arm, in a way similar to an arm support developed by (Rahman et al. 2000) and a common commercial arm support (JAECO 2007). An elastic cord spans the four bar mechanism so that the cord forces the mechanism to try to close, thereby lifting the arm. Depending on the weight of the driver's arm, the compensating force can be adjusted by extending the length of the cord by means of a lead screw, as proposed by (Rahman et al. 2000). Between the four bar mechanism and the attachment of the device to the driver's seat, there is another DoF that consists of a rotational joint that allows the arm support to rotate horizontally. At the distal end of the device, where the driver's forearm is to rest on the device, there is a sliding joint that allows it to move backwards and forwards. These three DoF were selected after a detailed benchmarking and in collaboration with the technical staff of Ficosa International, so that the device could be potentially used on commercial vehicles as an aftermarket driving accessory. They can be seen as the simplest combination of joints that comfortably accommodated the motion of the arm as it turned a steering wheel.

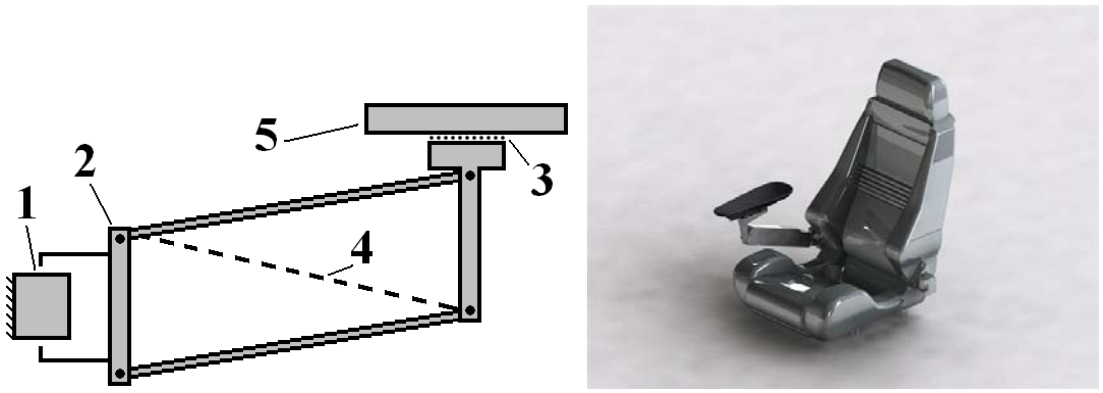

Figure 2.1. Mechanism diagram (left) Rendered armrest image (right). (1) Horizontal rotation (2) Vertical rotation (3) Linear bearing that allows frontal/rear displacement of the arm rest (4) Elastic element that creates an upward force to support the arm (5) Soft armrest

The driver's forearm rests on the top of the mechanism and is not strapped to the device. The range of motion of the mechanism is not as large as that of the human arm, but it covers the required range of motion during the action of driving. The device could be adjusted to the particular anthropometry of potential users by vertical and lateral adjustments of its attachment to the seat.

2.3.2 Driving simulator

We evaluated the dynamic arm rest using a custom-developed driving simulator. Subjects used a Logitech® MoMo Racing Force Wheel to steer a virtual car presented on a computer monitor in front of them (Figure 2.2). Subjects steered using only the dominant hand in the experiments described in this chapter. To measure hand grip forces we incorporated a hand grip filled with water, connected to a Viatran® 247 pressure transducer. The hand grip was attached to the steering wheel at 3 o'clock, and expanded the steering wheel diameter to a more realistic dimension (0.38 m). Hand grip pressure was sampled using a LabJack® U12, a USB A/D data

acquisition device. The resistance of the steering wheel was selected to be a light torsional spring with null displacement about the 0 degree rotation using the Logitech MoMo software.

Figure 2.2. Experimental Setup. (1) Steering Wheel (2) Hand Grip (3) Pressure transducer (4) A/D Data Acquisition Device

The graphical interface for the driving simulator was developed in Visual Basic, and is similar to a car racing game from a "first person" perspective, showing the road as if seen from behind the cockpit of the car (Figure 2.3). From the main menu three driving tracks can be selected Easy ('E'), Medium ('M'), and Difficult ('D'), each track harder than the previous one in terms of the number and sharpness of turns. The tracks simulate driving on a flat highway through a desert. For the experiments described here, the velocity of the car on each track was set to a fixed speed, in order to remove the confounding variable of speed control. Note that each track type was created as a series of straight segments, therefore all turns were sharp and there was always some tracking error in turns, even for the best driver.

Figure 2.3. Driving simulator. (1) Steering Wheel (2) Hand Grip (3) Pressure transducer (4) A/D Data Acquisition Device/ Main menu (left) Driving a sample scenario (right)

2.3.3 Experimental protocol

A total of 23 subjects (17 males, 6 females, and aged 20-32) participated in the subject. The Institutional Review Board of U.C. Irvine approved the experiments, and subjects provided informed consent. The experiment consisted of driving along the three tracks ('E', 'M' and 'D') with no arm support and the same three tracks with arm support. The order in which these six scenarios were experienced was randomized for each subject in order to reduce possible order of exposure effects. After a short test drive to get acquainted with the device, the subject drove each scenario for 2 minutes. The subject was allowed to take a break between tests. Each subject was instructed to drive the virtual car trying to follow a white dashed line located at the center of the road. Subjects were also instructed to maintain all the fingers in contact with the gripper while driving (Figure 2.4). No further instructions were given regarding the amount of force to be exerted on the gripper. The velocity of the car was set to remain constant for each scenario, although easier tracks were configured with higher speeds in order to simulate real driving scenarios. The constant velocity for each track was

approximately 105km/h (65mph), 90km/h (55mph) and 75km/h (45mph) for the 'E', 'M' and 'D' tracks respectively.

Figure 2.4. Subject driving the simulator with the dynamic arm rest

2.3.4 Data collection and analysis

During each steering test, the simulator recorded the coordinates of the car's path and the analogue voltage signal representing the grip pressure at 20 Hz. We calculated the steering error as the minimum distance between the car and the white dashed line in the center of the road at each time sample. Steering reversals were defined as changes in the direction of the steering wheel motion (local maxima/minima of the steering error). They were determined by identifying the zeroes of the first derivative of the steering error. Prior to taking the first derivative, the steering error was smoothened using the moving average method (a span of 5 samples was used in the average). The size of a steering reversal was defined as the area determined by the sum of all the driving errors occurred between steering reversals. A graphical example (Figure 2.5) shows how steering reversals are related

to the zeroes of the first derivative of the steering error. To analyze the grip force and steering error data we performed a two-way repeated measures ANOVA at the *p=0.05* confidence level. Statistical differences of the outcome variables steering error and grip force for each track difficulty were evaluated for the 'with' and 'without' dynamic arm rest conditions using paired t-tests with a significance level of *p=0.05*. Although we took *p = 0.05* as the cut-off level for statistical significance as is commonly accepted, we report the exact p-value obtained for each comparison to inform the reader of the actual probability of an erroneous conclusion of a significant difference for each comparison.

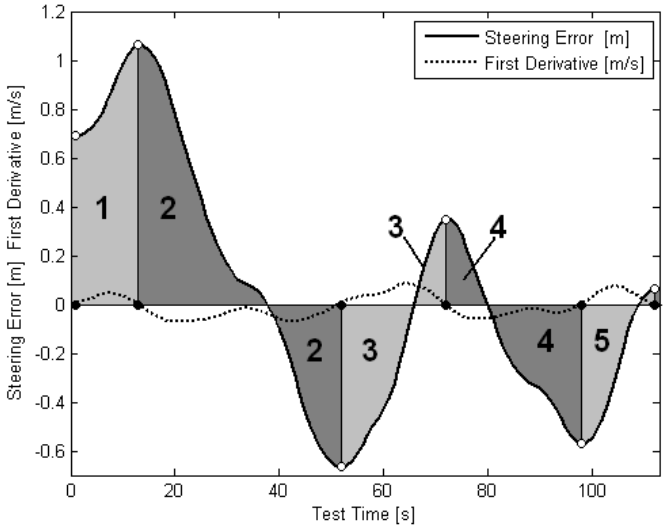

Figure 2.5. Sample of a subject's trial. Sample of a subject's steering error (solid line) and the steering error first derivative (dashed line) during a single test. Steering reversals are changes in the direction of the steering wheel, which correspond to local maxima or minima in the steering error (white circles). We identified steering reversals by detecting the zeroes of the first derivative of the steering error (black filled circles). The numbered areas identify the area corresponding to each reversal.

Our design criteria for the user attachment was that the attachment should be comfortable, hold the arm securely to the device, and allow a person with severe

spastic hemi-paresis to self-attach the arm to the device. The T-WREX used the Elbow Ranger (DJ Orthopedics, $70) to hold the arm. The Elbow Ranger has lower and upper arm cuffs that attach with Velcro that prevent the arm from slipping. The Elbow Ranger also has an elbow hinge with maximum and minimum range of motion settings that may be used as an added safety measure to limit the range of motion of the patient if needed. Use of an off the shelf brace reduced design cost, while ensuring a well-engineered, comfortable fit for the user. The brace was also fitted with a customized pressure sensing hand grip that was equipped with a hydraulic bladder connected to a pressure transducer (Viatran Corp., 2476AHG, 0-50 PSIG). The handgrip allowed Java Therapy to incorporate hand grasp functionality to the therapy games.

2.4 Results

We measured the effect of the dynamic arm rest on the steering error and the grip pressure of 23 young adult subjects as they steered along three virtual tracks of differing difficulty. An example of the data captured in a sample test is shown in (Figure 2.6).

The error and pressure means for each type of track and support condition are summarized in Table 2.1 and Table 2.2, and the differences in error and pressure with and without the arm support are shown in (Figure 2.7). Use of the arm support decreased steering error (ANOVA, $p=0.005$) and decreased grip force pressure (ANOVA, $p<0.001$). These reductions were significant for all three track types, (paired t-test, $p=0.036$, $p=0.004$ and $p=0.038$ for 'E','M' and 'D' tracks for steering error, and $p=0.0001$, $p=0.0003$ and $p=0.0014$ for grip pressure). The average

reduction in the mean steering error was 5.9% ('E'), 13.0% ('M') and 6.1% ('D'). The mean pressure reduction was 35.6%, 26.7% and 30.1% for the 'E', 'M' and 'D' tracks, respectively. Steering error (ANOVA, $p=0.001$) and grip force pressure (ANOVA, $p<0.005$) increased for more difficult tracks.

To understand how use of the arm support reduced steering error, we analyzed steering reversals (Table 2.3 and Table 2.4), where a reversal was defined as a change in direction of the steering wheel motion. This parameter has been used previously as an indicator of a person's driving skills (Brown and Huffman 1972; Greenshields and Plat 1967), with more skilled drivers using fewer steering reversals. We found that use of the arm support significantly reduced the number of steering reversals for the 'E' track ($p=0.031$) and the size of the steering reversals for the 'M' track ($p=0.007$). Use of the arm support also caused a marginally significant reduction in amplitude of the steering reversals for the 'H' track ($p=0.062$).

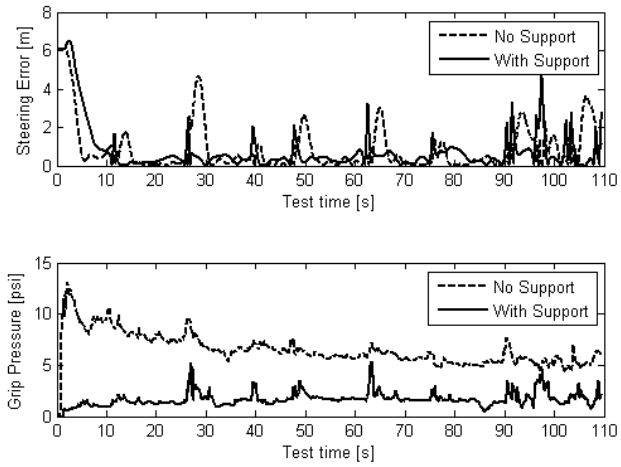

Figure 2.6. Sample of a subject's performance. Steering error (top) and grip pressure data (bottom) during a single test

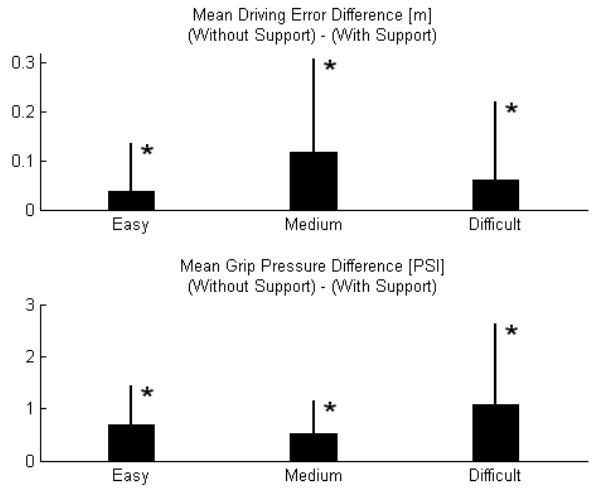

Figure 2.7. Mean Driving Error Difference and Mean Grip Difference. Top: Difference in mean steering error sorted by track type. A positive value indicates a reduction in error when arm support is applied. In all three tracks the reduction was significant. Bottom: Difference in grip pressure for each type of track. Similarly, the grip pressure was significantly reduced in all three cases. {*} Significant value (p<0.05)

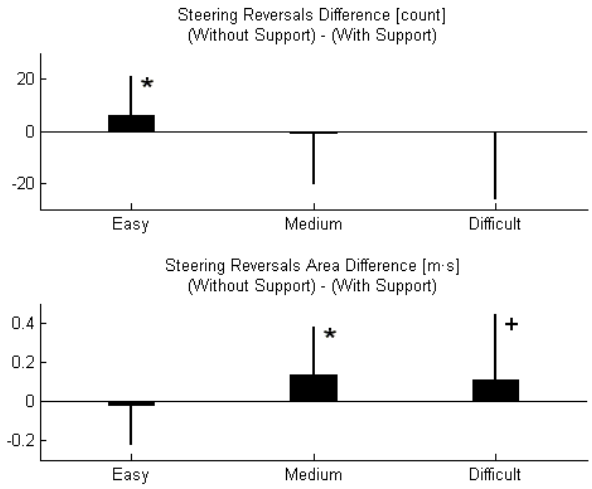

Figure 2.8. Steering reversals and Steering Reversals Area Difference. Top: Difference in number of steering reversals sorted by track type. A positive value indicates a reduction in the reversals count when arm support is applied. Only the 'E' case was significant (p<0.05). Bottom: Difference in steering reversals size (duration and amplitude) for each type of track. Only the 'M' case was significant. The 'D' case was marginally significant. {*} Significant value (p<0.05), {+} Marginally significant value (p=0.06).

TABLE 2.1. STEERING ERROR MEAN [M]
(STANDARD DEVIATION)

Condition	Easy	Medium	Hard
No Support	0.41 (0.11)	0.74 (0.19)	0.74 (0.13)
With Support	0.37 (0.06)	0.62 (0.17)	0.68 (0.12)

TABLE 2.2. GRIP PRESSURE MEAN [PSI]
(STANDARD DEVIATION)

Condition	Easy	Medium	Hard
No Support	1.75 (0.88)	2.10 (0.90)	2.69 (1.93)
With Support	1.07 (0.69)	1.57 (0.92)	1.61 (0.88)

TABLE 2.3. MEAN NUMBER OF STEERING REVERSALS [COUNT]
(STANDARD DEVIATION)

Condition	Easy	Medium	Hard
No Support	75 (16.2)	104 (20.1)	94 (20.2)
With Support	68 (16.6)	105 (17.1)	94 (12.9)

TABLE 2.4. MEAN SIZE OF STEERING REVERSALS [M·S]
(STANDARD DEVIATION)

Condition	Easy	Medium	Hard
No Support	0.59 (0.19)	0.78 (0.26)	0.92 (0.31)
With Support	0.61 (0.20)	0.65 (0.24)	0.81 (0.24)

2.5 Discussion

The reason for the decrease in hand grasp pressure with use of the arm support seems straightforward: the weight balancing effect of the support reduced the necessary gripping force on the steering wheel. Thus the subjects could reduce their grasp pressure and still maintain a hold on the steering wheel. The fact that the subjects did reduce their grasp pressure when given the opportunity by the arm rest is

consistent with studies of human motor control that indicate that the motor system attempts to minimize exertion when possible (Emken et al. 2007; Scheidt et al. 2000).

The significant decrease in steering error with use of the arm support was unexpected and the reasons for it are less clear. We detected that subjects made significantly fewer steering reversals on the relatively straight course, and significantly smaller reversals on the courses with more turns. These findings may explain the reduced steering error, and may be accounted for as follows. First, the arm support introduced some stiction, although it was designed to have low friction using high precision rolling bearings. The stiction may have helped keep the car aligned with the center line as long as the line remained straight, once the subject actively moved the car to the center line, despite inherent noise in the subjects' motor signals.

Second, the introduction of the dynamic arm rest also likely reduced the inherent noise that is present in motor signals. Human motor noise possesses a signal-dependent property, which is to say that the amount of variability in the force generated by a human increases with the mean force generated (Harris and Wolpert 1998). The arm rest reduced the mean force produced by the arm muscles to lift the arms, and may have therefore reduced force variability that contributed to steering reversals.

The reason for the decreased reversal sizes on tracks with more frequent turns may relate to the inertia that the arm rest added to the arm's movement. It is well known that the mass on a single degree of freedom dynamic system behaves as a low pass filter for the displacement signal.

2.6 Conclusion

We developed a spring-loaded, passive arm rest that moves up and down with the driver's forearm, allowing the driver to grasp the steering wheel in the recommended location while still receiving weight support for the arm.

Using a driving simulator that mimicked driving on highways, we found that young adult drivers significantly reduced their hand grasp pressure by about 30% and their steering error by about 5~10%. These results suggest that incorporation of a dynamic arm rest into an automobile might improve driving ergonomics and safety.

This conclusion should be taken in recognition of several limitations of the current study. The study involved driving simulations - not real driving - of short duration only. We also tested only highway type driving, for which the angle of all turns was less than 90 degrees. It is unclear how the dynamic arm rest would affect city-type driving. We also only tested driving with one hand, and future research should examine how driving with two hands and two arm rests compares to driving with two hands and no arm rest, or driving with one hand.

During testing we observed some practical problems with the dynamic arm rest design. The clearance between the arm-machine contact surface and the lowest element of the supporting structure needs to be optimized in order to reduce the interference with the driver's leg. Another issue is that if the driver executes a large turn (e.g. hand-over-hand turn), the arm may lose contact with the arm rest, which can then freely rotate to either side. This issue might be ameliorated by replacing the manually adjustable pre-load of the inner elastic element with a controlled motor that automatically retracts the arm rest into a standard arm rest position if the driver's arm

loses contact with it. Such a mechatronic feature could also be used to automatically configure the weight support level for each driver.

We did not study rapid lane change maneuvers, which frequently occur, for example, when driving in traffic. An important direction for future research is to determine how the arm support affects safety during such maneuvers. If it negatively affects safety, the arm support could possibly be moved to a dock either at the driver's discretion or automatically based on sensing of the ongoing steering characteristics.

To conclude, we note that we tested the dynamic arm rest with young, unimpaired adults. However, the usefulness of a dynamic arm rest may be even greater for people with a disability or for elderly adults, who experience age-related decreases in arm and hand strength, and for whom such an arm rest may improve comfort of driving. The greying of the populations in industrialized nations may therefore help drive the introduction of dynamic arm rests, if the results of this study are confirmed for actual driving.

Chapter 3 Closed-chain Robot for Assisting in Manual Exercise and Rehabilitation

3.1 Introduction

This chapter describes a Closed-chain Robot for Assisting in Manual Exercise and Rehabilitation (CRAMER), a simple and low-cost mechanism that provides three degrees of freedom assistance to the human wrist. The design of CRAMER was inspired by the bones in the human forearm. This chapter presents the design of CRAMER and analyzes its kinematics.

3.2 Background and Motivation

Limitations in wrist and forearm motion are key limiting factors to motor recovery following neurologic injuries such as stroke and spinal cord injury (Sadowsky et al. 2002). Rehabilitation exercise can improve the ability to make these motions (Burgar et al. 2000; Giszter 2008), but existing exercise devices for the distal upper extremity are either simplistic, using a reduced number of degrees of freedom compared to the three degrees of freedom of the wrist and forearm, or cumbersome and bulky.

In recent years there have been numerous projects targeted at wrist and forearm rehabilitation (Ball et al. 2007; Charles et al. 2005; Hu et al.; Krebs et al. 2007; Takahashi et al. 2005; Williams et al. 2001). In this section we will review several of the most significant ones.

After the promising clinical results of the pioneering MIT-MANUS robot on upper-limb shoulder/elbow rehabilitation (Krebs et al. 2007), a 3 DOF wrist module was attached to it in order to expand the capabilities of the robot (Charles et al. 2005; Krebs et al. 2007). This combination offered the opportunity to compare the outcomes of functional upper limb training as opposed to particular segment exercising (Figure 3.1).

Figure 3.1. MIT-Manus with a wrist module. Human arm interacting with this 2 DOF device (Krebs et al. 2007).

Furthermore, this research group used this combination of robots to evaluate the outcome effects of proximal versus distal limb segments training sequence. After 6 weeks of robotic wrist rehabilitation, followed by 6 weeks of shoulder/elbow training, the subjects presented an increase of 10 points in the Fugl-Meyer scale (Fugl-Meyer et al. 1975).

Another wrist mechanism compatible with the MIT-MANUS platform is presented in (Williams et al. 2001). This cable-driven device allows for the three main degrees of freedom of the wrist: flexion/extension, radial/ulnar deviation and pronation/supination (Figure 3.2).

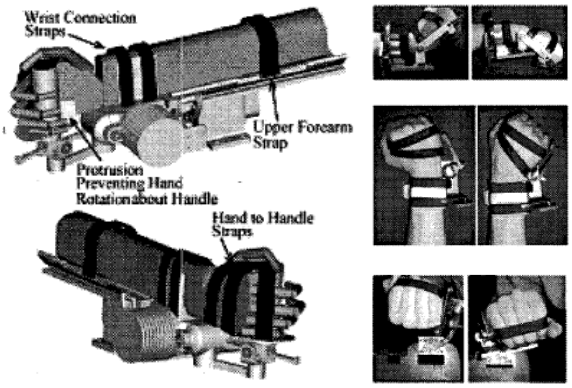

Figure 3.2. Robot for wrist rehabilitation. Rendered image of the serial mechanism driving the forearm and the wrist (left) Degrees of freedom of the actual mechanism (right) (Williams et al. 2001)

The RICE-WRIST (Gupta and O'Malley 2006) is a 5 DOF haptic arm exoskeleton for training and rehabilitation in virtual environments. The supination of the forearm is achieved by means of a closed ring structure, while the flexion/extension and radial/ulnar deviation are driven by means of a mechanism based in the design of the Stewart Platform (Stewart 1965). Another mechanism based on a Stewart Platform is presented by (Takaiwa and Noritsugu 2005). This parallel mechanism is not an exoskeleton, but provides the means to drive a human hand along all of its DOF. The hand grabs onto a joystick-like handle driven by a pneumatically actuated platform.

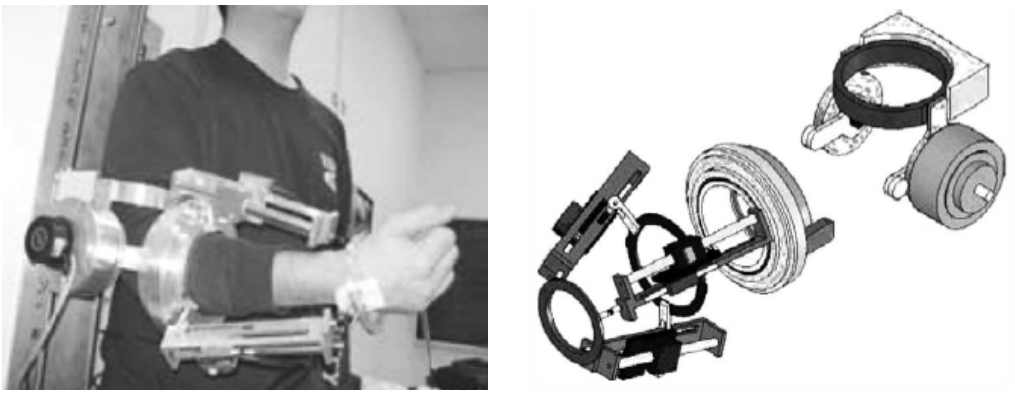

Figure 3.3. RICE-Wrist robot. Human subject operating the RICE-Wrist robot (left) Exploded view of the CAD assembly of the RICE-Wrist (right) (Gupta and O'Malley 2006)

Developed at UCI in 2006, the H-WARD is a 3 DOF, pneumatically actuated, standalone wrist rehabilitation robot (Takahashi et al. 2005). Although supination/pronation and ulnar/radial deviation are not contemplated in this design, *H-WARD* offers grasping and releasing assistance while simultaneously keeping the palm of the hand unobstructed, allowing sensory feedback at the palm of the hand during rehabilitation (Figure 3.4).

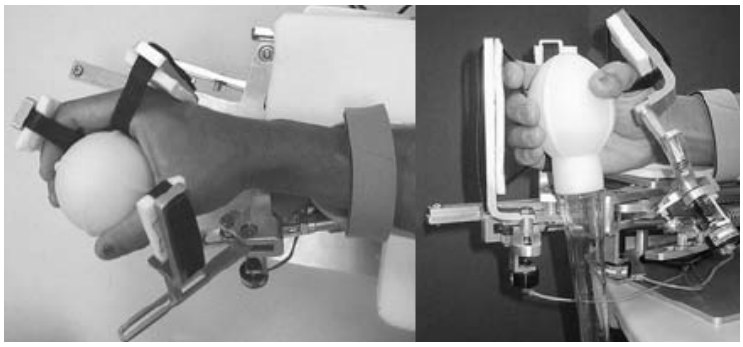

Figure 3.4. UCI's H-WARD wrist robot. H-WARD drives the fingers with a mechanism that attaches on the dorsal side of the fingers, allowing the palm of the hand to be exposed in order to increase cutaneous feedback while grasping (Takahashi et al. 2005)

Research groups like (Hesse et al. 2003) have focused on robot-assisted bilateral forearm and wrist movements. The device is a reconfigurable 1 DOF for forearm supination/pronation or wrist flexion/extension. Simultaneously, the impaired and the unimpaired limb underwent therapy. According to the authors, voluntary movements of the unimpaired limb have an important role in the neurological recovery of the impaired limb.

Making rehabilitation devices inexpensive and portable is the goal of many research groups. In (Koeneman et al. 2004), a pneumatic muscle drives a 1 DOF crank-shaft mechanism that provides wrist flexion/extension (Figure 3.5). This muscle, known as the McKibben Artificial Muscle (Schulte 1962), is normally extended, and contracts when inflated.

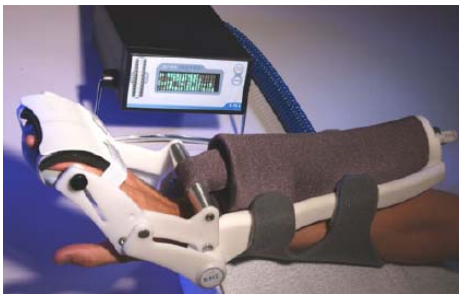

Figure 3.5. Single DOF wrist flexion mechanism driven by a pneumatic muscle actuator

3.3 CRAMER Design

CRAMER is a lightweight 3 DOF parallel mechanism actuated by 4 small, yet powerful, servomotors. The inspiration for the design of CRAMER was the human forearm. In the human forearm, the Ulna and the Radius bones prescribe a unique and complex motion in order to supinate/pronate (Kecskeméthy and Weinberg 2005).

The hand is strapped to a grip that can slide along two rods. The location of the two rods determines the translation and orientation of the hand. A wrist cuff is necessary in order to prevent the wrist from moving laterally or forward (axially in the direction of the forearm). Without this constraint, the location of the virtual center of rotation of the wrist is not fully defined, and the mechanism does not work properly. The wrist, modeled as a spherical joint, acts as the link closing the parallel mechanism formed by the two rods. Further detail on the kinematics of CRAMER can be found in 3.4.

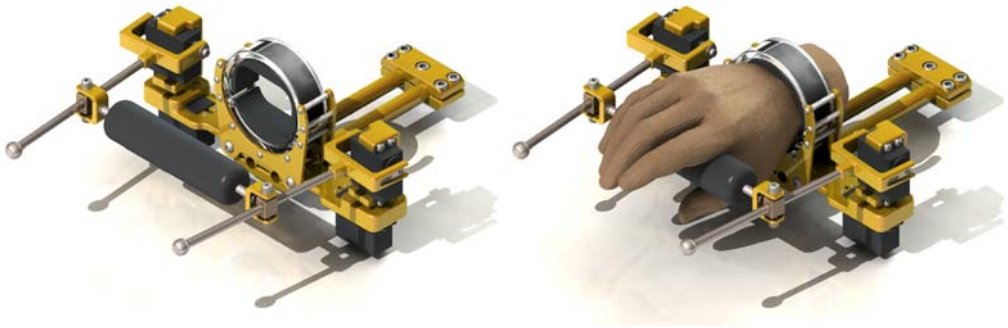

Figure 3.6. Rendered image of CRAMER (left) Rendered model of CRAMER including a human hand (right)

The device allows for the three rotations of the wrist (Figure 3.7). These rotations are: supination/pronation, radial/ulnar deviation, and flexion/extension. Wrist flexion is the downward movement of the wrist resulting in the palm facing inward. Consequently, extension is the upward movement of the wrist to which results in the palm facing outward (as if it were in contact with a vertical wall). Forearm supination is the rotation about the forearm that causes the hand to in a “palm up” posture. Forearm pronation is the antagonist movement to supination; therefore, the rotation of the forearm causes the hand to be in a “palm down” position. Radial and ulnar

deviation is the side-to-side movement of the hand at the wrist, toward or away from the thumb (Wu et al. 2005).

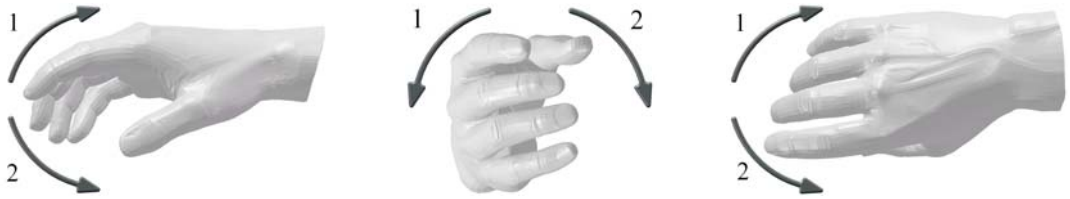

(a) (b) (c)

Figure 3.7. Degrees of freedom at the wrist. (a) 1-Extension / 2-Flexion (b) 1-Supination / 2-Pronation (c) 1-Ulnar Deviation / 2-Radial Deviation

CRAMER is powered by four Hitec HSR 5995TG hobby servo motors. Despite their relative small size, each servomotor can produce a maximum torque of 30kg·cm.

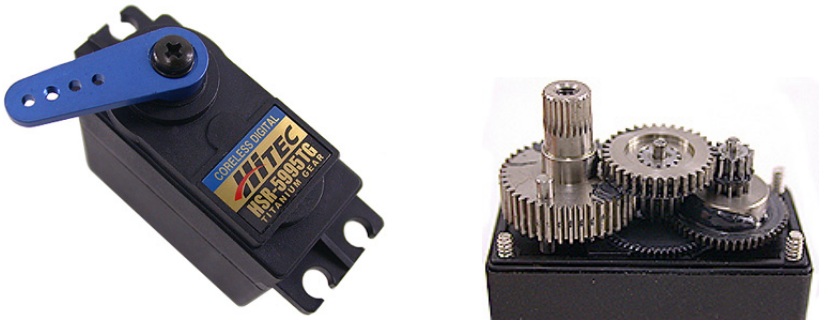

Figure 3.8. Servomotor, cover (left) and titanium gears (right)

3.4 Kinematic and Jacobian Equations

Similarly to the actuation of the shoulder joint on BONES (Chapter 4), CRAMER is a 3 DOF parallel mechanism that uses 4 actuators. In the case of BONES, the spherical joint at the shoulder is constrained by a set of brackets that prevented the exoskeleton from exerting forces in the direction of the Humerus (Figure 4.7). For CRAMER, there is no such hardware constraint. The wrist itself acts as its own

spherical joint constraint. As opposed to the hardware shoulder constraint in BONES, the wrist mechanism relies on the human wrist to actually complete the parallel mechanism. The robot cannot function properly without a human wrist.

3.4.1 Kinematic equations

Consider $\{F_0\}$ a coordinate system centered at O, located at the virtual center of rotation of the human wrist (Figure 3.9). The x_0-axis is in the direction of the forearm, with the positive direction distal to the elbow. The y_0-axis is perpendicular to the palm, pointing away from the palm top. The remaining axis, z_0, completes the coordinate system so that $\{F_0\}$ is right handed. Let θ_S be the angle of supination, defined as a rotation about $x_{0,0}$. Furthermore, θ_R describes the radial deviation about $y_{0,1}$. Finally, θ_F represents the wrist flexion, which corresponds to a rotation about $z_{0,2}$.

We define a new coordinate system $\{F_{1,0}\}$ as the translation of $\{F_0\}$ from O to A. Let $\{F_{1,1}\}$ be secondary coordinate system, with origin A, defined as a rotation of $\{F_{1,0}\}$ about the $y_{1,0}$-axis. The angle of rotation about $y_{1,0}$ is $q_{1,1}$. Consider a third reference frame, $\{F_{1,2}\}$, located at A and resulting from the rotation of $\{F_{1,1}\}$ about $z_{1,1}$. The quantity of this rotation is $q_{1,2}$. Note that the axes $x_{1,0} \equiv x_{1,1} \equiv x_{1,2}$ are aligned in the direction of AB.

Similarly, $\{F_{2,0}\}$ is the translation of $\{F_0\}$ from O to C, $\{F_{2,1}\}$ is the result of rotating $\{F_{2,0}\}$ about $y_{2,0}$ and $\{F_{2,2}\}$ is the result of rotating $\{F_{2,1}\}$ about $z_{2,1}$. Correspondently, $q_{2,1}$ is the angle of the rotation about $y_{2,0}$ and $q_{2,2}$ is the quantity of the rotation about $z_{2,1}$. Furthermore, $x_{2,0} \equiv x_{2,1} \equiv x_{2,2}$ is aligned with CD.

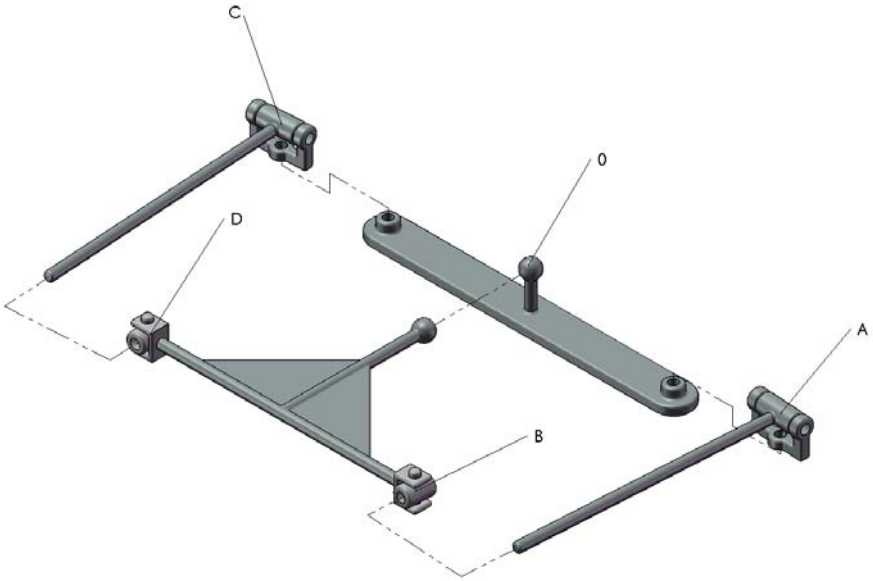

Figure 3.9. Exploded view of a simplified model of CRAMER

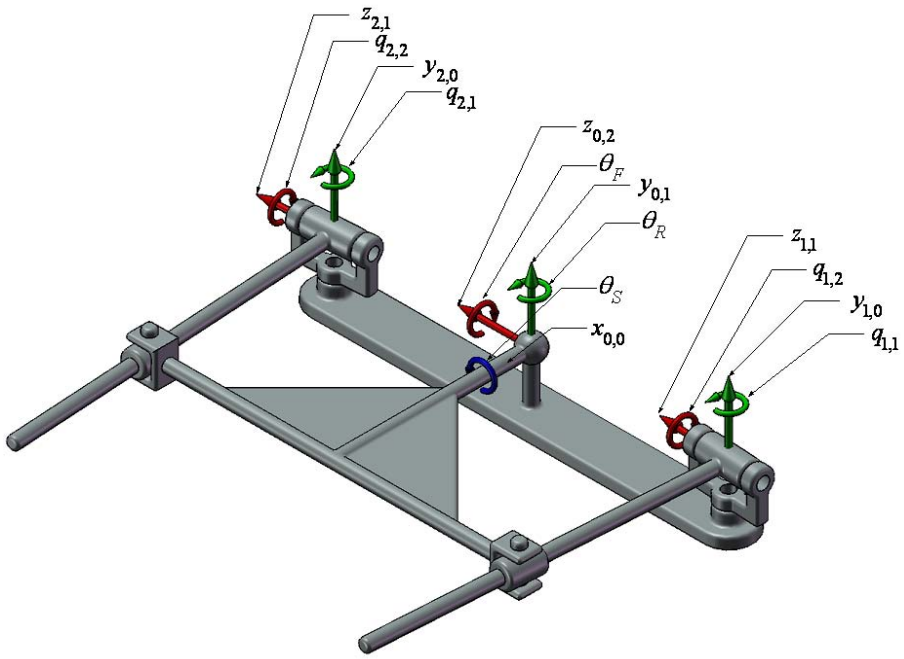

Figure 3.10. CRAMER's main axes and angles of rotation

We start describing the kinematic chain from O to B and O to D using a series of homogeneous transformations. We denote B_0 and D_0 as the point locations of B and D when the wrist is at the Home position ($\theta_F = \theta_R = \theta_S = 0$). The position of B and D as a function of θ_F, θ_R and θ_S is defined by

$$B = R_z(\theta_F) \cdot R_y(-\theta_R) \cdot R_x(\theta_S) \cdot B_0 = M \cdot B_0, \tag{3.1}$$

and

$$D = R_z(\theta_F) \cdot R_y(-\theta_R) \cdot R_x(\theta_S) \cdot D_0 = M \cdot D_0, \tag{3.2}$$

where

$$M = \begin{bmatrix} c(\theta_F)c(\theta_R) & -s(\theta_F)c(\theta_S)-c(\theta_F)s(\theta_R)s(\theta_S) & s(\theta_F)s(\theta_S)-c(\theta_F)s(\theta_R)c(\theta_S) \\ s(\theta_F)c(\theta_R) & c(\theta_F)c(\theta_S)-s(\theta_F)s(\theta_R)s(\theta_S) & -c(\theta_F)s(\theta_S)-s(\theta_F)s(\theta_R)c(\theta_S) \\ 0 & c(\theta_R)s(\theta_S) & c(\theta_R)c(\theta_S) \end{bmatrix}. \tag{3.3}$$

For simplicity, in (3.3) we used the following abbreviations c(θ)=cos(θ) and s(θ)=sin(θ).

Closing the parallel mechanism's chain via BA and DC we determine the vector q as a function of θ. Component-wise, the actuator positions $q_{1,1}$, $q_{1,2}$, $q_{2,1}$ and $q_{2,2}$ are defined by

$$q_{1,1} = \begin{cases} -\arctan\left(\dfrac{B_z(\theta) - A_z}{B_x(\theta) - A_x}\right) & for\ B_x \neq A_x \\ \pm\pi & for\ B_x = A_x \end{cases}, \tag{3.4}$$

$$q_{2,1} = \begin{cases} -\arctan\left(\dfrac{D_z(\theta) - C_z}{D_x(\theta) - C_x}\right) & for\ D_x \neq C_x \\ \pm\pi & for\ D_x = C_x \end{cases}, \tag{3.5}$$

$$q_{1,2} = \begin{cases} \arcsin\left(\dfrac{B_y - A_y}{\|B_y - A_y\|}\right) & for\ B_y \neq A_y \\ 0 & for\ B_y = A_y \end{cases} \tag{3.6}$$

and

$$q_{2,2} = \begin{cases} \arcsin\left(\dfrac{D_y - C_y}{\|D_y - C_y\|}\right) & for\ D_y \neq C_y \\ 0 & for\ D_y = C_y \end{cases}. \tag{3.7}$$

Note that $B_x = A_x$ and $D_x = C_x$ does not belong to the reachable workspace of the mechanism, therefore the equations are non-singular.

Given a set of desired θ_F, θ_R and θ_S within the wrist natural range of motion, then equations (3.4) through (3.7) provide the means to convert the wrist angles, θ, into actuator angles, q.

$$q = f(\theta), \tag{3.8}$$

In Figure 2.1, several configurations of CRAMER are shown.

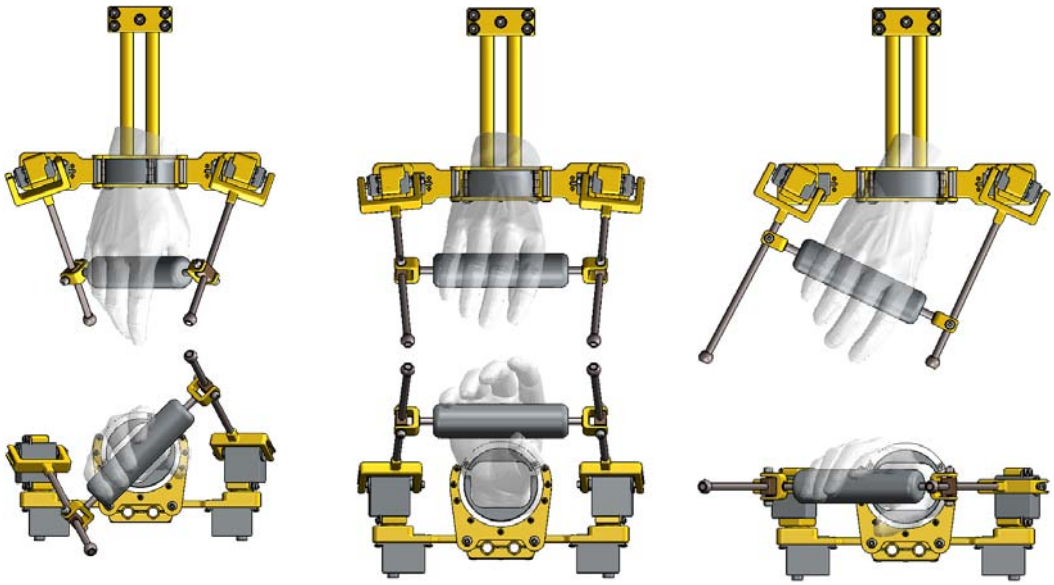

(a) (b) (c)

Figure 3.11. Some configurations of CRAMER. (a) Supination. (b) Extension. (c) Ulnar Deviation.

The range of motion of CRAMER is summarized in Table 3.1.

TABLE 3.1. RANGE OF MOTION OF CRAMER [DEG]

	CRAMER (Min.)	CRAMER (Max)	CRAMER Range of Motion	ADL Range of Motion
θ_R	-15	10	175	170
θ_F	-70	90	25	90
θ_S	-90	85	160	115

The desired ADL angles are obtained from (Perry et al. 2007)

3.4.2 Jacobian equations

The Jacobian matrix, $J(\theta)$, relates velocities at the end-effector and the velocities of the servo-motors. Furthermore, the transpose of the Jacobian matrix relates the torques applied to the wrist and the torques applied by the actuators.

Taking the time derivative of *equation reference goes here* we obtain

$$\dot{q} = \frac{dq}{dt} = \frac{\partial f}{\partial \theta}\dot{\theta} = J(\theta)\dot{\theta}. \tag{3.9}$$

The computation of (3.9) was developed in (Spencer 2008; Spencer et al. 2008). For the complete derivation of $J(\theta)$, please see Appendix A .

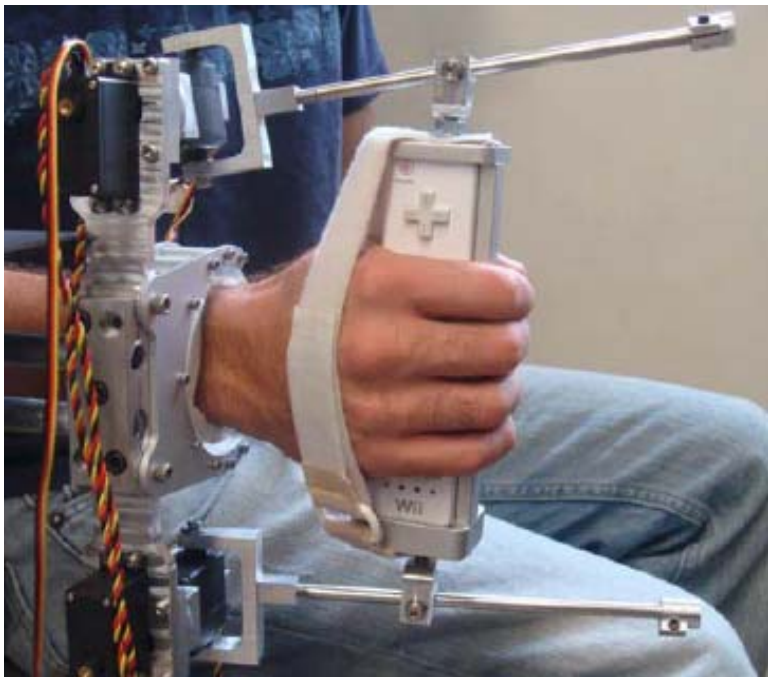

Figure 3.12. CRAMER adapted with a Nintendo Wii remote.

3.5 Conclusion

We have developed a novel, low-cost forearm and wrist rehabilitation mechanism that accommodates much of the natural range of motion of the three degrees of freedom of the human wrist and forearm. A colleague has integrated a Nintendo Wii remote into CRAMER (Figure 3.12) in order to allow patients to play the motion-based games that have been developed for the Wii (Spencer et al. 2008).

Future work on CRAMER should be focused on the possibility of making the device wearable, and on incorporating alternative actuators in order to generate higher torques, so the device is strong enough to assist patients with abnormal, elevated tone.

Chapter 4 Biomimetic Orthosis for the Neurorehabilitation of the Elbow and Shoulder (BONES)

4.1 Introduction

This chapter presents BONES, a novel design for a 4 DOF pneumatically-actuated upper-limb rehabilitation robot. The device accommodates a wide range of motion of the human arm, while also achieving low inertia and direct-drive force generation capability at the shoulder. A key accomplishment of this design is the ability to generate arm internal/external rotation without any circular bearing element such as a ring, a design feature inspired by the biomechanics of the human forearm. The chapter also describes the rationale for this device and its main design aspects including its kinematics, range of motion, and force generation capability.

4.2 Background and Motivation

Robotic devices that interact with the upper limb during rehabilitation process can be classified under several criteria, ranging from passive supports to active wearable devices. The main features used to characterize an orthosis are the degrees of freedom

of the device and its workspace (compared to the upper-limb's range of motion). Other features associated with these mechanisms are the ability to passively cancel the effect of gravity and the way in which in forces are applied the subject's arm (end-effector oriented devices apply force only to the hand).

Most previous robotic therapy devices have used a reduced number of DOF compared to the human arm (Coote et al. 2003; Hesse et al. 2005; Hogan et al. 1995; Kahn et al. 2006; Reinkensmeyer et al. 2000; Riener et al. 2005). Therefore, the movements trained with these devices are not fully naturalistic. Motor learning research suggests that motor learning is task specific (Schmidt and Lee 1998): i.e. that transfer of skill to other movements following training of one movement is limited. Therefore, one way to improve robotic therapy may be to develop devices that allow patients to practice movements that are kinematically more similar to activities of daily living.

Naturalistic arm movements can be accommodated with 5 or 6 DOF industrial robots (Lum et al. 2005; Toth et al. 2005), but these robots do not match the workspace of the human arm, limiting functional movements and raising safety issues. Several groups are also developing robotic exoskeletons to meet the goal of more naturalistic arm movements (Bergamasco et al. 1994; Frisoli et al. 2005; Hurmuzlu et al. 1998; Nef et al. 2007a; Sugar et al. 2007). These devices typically use a serial-chain design in which actuators are mounted on progressively more distal serially-connected links of the robot. Because of the serial-chain topology, a common strategy to achieve upper arm internal/external rotation is the use of serially-mounted ring bearings with an actuator mounted directly on the ring (Bergamasco et al. 1994;

Carignan et al. 2005; Frisoli et al. 2005; Mihelj et al. 2006; Schiele and van der Helm 2006; Zhang et al. 2007). As we move distally along serial-chain mechanisms, weight and inertia reduction of distal links becomes more imperative. Reducing weight and inertia with this serial-chain strategy, while still achieving good force control typically requires use of small, highly geared actuators and force feedback, a strategy that has been implemented with success (Mihelj et al. 2006; Nef et al. 2007a). However, this strategy has the limitations that the endpoint impedance of the robot at high frequencies tends to infinity, and the weight and inertia of the robot are necessarily determined by the actuator selection.

An alternate strategy to achieving a lightweight robot with good force control is to use a parallel mechanism with mechanically grounded actuators. This strategy has the advantage that it allows large, direct-drive actuators to be used to generate force, since the weight of the actuators themselves need not be moved. Extending such a design to more than 2 DOF is difficult though because of the need for complex mechanisms (Adelstein 1998).

As an example of parallel, mechanically grounded robot we select the MIT-MANUS (Krebs et al. 1998). As an example of serial topology rehabilitation robots, we highlight three different robots: ARM-In (Mihelj et al. 2007; Nef et al. 2007b), T-WREX (Rahman et al. 2004; Rahman et al. 2000) and Pneu-WREX (Sanchez et al. 2006; Sanchez et al. 2005). A brief description of these 4 robots follows.

The MIT-MANUS robot (Figure 4.1) uses two mechanically grounded actuators to control planar motion of the robot end effector (Krebs et al. 1998). The core of the

MIT-MANUS is a 2 DOF direct-drive five-bar linkage SCARA mechanism driven by brushless motors.

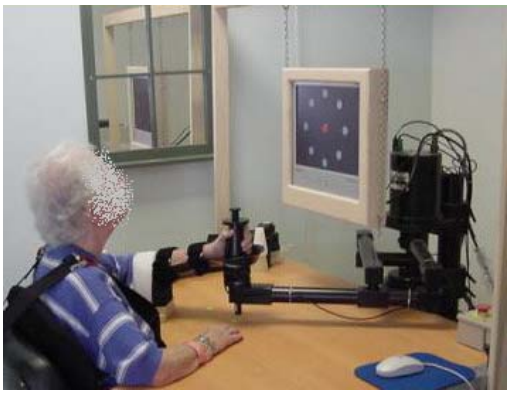

Figure 4.1. A patient interacting with the MIT-MANUS

The ARM-In features a total of 6 DOF: 4 main DOF of a human arm plus 2 DOF at the forearm level. Equipped with position, force and torque sensors, ARM-In uses a graphical computer interface in order to interconnect the exoskeleton to a series of rehabilitation games. The latest version of ARM-In robots (Mihelj et al. 2007) is equipped with a new shoulder actuation principle that accommodates shoulder elevation in order to correct the shoulder rotation center during shoulder flexion.

Figure 4.2. ArmIN II

The Wilmington Robotic Exoskeletal, or T-WREX, is a wheelchair arm exoskeleton that offers 4 DOF (Figure 4.3). This 2-link device is gravity balanced by means of two rubber bands. Subjects in the preliminary tests used T-WREX at home for two weeks. Results showed a significant improvement in tasks such as self-feeding and object picking (Sanchez et al. 2006).

Figure 4.3. T-WREX

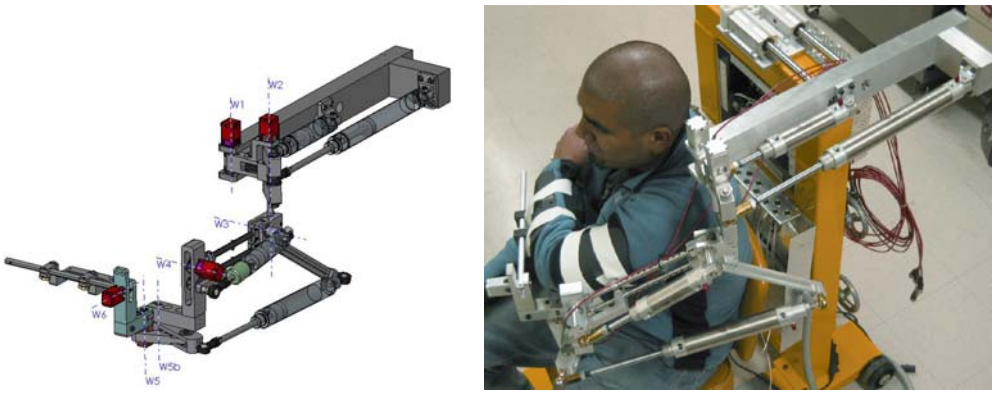

Figure 4.4. Pneu-WREX. CAD Model (left) Healthy subject on the first prototype of Pneu-WREX (right)

Pneu-WREX (Figure 4.4) is the actuated version of T-WREX. This robot offers a naturalistic workspace using 5 DOF, gravity-balance and backdriveability by means of pneumatic sensorized actuators (Sanchez et al. 2005). Experimental results with this robot showed that an active gravity compensating mechanism has a beneficial effect on reaching tasks. Pneu-WREX does not allow shoulder-external rotation, as it was based on a passive weight supporting orthosis design (Rahman et al. 2000) that did not include this degree of freedom in order to improve the weight balance. However, feedback from therapists suggests that this degree of freedom is perceived as very important for stroke rehabilitation. In order to provide this additional degree of freedom, we developed BONES.

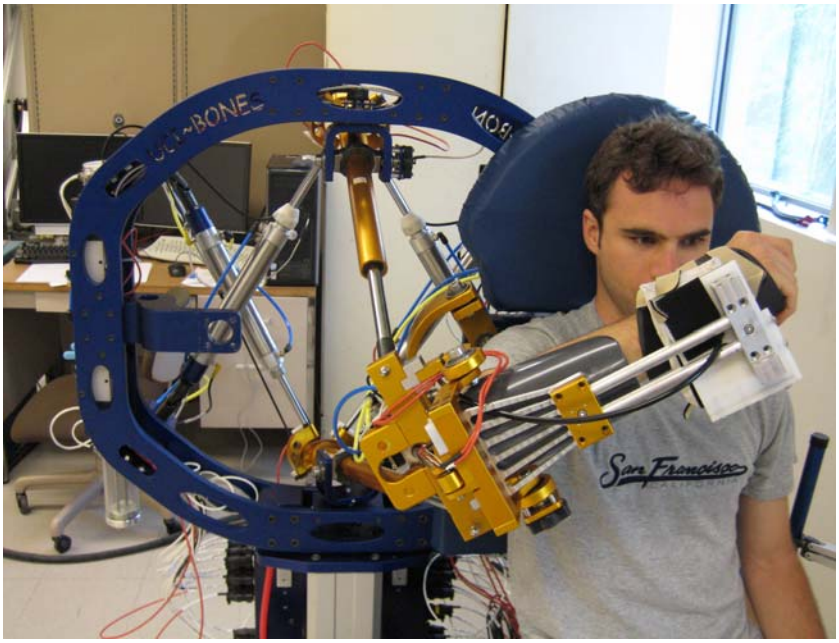

Figure 4.5. Unimpaired subject on the first version of BONES.

4.3 Stroke Rehabilitation and Robotic Therapy

Stroke is a sudden disturbance of the blood supply to the brain, which causes partial loss of brain function. Last year there were about 780,000 stroke episodes in the U.S., a number that has increased yearly over the past decade due to an increase in the mean age of the U.S. population. From 1994 to 2004, the stroke survival rate also improved 24.2 percent. The estimated direct and indirect cost of stroke for 2008 is $65.5 billion (Rosamond et al. 2008).

The result of more people having and surviving strokes is an increased need for rehabilitation services. Stroke patients with hemiparesis usually suffer difficulty with daily activities such as reaching, grasping, or walking (National Institute of Neurological Disorders and Stroke 2008). Stroke survivors undergo rehabilitation therapy to improve movement ability, and it has been demonstrated that rehabilitation

progress depends on the training intensity (Kwakkel et al. 2004). However, because rehabilitation is time intensive, health care providers limit the amount of therapy they will cover. Patients are receiving less therapy now than 20 years ago due to economic constraints on the U.S. health care system (Schmidt et al. 2002).

The process of neurological rehabilitation depends on the patient's ability to relearn how to trigger a proper response when a stimulus is given to move a specific limb or muscle – i.e. motor plasticity. Plasticity can be defined as the alteration of the properties of neurons and muscles, including their connectivity outline, ultimately leading to an alteration of their function (Seeley et al. 2003).

In recent years there has been increasing interest in using robotic devices to help automate rehabilitation therapy for stroke patients (Brewer et al. 2007; Burgar et al. 2000; Coote et al. 2003; Denève et al. 2008; Frisoli et al. 2007; Gupta and O'Malley 2006; He et al. 2005; Herder 2005; Jackson et al. 2007; Jiping et al. 2005; Kikuchi et al. 2007; Kramer et al. 2007; Li-Qun et al. 2007; Loureiro et al. 2003; Lum et al. 2002; Lum et al. 2005; Mayr et al. 2008; Mihelj et al. 2007; Nagai et al. 1998; Nef et al. 2007b; Perry et al. 2007; Rahman et al. 2004; Riener et al. 2005; Rosen et al. 2005; Sanchez et al. 2005; Sledd and O'Malley 2006; Sugar et al. 2007). Such devices may ultimately allow patients improved access to repetitive aspects of movement training at a reduced cost. These devices have shown initially positive clinical results: patients who receive robotic therapy in the chronic or acute stages following stroke significantly improve their movement ability (Kwakkel et al. 2004). However, movement ability gains due to robotic therapy are small, and typically do not transfer to activities of daily living (Kwakkel et al. 2004). Advantages of

rehabilitation robots are often hard to quantify due the length of the assessment period and patient-dependent variability of results (Siciliano and Khatib 2008). A key question for the field is therefore “How can robotic therapy be optimized to improve these initially positive clinical results?”

A common outcome of rehabilitation studies is that function improvement is directly linked to patient engagement in the rehabilitation process, independently of the nature of the rehabilitation approach (robotic or non-robotic) (Sanchez et al. 2006; Schmidt et al. 2004). Furthermore, there exists evidence that robotic movement training techniques, such as active constrained therapy, robotic-induced force fields and others, may present greater movement improvement when compared to repetitive movement practice alone (Housman et al. 2007; Kahn et al. 2006; Krebs et al. 1998; Kwakkel et al. 2008; Lum et al. 2005; Sanchez et al. 2006; Toth et al. 2005). Following, some of the most relevant clinical testing studies are presented:

Among the pioneer rehabilitation robots to undergo clinical testing, we find the MIT-Manus (Krebs et al. 1998). Results obtained with this robot, showed that the use of robotic therapy had no adverse effects and was well tolerated by the patients. They also proved that exercise therapy influenced motor recovery. In a more recent study, the ARM-GUIDE (Kahn et al. 2006) was used to compare efficacy of assisted robot-based therapy versus unassisted therapy. Results from this experiment showed that both groups presented similar improvements, concluding that assisted robotic therapy did not provide any additional value other than the movement practice itself. A study from the Biomechatronics Laboratory at the University of California Irvine (Sanchez et al. 2005), concluded that improvement of stroke patients using robotic therapy did

not differ much when compared to a control group who followed simple table-top reaching exercises. Other studies (Kahn et al. 2006; Lum et al. 2005) concluded that when it comes to function recovery, the main factor is the total therapy time accrued. Nevertheless, another key element linked to successful robotic therapy is the capability of the robotic device to generate human-like movements and forces (Carignan et al. 2005; Frisoli et al. 2005; Schiele and van der Helm 2006)

A clear advantage of robotic devices is the ability to quantify the performance of a subject's rehabilitation history. Whether quantifying force levels, path-tracking errors, response times or other quantifiable parameters, robots offer a clear advantage when compared to human therapist's subjective quantification of the patient's progress.

These findings converge towards a common goal for stroke rehabilitation: to make efficient rehabilitation accessible and affordable to a broader range of patients. Since the main elements against successful improvement of rehabilitation therapy are fatigue and inattention of the patient (Jan Nijhof and Gabriel 2006; Kahn et al. 2006; Loureiro et al. 2003; Nef et al. 2006), another key factor to a successful rehabilitation progress is the capability to maintain the engagement level and excitement of the patient during the therapy sessions.

In order to maintain the level of engagement, interactive games have proven to work positively towards engaging stroke patients (Sanchez et al. 2005). Such games, driven by robotic devices, can transform the monotony of a repetitive self-assisted rehabilitation exercise into a challenging, exciting, quantifiable robotic assisted therapy session. Among these rehabilitation games, we find *Java Therapy*

(Reinkensmeyer et al. 2002), a software system for guiding repetitive movement practice. It can be used with inputs such as a force feedback joystick or other more complex devices. The main goal of this program is to make rehabilitation therapy affordable and home-based, instead of having hospital-based therapy. Low cost in-home therapy tools can engage the patient and stimulate him/her to exercise more regularly. The system can keep a record of the patient's progress and via web transmit the patient's progress to their caregivers. Another graphical interface for robotic rehabilitation systems is the GENTLE/s, a system which integrates haptic and Virtual Reality technologies driven by a gravity compensated suspended arm orthosis (Loureiro et al. 2003). The aim of this project is to make quality machine-based rehabilitation available in the patient's home following hospital discharge.

Reducing muscle fatigue, while maintaining the effectiveness of the therapy, can be achieved by cancelling the effect of gravity of the assistive device. It has been suggested that gravity compensation increases the active range of motion during reach (when compared to gravity non-compensated reach). In (Prange et al. 2007), increased range of motion during gravity compensation is linked to lower levels of muscle activity, thus reducing the level of muscle fatigue during therapy.

Strategies for optimizing robotic therapy include designing improved exercise protocols, developing more sophisticated control algorithms, and improving the mechanical design of the robots. This thesis focuses on the last strategy: improved mechanical design.

4.4 Design description

BONES is a new robot that uses a simple parallel mechanism with mechanically grounded actuators to achieve 3 DOF shoulder movement, including shoulder internal/external rotation (Radomski and Trombly Latham 2008). The robot incorporates a serially-placed actuator for elbow flexion/extension, but uses a pneumatic actuator for this DOF to achieve large force output with light weight (Figure 4.5).

The inspiration for the design used in BONES (Figure 4.6) was the human forearm. We extended the same biomimetic principle that CRAMER is based on (see 3.3 for further detail and references) and adapted it to the shoulder. We used a simplified model of the human internal forearm mechanism consisting of an external pair of actuators that wrap around the upper arm, hence the word ‘biomimetic’.

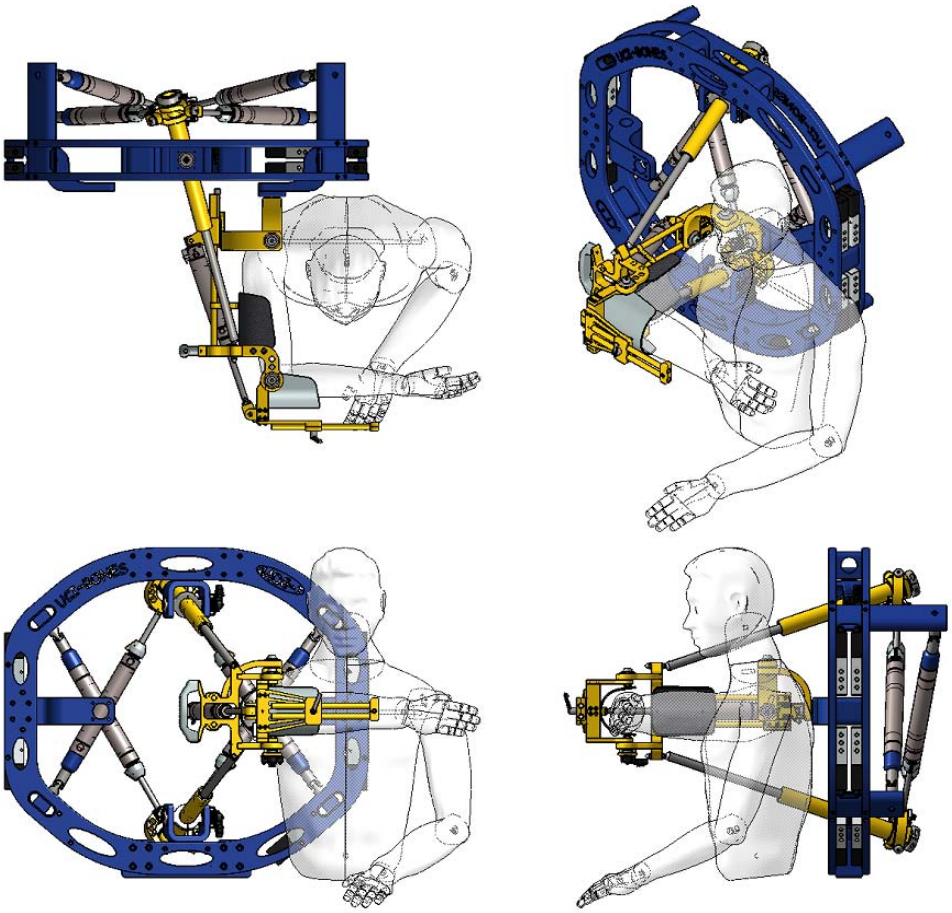

Figure 4.6. Several CAD views of the main components of BONES.

4.4.1 Mechanism Design Details

The upper arm exoskeleton (Figure 4.7) mimics the upper arm motion as a spherical joint (Woodson et al. 1992) rotating about the shoulder (Figure 4.9, point S). The rotation of the subject's Humerus is aligned along the x-axis (S to E). The elbow joint coincides with the upper arm's x-axis at point E. The upper arm lengths (LH) can be adjusted in order to accommodate a wide range of subjects.

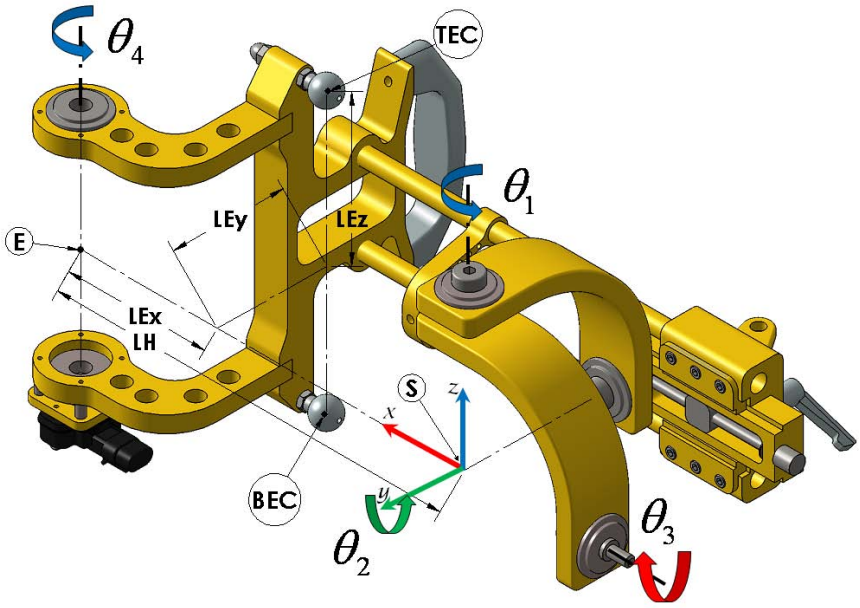

Figure 4.7. CAD model of the upper arm exoskeleton. S represents the location the subject's shoulder. E represents the location the center of the subject's elbow. TEC is one of the two points through which the upper arm exoskeleton is actuated. BEC is the second point through which the actuation takes place.

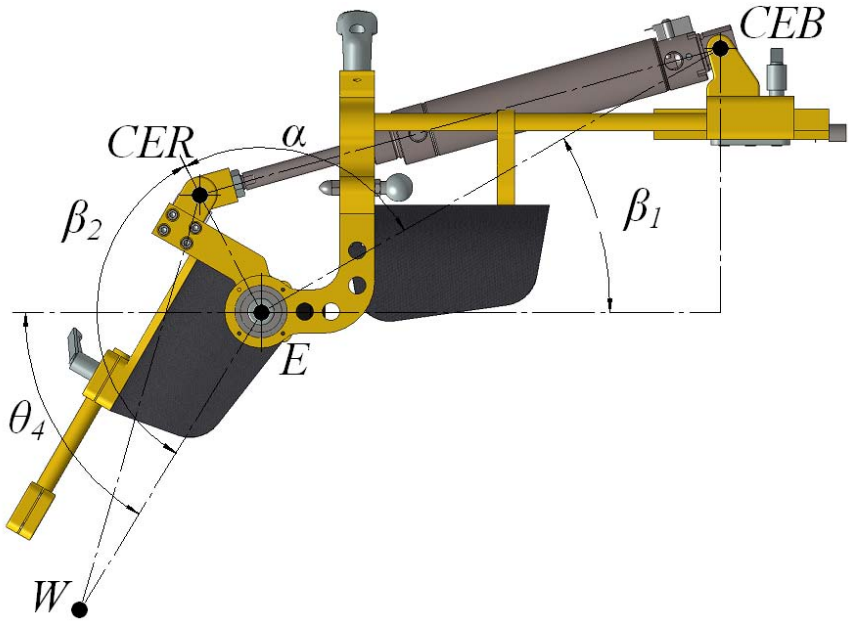

Figure 4.8. Elbow flexion/extension mechanism.

The arm is actuated at the elbow by means of two rods that can passively slide. One rod pivots with respect to static point YT (at the center of rotation of the top yoke which is attached to the actuators) and is attached to the arm exoskeleton at point TEC. Note that TEC is not aligned with the elbow rotation axis, yet the point is close to the location of the subject's elbow theoretical center. For simplicity we named this point Top Elbow Connection (TEC). Similarly, the other rod pivots at YB (bottom yoke center of rotation) and is attached to the arm at BEC (bottom elbow connection point).

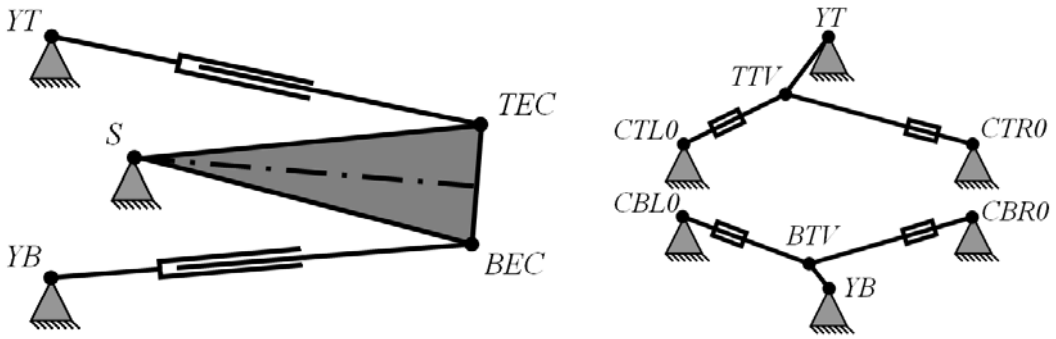

Figure 4.9. Rear Diamond and Upper Arm Geometry. (left) Elbow motion diagram. (right) Rear 'Diamond Structure' actuation diagram.

Both rods extend past YT and YB, respectively, towards the back of the robot's frame. The rear end of each these rods is actuated by two pneumatic cylinders using the scheme depicted in Figure 4.10 (we refer to this configuration as the 'Diamond Structure'). The Diamond Structure includes two geometric tetrahedrons. The static base of the first tetrahedron is defined by $CTL0$, YT and $CTR0$. The vertex of the first tetrahedron is TTV ('Top Tetrahedron Vertex'). Similarly, the second

tetrahedron has a base defined by $CBL0$, $CBR0$ and YB. Its corresponding vertex is BTV (Bottom Tetrahedron Vertex). The upper rod contains the points TTV (rear end), YT (yoke pivot point) and TEC (elbow actuation point). Similarly, the lower rod aligns BTV, YB and BEC.

The distances from BTV to YB and from TTV to YT are fixed, but the distance from YT to TEC and from YB to BEC varies passively depending on the position of the exoskeleton. If points TTV and BTV are moved to the right, the arm moves to the left. When points TTV and BTV are moved downward, the arm moves up. If TTV and BTV are displaced in opposing directions, the elbow rotates about the x-axis (internal/external rotation). In Figure 4.10 several configurations for the rear Diamond are shown.

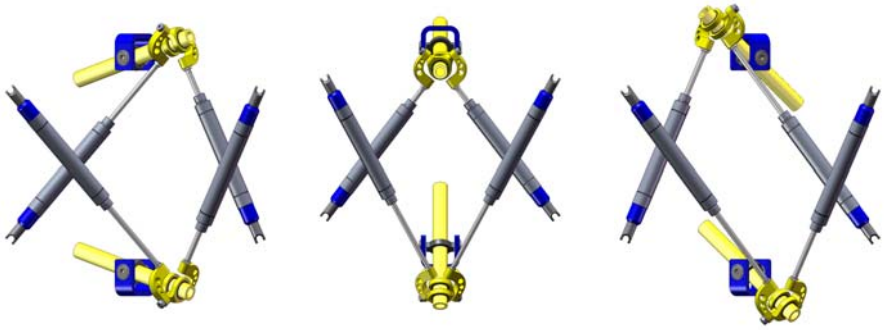

Figure 4.10. Rear view of the 'Diamond Structure' for the elbow.

In order for the pairs of cylinders to actuate the tetrahedron vertices we designed a mechanism (Figure 4.11) that mimics a spherical joint by intersecting the two cylinder axis and the rod axes at TTV (or BTV).

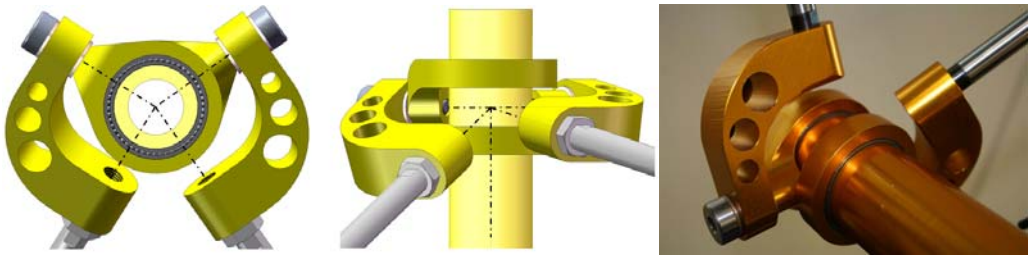

Figure 4.11. Novel spherical joint mechanism. (left and center) CAD model of spherical joint mechanism. (right) Actual part used in the first BONES prototype.

4.4.2 Range of Motion

The range of motion (ROM), or workspace, achieved by BONES is summarized in Table 4.1. Note that we define home position to be $[\theta_1, \theta_2, \theta_3, \theta_4] = [0, 0, 0, 0]$, according to the angles described in Figure 4.7. In this position the upper arm is horizontal, aligning the elbow and the shoulder at the same elevation, and the forearm fully extended. The ROM is close to human ROM, except at the elbow, where we limit elbow flexion to prevent the robot from contacting the subject's torso.

TABLE 4.1. RANGE OF MOTION OF BONES [DEG]

	BONES (Min.)	BONES (Max)	BONES Range of Motion	ADL Range of Motion
θ_1	-49	50	99	110
θ_2	-33	40	73	100
θ_3	5	81	76	135
θ_4	12	84	72	150

Angles are measured with respect to the home position shown in Figure 4.7.
The desired ADL angles are obtained from (Perry et al. 2007)

4.4.3 Hardware, actuators, and sensors

We incorporated pneumatic cylinder actuators and sensors into BONES as described next. It would also be possible to use the same mechanism design with

other types of actuators, including linear or rotary electric motors. Direct drive rotary actuators could be mounted at the yokes, for example.

The main structural frame (Figure 4.6) consists of two oval-shaped aluminum plates (76.2cm x 86.3cm) separated by a 6.4cm gap. The gap between the two plates is used to enclose 10 Festo MPYE-5-1/8-LF-010-B proportional directional control valves. This gap is also used to route the sensor wiring, power supply and air supply in order to provide protection and making the overall design more aesthetically pleasing.

Previous work from our research group (Wolbrecht 2007; Wolbrecht et al. 2006) revealed the importance of having the pneumatic valves and the pressure sensors as close to the cylinder as possible in order to minimize pressure loss, latency due to pressure wave dynamics and obtain more accurate cylinder pressure measurements. In order to locate the pressure sensors close to the cylinder chambers, we customized both ends of the double actuated Bimba cylinders to provide an attachment port for a Honeywell ASCX100AN pressure sensor (Figure 4.12). We machined a flat surface on both ends of the cylinder and drilled a precision hole into the chamber, allowing the pressure sensing port to become embedded directly inside the cylinder chamber. This solution enables a clean and direct pressure reading, while minimizing the required plumbing parts. During the machining process the chamber was pressurized at 0.68MPa (100PSI) so that any possible contaminating lubricant fluid or chip was blown away from the cylinder chamber.

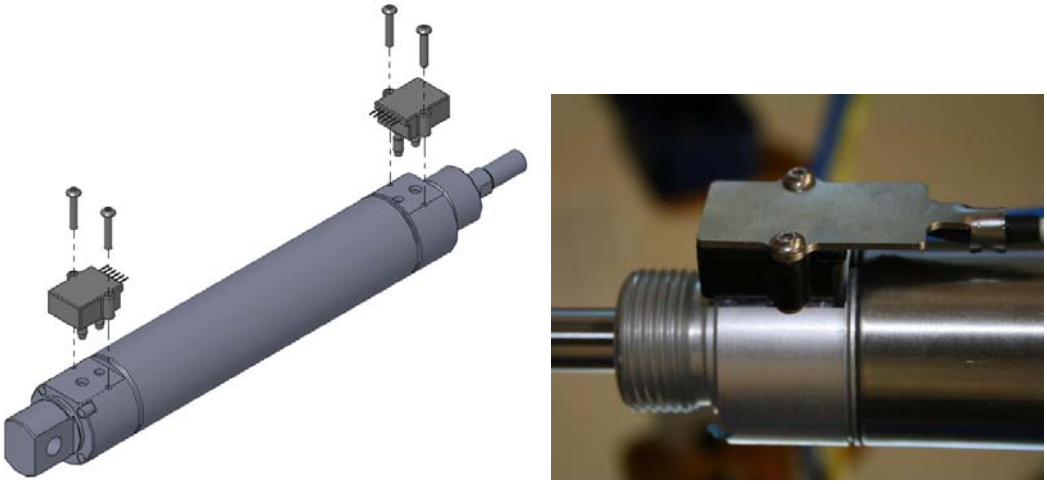

Figure 4.12. Novel pressure sensor placement. (left) CAD exploded view of the assembly of the post-processed cylinder and the pressure sensor. (right) Actual view of the finished assembly.

Five PFC-XLBP Bimba low friction, position feedback cylinders are used to actuate BONES. Diamond Structure is composed by four Bimba PFC-176.5-XBPL and the elbow is driven by a Bimba PFC-175-XBPL. Although the mechanism presents 4 DoF, we use one extra cylinder in the rear Diamond Structure (Figure 4.9) in order to achieve higher forces, higher stiffness control and add redundancy of measurements for safety purposes.

BEI Duncan 9855R5K low profile potentiometers are located at the elbow joint and at each of the two revolute axes of the yokes (located at point YT and BT in Figure 4.9).

The bearing surfaces for all revolute joints (elbow joint, shoulder spherical link and upper and lower yokes) use flanged tapered A4138B Timken bearings. We use tapered bearings to minimize backlash while maintaining a smooth, low friction rolling joint. The overall assembly presents very low backlash and friction simultaneously.

The device can be adapted to the anthropometry of a wide range of stroke patients. The arm length (from S to E) can be adjusted to accommodate 27.9 cm (11 in) to 44.4 cm (17.5 in) long arms. Furthermore, in order to align the subject's shoulder to the exoskeleton's S point, the mechanism is provided with an electrically adjustable 30.5 cm (12 in) stroke pedestal and a motorized chair base capable of fine tuning the subject's elevation by 10.1 cm (4 in) in the vertical direction, and 5.1 cm (2 in) in the lateral direction. BONES can also be easily reconfigured from right left arm configuration and vice versa.

4.4.4 Kinematics

In this section, we present the inverse kinematics for the mechanism, which allow us to solve for the cylinder coordinates to produce a desired joint motion of the human arm.

Although there exist recommendations from the International Society of Biomechanics on how to define a joint coordinate system for the upper limb (Šenk and Chèze 2006; Wu et al. 2005), for simplicity we used the homogenous transformations similar to the Euler angles proposed in (Wu et al. 2005). While the rotation sequence XZX is the common Euler angle formulation found in (Murray et al. 1994), we used the sequence ZYX which has singularities when Y is ±90 degrees. In our case, this singularity is not in the range of motion of the robot. To solve the kinematics of the robot, we defined the following coordinate systems, angles and transformations:

$\{F_0\}$ is the reference frame with origin at S, and x_0-axis aligned to the line defined by S and E. The z_0-axis, as shown in Figure 4.7, is vertical pointing upward, orthogonal to the x_0-axis. Accordingly, the y_0-axis completes $\{F_0\}$ as an orthogonal right-handed coordinate system. The angle θ_1 represents a rotation about the z_0-axis. The coordinate system $\{F_1\}$ is the result of rotating $\{F_0\}$ with respect to z_0. Furthermore, θ_2 represents a rotation about the y_1-axis. $\{F_2\}$ is the result of rotating $\{F_1\}$ about y_1. In addition, θ_3 represents a rotation about the x_3-axis. In a similar process as the one described in Chapter 3, the explicit functions of TEC and BEC (both defined in the previous section) in the coordinate system $\{F_0\}$ are

$$TEC = R_z(\theta_1) \cdot R_y(-\theta_2) \cdot R_x(\theta_3) \cdot TEC_0 \tag{4.1}$$

and

$$BEC = R_z(\theta_1) \cdot R_y(-\theta_2) \cdot R_x(\theta_3) \cdot BEC_0 . \tag{4.2}$$

Note that, according to the dimensional parameters described in Figure 4.7, the homogeneous coordinates of TEC_0 and BEC_0 are

$$TEC_0 = \begin{bmatrix} LEH - LE_z \\ -LE_y \\ LE_z \\ 1 \end{bmatrix} \quad \text{and} \quad BEC_0 = \begin{bmatrix} LEH - LE_z \\ -LE_y \\ -LE_z \\ 1 \end{bmatrix}.$$

Within the workspace of the human arm, for any given combination of roll, pitch and yaw transformations the location of TEC and BEC is unique.

Once the location of TEC and BEC is defined, we continue the kinematics analysis at the Diamond Structure. We express the location of the rear end of the upper and bottom rods in terms of the elbow connection points as

$$TTV = -\frac{TEC - YT}{|TEC - YT|}|TTV - YT| + YT \tag{4.3}$$

and

$$BTV = -\frac{BEC - YB}{|BEC - YB|}|BTV - YB| + YB\,. \tag{4.4}$$

Having determined the location of TTV and BTV, we define the cylinder coordinates for the four cylinders in the Diamond Structure (Figure 4.9) and the elbow cylinder (Figure 4.8) as

$$q = \begin{bmatrix} |TTV - CTL0| \\ |TTV - CTR0| \\ |BTV - CBL0| \\ |BTV - CBR0| \\ |CER - CEB| \end{bmatrix}. \tag{4.5}$$

The elbow joint coordinate can be determined independently from the previous calculations due to the fact that the elbow is decoupled from the Diamond Structure actuators. We define the edges of the triangle defined by the points CEB, E and CER (Figure 4.8) as follows:

$$a = |CER - CEB| \tag{4.6}$$

$$b = |E - CER| \tag{4.7}$$

$$c = |E - CEB| \tag{4.8}$$

Using law of cosines we obtain the following relation,

$$a^2 = b^2 + c^2 - 2bc\cos(\alpha). \tag{4.9}$$

From (4.5) and (4.6) we can establish the relation $a = q_5$. According to the notation used in Figure 4.8, it holds that

$$\theta_4 + \pi = \beta_1 + \alpha + \beta_2. \tag{4.10}$$

Finally, using (4.9) and (4.10), the fifth cylinder coordinate as a function of the elbow angle, θ_4, is determined by

$$q_5 = \sqrt{b^2 + c^2 - 2bc\cos(\theta_4 + \pi - \beta_1 - \beta_2)}. \tag{4.11}$$

where β_1, β_2 are constant.

4.5 Force generation

4.5.1 Relating Cylinder Forces, Joint Torques, and Endpoint Forces

If the set of desired arm angular velocities are known, the required cylinder linear velocities are given by:

$$\dot{q} = \frac{dq}{dt} = \frac{\partial f}{\partial \theta}\dot{\theta} = J_c(\theta)\dot{\theta}, \tag{4.12}$$

where $q(t) \in \Re^5$, $\theta(t) \in \Re^4$, $f(\theta): \Re^4 \to \Re^5$, and thus $J_c \in \Re^{5\times 4}$. The transpose of the Jacobian relates the torques applied to the arm, τ, to the forces by the actuators, F_c:

$$\tau = J_c^{\mathsf{T}}(\theta) F_c. \tag{4.13}$$

We use two different Jacobians for BONES. One relates cylinder velocities to the robot joint velocities. The other relates robot joint velocities to wrist/forearm velocities in a world-centered frame. The first Jacobian is important for relating the

actuators forces to the joint torques. The second Jacobian is important for determining the forces that the robot applies to the subject in endpoint coordinates.

The location of the wrist can be described by the kinematic chain formed from the 4 joint angles in the shoulder and elbow, similarly to how TEC and BEC were defined but with an additional transformation for the elbow. Using this transformation, three DOF of the wrist can be easily defined as the resulting position of the wrist. A coordinate for the last DOF of the wrist needs to be defined from the rotation matrix of the transformation. Using the swivel angle (Kang et al. 2005) as this final coordinate, a coordinate transformation from shoulder and elbow angles to wrist position and arm swivel can be defined as

$$q_w = g(\theta). \tag{4.14}$$

Taking the derivative of this equation with respect to time gives us the arm Jacobian in

$$\dot{q}_w = \frac{dq_w}{dt} = \frac{\partial g}{\partial \theta}\dot{\theta} = J_a(\theta)\dot{\theta}. \tag{4.15}$$

The cylinder Jacobian is found using (4.12) on (4.1)-(4.5).

In order to solve the Jacobian that relates the pneumatic actuator velocities and the end-effector motion (wrist), we divide the path from one to the other in four intermediate steps (Figure 4.13). The first stage relates the velocity vector of the pneumatic cylinders and the velocity at TTV and BTV (points defined in Figure 4.9). Determining the velocity of these two points leads to the second intermediate stage: solving for the velocity of BEC and TEC. Consequently, the third phase links the configuration of the upper arm ($\dot{\theta}$ from Figure 4.7) as a function of the velocities

of *BEC* and *TEC* . Because the elbow actuation is decoupled from the three previous stages, in the fourth and final intermediate step we add the elbow flexion/extension mechanism in order to determine the velocity of the end effector.

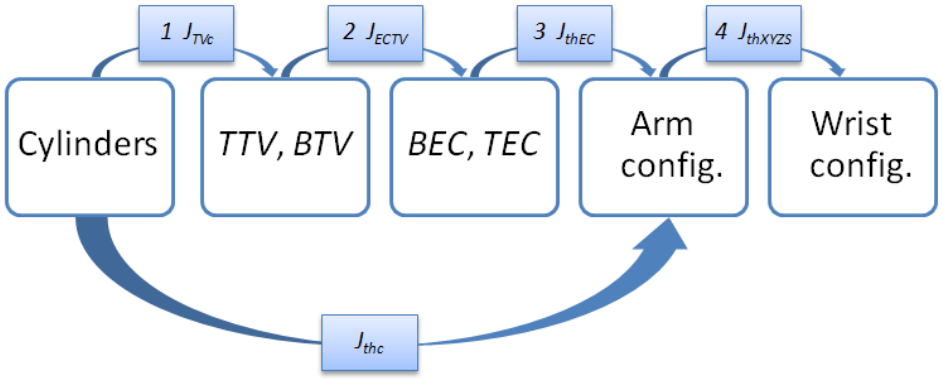

Figure 4.13. Intermediate steps relating the end-effector and the actuators, and their respective Jacobian matrices. Steps 1 through 3 are dependent on the 4 pneumatic cylinders at the rear diamond. The last step adds the decoupled cylinder located at the elbow.

The detailed derivations for the Jacobian equations are provided in Appendix A.2.

4.5.2 Geometric Design, Special Considerations

In serial robots, in which links are highly independent from each other, the dimensioning of geometrical design parameters in one link will have limited effects on the parameters in another link. Because of the parallel topology of BONES, each geometrical design parameter can affect simultaneously the RoM, Jacobian Matrix conditioning, maximal force capability and patient safety (moving parts could potentially collide with the patient's body). For example if we increase LE_z (Figure 4.7) in order to increase the distance between *TEC* and *BEC* , we will improve the mechanical advantage of the internal/external rotation but at the same time we will be

reducing the safety factor of the robot: *BEC* ("Bottom Elbow Connection" point) will be closer to the patient's body. Many of the design parameters present this duality between enhanced mechanical advantage versus reduced safety.

One of the most critical design aspects of BONES are the locations of *S* (the shoulder center), *TEC* and *BEC* (Figure 4.7). These points play a very important role in transforming the forces from the sliding bars into torques at the upper arm exoskeleton structure. A change in the geometrical location of *TEC* and *BEC* will have a direct effect on the force capabilities, RoM and safety.

Recall the coordinates of *TEC* and *BEC* from (A.4) and (A.5)

$$TEC = \begin{bmatrix} c_y c_p LH + \left(s_y s_r + c_y s_p c_r\right) LE + S_x \\ s_y c_p LH + \left(-c_y s_r + s_y s_p c_r\right) LE + S_y \\ s_p LH + c_p c_r LE + S_z \end{bmatrix},$$

$$BEC = \begin{bmatrix} c_y c_p LH - \left(s_y s_r + c_y s_p c_r\right) LE + S_x \\ s_y c_p LH - \left(-c_y s_r + s_y s_p c_r\right) LE + S_y \\ -s_p LH - c_p c_r LE + S_z \end{bmatrix}.$$

With the original set of values in the first design of BONES, we observed that the robot was very weak in some directions. For example, for an arm in the home position ($[\theta_1, \theta_2, \theta_3, \theta_4] = [0, 0, 0, 0]$) the robot was barely strong enough to lift its own weight. This was due to the fact that in order to move the arm in a pure elevation (about θ_2), the robot had to provide additional external rotation to compensate for the moment arm produced by the forearm against gravity. Because of the relatively short distance between *TEC* and *BEC*, the robot had a reduced moment arm to generate internal/external rotation torques, therefore all the pneumatic power had to be

invested in overcoming the external rotation, leaving a reduced amount of lifting power. In such a scenario, the pneumatic valves were working close to saturation.

To assess the best design values for these sensitive dimensions we crafted an optimization function in which the capability to lift the arm (exoskeleton+human arm) was the cost function. We optimized three parameters. The first one affected the y coordinate of the shoulder origin, S. Parameter 2 represents a vertical translation of TEC and Parameter 3 a horizontal translation of BEC. Figure 4.14 shows the direction of the translation related to each parameter.

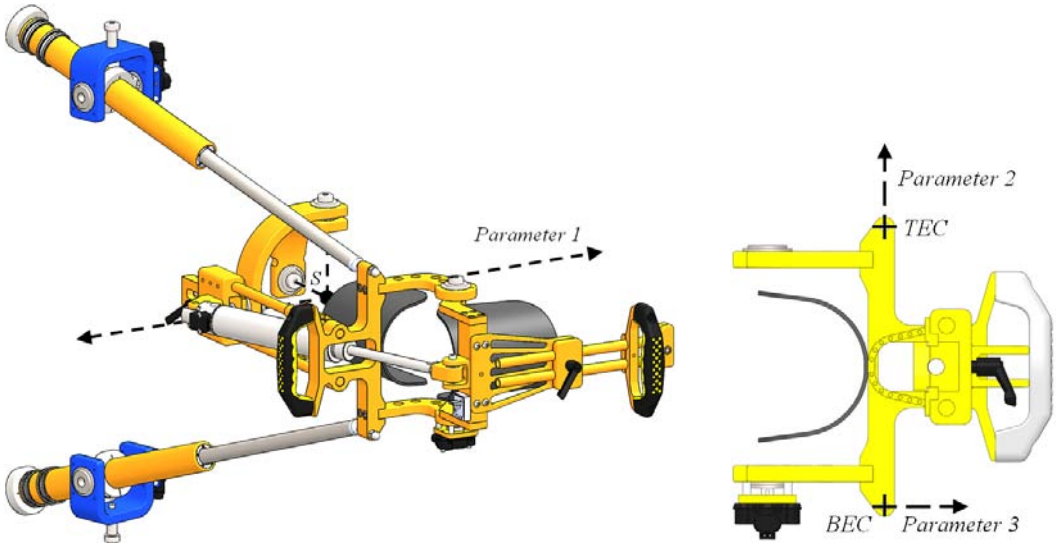

Figure 4.14. Design optimization based on three parameters. Parameter 1 translates S in the y direction (left) Parameter 2 moves TEC in the z direction. Similarly, Parameter 3 moves BEC In the y direction (right)

We consider the force capability of the robot at any given arm configuration as a vector-space defined by combinations of maximum/minimum force capabilities of each of the 4 pneumatic cylinders in the rear diamond. For any given shoulder

configuration, there exist 16 points, each representing a combination of all 4 cylinders applying maximum force in either direction. A line between two points represents combinations of 3 cylinders providing maximum force ("push" or "pull") and the remaining cylinder is unconstrained by any force condition. A plane corresponds to a combination of two force-constrained cylinders and two unconstrained ones.

We can characterize the maximum lifting capability as the highest intersection point between the polygonal volume and a vertical vector representing the weight of the arm in the direction of gravity, i.e. the combination of pneumatic forces able to produce the highest pitch torque (pure rotation about θ_2). Furthermore, if we analyze the shape of this volumetric representation, we can characterize the strongest and weakest directions of motion. A rounder volume indicates a situation in which the robot is capable of transitioning from that position to another with no preferred direction. A narrow polygon with a dominantly long dimension shows the preferred (strongest) direction of motion in that configuration. It is desirable that, in any given configuration, the robot is capable of generating forces in all directions.

We superimposed a sphere representing a 22Nm torque applied in any given direction, associated to the maximum torque required in ADLs (Table 4.2). If the robot was not able to provide more than 22Nm in a specific direction, the normal plane to that direction was at a distance of less than 22Nm away from origin, therefore the plane would intersect the sphere, and a spherical cap would become visible. If the robot was capable of exceeding 22Nm in any direction, from a specific arm configuration, the sphere was no longer visible. For example, with the original dimensions (before optimizing) and the arm located at $[\theta_1, \theta_2, \theta_3] = [-50^o, 0^o, 0^o]$, the

robot was unable to exert a positive roll torque (external rotation of the arm), nor was it capable of elevating the arm (pitch). In this configuration, the robot was very strong only in one direction: along an undesirable combination of internal rotation and elevation of the arm.

Changing Parameters 1, 2 and 3 reshaped the volumetric representation of the force capability. A set of optimized dimensions enabled the robot to successfully provide greater torques in the desired directions. An example of how modifying Parameter 2 and 3 affected the shape of the polygonal volume is shown in Figure 4.15 (Parameter 1 was set to zero in this example).

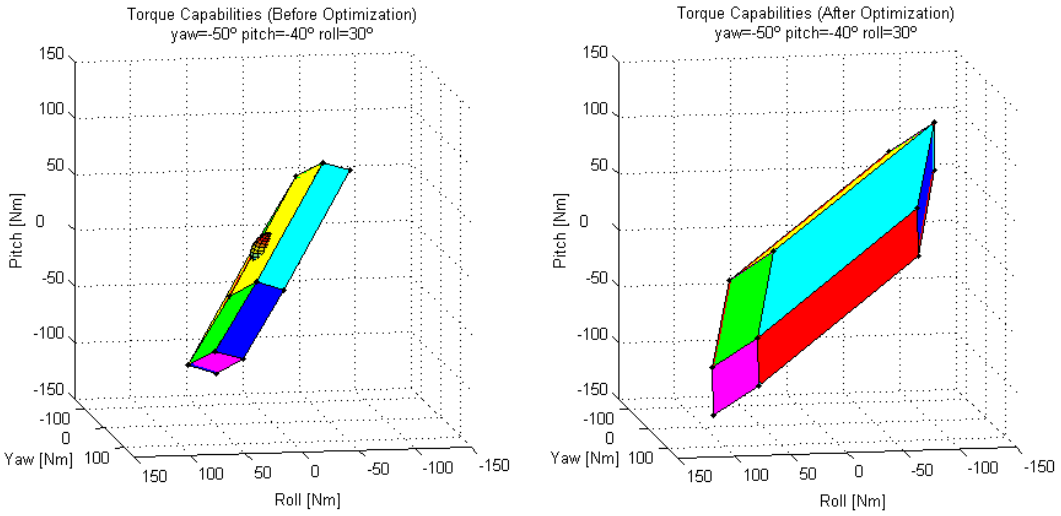

Figure 4.15. Polygonal volumes represent maximal force capability. If the sphere is partially visible, the robot won't be able to exceed 22Nm in a particular direction. The left plot shows the torque generation polygon of the initial BONES design, while the right plot shows the effect of setting $Parameter_2 = 2.25in$ **and** $Parameter_3 = 3in$ **.**

After experimenting with some preliminary estimates for each parameter, we realized that Parameter 1 had a greater influence on the capability of the robot to lift

the weight of the arm and the weight of the exoskeleton. Parameter 2 and 3 had a limited effect on the arm weight lifting capability, yet both parameters had the potential to fine tune the shape of the force representation in order to meet our goals.

Therefore, we optimized Parameter 1 in order to achieve sufficient arm lifting power. We considered 22Nm to be the threshold below which the robot would not be able to provide the maximum torque necessary to lift the arm and the exoskeleton in typical activities in daily living (Table 4.2). The cost function for this optimization method was defined as the ratio of maximum elevation torque achievable by the robot with respect to the 22Nm threshold.

The geometrical representation of the maximum lift corresponds to the distance from the center of the torque coordinate system to the intersection point of the gravity vector (vertical line) and the polygonal volume. For each polygonal volume, the intersection with a vertical line leaves two solution points. We only considered the point with the highest z-component. In Figure 4.16 we show the highest plane intersecting a vertical line centered at the origin, for several values of Parameter 1. For clarity purposes, we deleted the remaining 15 planes. Figure 4.17 shows the arm lifting ratio as a function of Parameter 1.

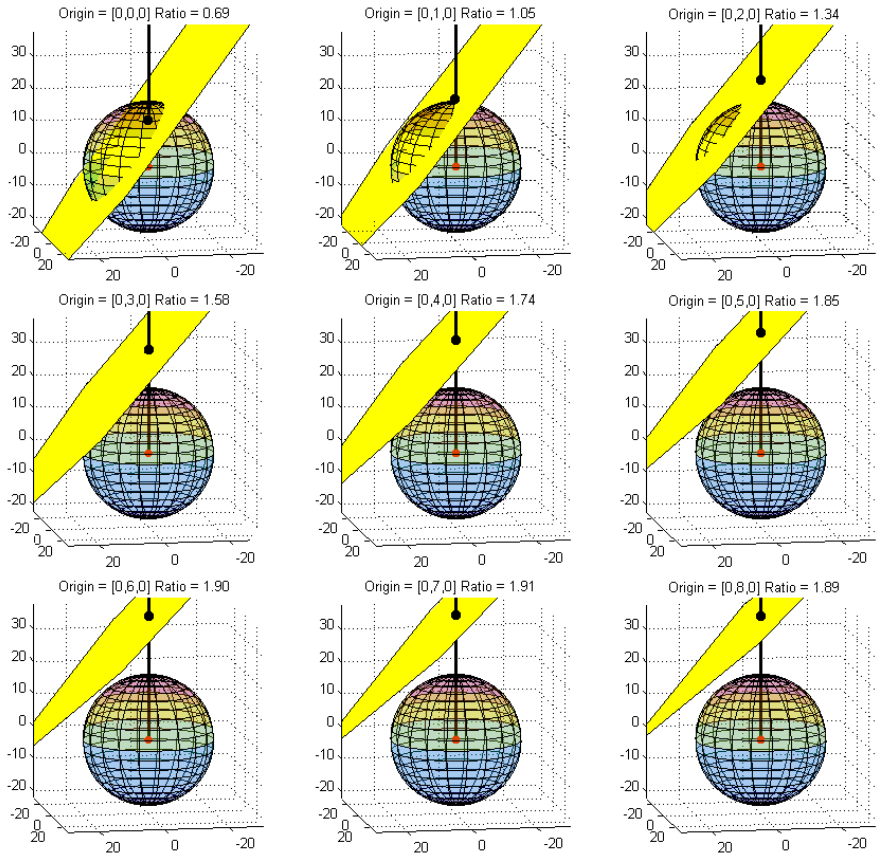

Figure 4.16. Arm weight lifting capability as a function of shoulder center shifting, geometrical representation. The vertical axis represents the torque (in Nm) applied to lift the arm (about θ_2)

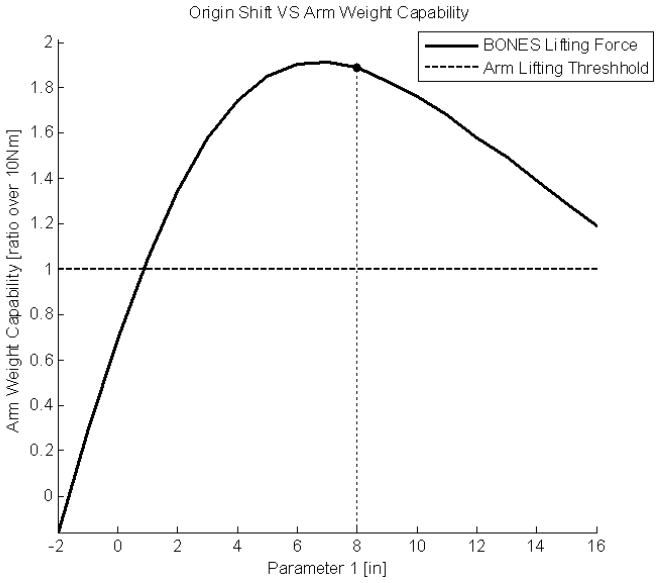

Figure 4.17. Lifting ratio as a function of shoulder center shifting, graphical result

After analyzing the results from the first optimization process, we set $Parameter_1 = 8in$, with a corresponding ratio 89% exceeding over the threshold. Although the optimization method would encourage a designer to set Parameter 1 to a value with a higher ratio, we took into consideration some additional benefits difficult to quantify, such as the ability to reconfigure BONES from left arm to right arm as simply as possible. By setting $Parameter_1 = 8in$, we moved the shoulder to the sagittal symmetry plane of the supporting frame. If the robot had to be reconfigured from left to right arm configuration, any point located at the sagittal plane would remain in the same location, therefore reducing the number of parts that need reassembly during the reconfiguration process.

After determining the optimal value for Parameter 1, we continued the optimization process with Parameter 2 and 3. For these two parameters, our goal was to optimize the ratio between the shortest and the longest axis of the polygonal volume in order to discourage any undesirable direction to be stronger than the rest. By making the major axis and the minor axis similar, we were reshaping an ellipsoid-like volume into a sphere, therefore equalizing the maximal applicable strength for any given direction. This ratio is related to the condition of the Jacobian matrix. When a Jacobian matrix is poorly conditioned in a given direction, the eigenvalue corresponding to that direction presents a large condition number. The poorly conditioned eigenvalue will cause difficulties in the numerical calculation along that direction, as if we were approximating a singular point (Merlet 2006; Saad 1989). The forces along the corresponding eigenvector will be very low, compared to better

conditioned directions (with lower condition numbers). Therefore, it is desirable that the Jacobian matrix remains as well conditioned as possible, with condition numbers as low as possible in all directions. A well conditioned Jacobian will translate directly into a system capable of offering similar forces in all directions.

The plot of the ratio between the smallest and the largest axis as a function of Parameter 2 and Parameter 3 is shown in Figure 4.18. According to the results obtained, we selected $Parameter_2 = 2.25in$ and $Parameter_3 = 3in$.

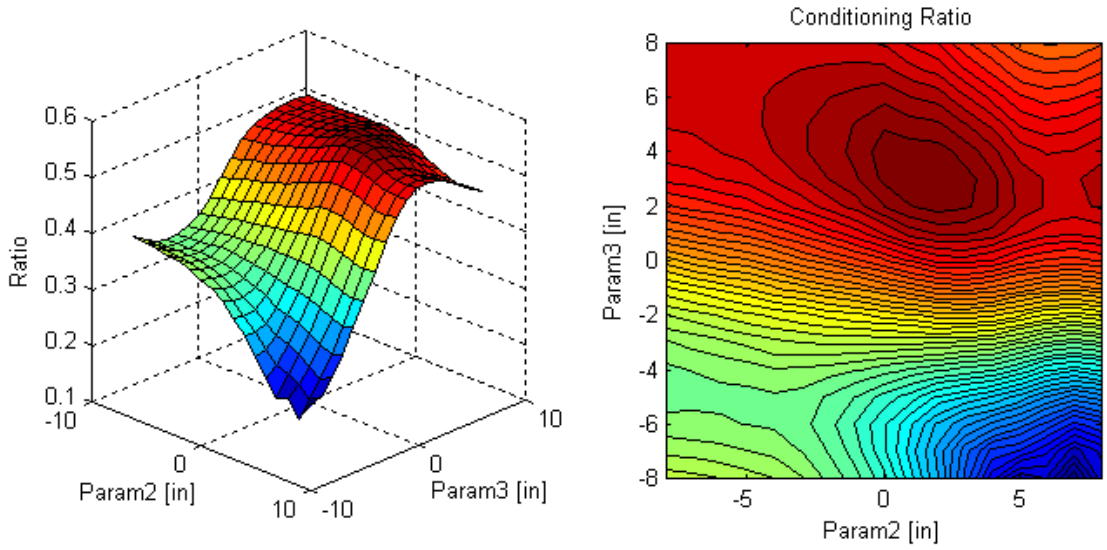

Figure 4.18. Longitude of the shortest volume axis over the longitude of the longest volume axis as a function of Parameter 2 and Parameter 3

4.5.3 Passive Gravity Support

An elastic element provides weight support for the exoskeleton. In case of emergency or power outage, the exoskeleton returns to the home position, so the subject's arm does not fall. The spring-like element also biases the force operating range of the actuators so that they have a greater, bi-directional range. The initial

adjustment of the elastic element was determined from (4.13) at the home position, but the final location of the attachment points was a trial-and-error process.

For further detail on the Passive Gravity Support, please refer to Chapter 5.

4.5.4 Joint Torque Range

We attached 3.81cm (1.5in) diameter pneumatic cylinders to the device, and operated them at 6.3bar (90 PSI). With these numbers, the peak force generating capability of BONES is summarized in Table 4.2.

TABLE 4.2. TORQUES APPLIED TO THE ARM [NM]

	BONES	Impaired Arm	Unimpaired Arm	ADL
τ_1	76.8	27.2	53.9	8
τ_2	50.0	41.2	53.5	10
τ_3	42.2	19.1	35.6	1
τ_4	68.0	38.7	80.9	3.5

Impaired limb data from (Dewald and Beer 2001). ADL extracted from (Perry et al. 2007).

For BONES, we are targeting patients with severe to moderate arm impairment, i.e. Upper Extremity Fugl-Meyer Score less than 35 out of 66 max (Fugl-Meyer et al. 1975). For this level of impairment, the device's maximum torque is larger than the impaired arm's maximum torques. If higher force levels are required, larger diameter cylinders can replace the existing ones, or supply pressure can also be increased.

TABLE 4.3. INERTIA OF THE EXOSKELETON [$g \cdot cm^2 \times 10^3$]

	axis	BONES	Human
Upper arm	X	165	39.8
	Y	696	204.4
	Z	740	190.5
Forearm	X	53	18.8
	Y	281	124.8
	Z	414	122.4

Human data values have been extracted from (National Aeronautics and Space Administration 1995).

The upper arm exoskeleton weighs 3438g (including the elbow actuator). The forearm exoskeleton module weighs 921g for a total arm weight of 4359g. An average (across sexes) human upper arm weighs approximately 2500g, and a human forearm, 1720g, for a total of 4220g (National Aeronautics and Space Administration 1995). Thus, the mass of the exoskeletal parts that the subject has to move is comparable to the mass of a human arm. This relatively lightweight exoskeleton is made possible by the use of the parallel mechanism and mechanically grounded actuators. Indeed, the total weight of the robot, including the actuators, is 18.5kg. Mass could be further reduced in the next version of BONES by reducing part size.

4.6 Conclusion

This chapter presented the design and kinematic analysis of BONES, a novel robot that allows naturalistic motion of the human arm using mechanically grounded, direct drive actuators at the shoulder. Direct drive actuation is achieved with a relatively simple mechanism inspired by the human forearm. The range of motion, inertia, and force generating capacity of the mechanism are well matched to the

human arm. In the clinic, we plan to use BONES to assist, resist, and perturb naturalistic arm movements, for the purpose of re-training movement ability after stroke. Development of BONES will allow us to rigorously test whether functional transfer of robotic therapy is improved by practicing more naturalistic movements, and will allow implementation of a wide variety of force assistance algorithms.

Chapter 5 Weight compensation

5.1 Introduction

This chapter describes the mechanism that passively counteracts the weight of the BONES exoskeleton (Chapter 4). Using springs in parallel with the pneumatic cylinders, we can partially reduce the effect of weight of the exoskeleton on a subject's arm. Due do the complex and highly non-linear kinematics of BONES, perfect spring gravity compensation would require a complex system of cam pulleys. Our solution does not achieve a perfect compensation for all positions, but provides a mechanically simple and effective partial balancing effect, most effective around the home position described in (Rahman et al. 1995). Our spring system also serves the purpose of safely supporting the arm during an emergency stop leading to a drop in air pressure supply to the pneumatic cylinders.

5.2 Overview

In order to determine the effect of gravity on the robot exoskeleton we must define the position of the Center of Mass (*CoM*) of the exoskeleton (including the

human arm). Once the *CoM* is known for any configuration, we calculate the joint torque created by the weight of the exoskeleton at the shoulder rotation point. The next step is to transform the joint torque required to counterbalance the arm into the force required by the springs in order to balance the system. Since the springs will be placed in parallel with the pneumatic cylinders, we can use the Jacobian from (4.5).

5.3 Determining the location of the Center of Mass (*CoM*)

The desired torque we want to counterbalance at the home position is a function of the weight of arm, the weight of exoskeleton, the pitch elevation and the arm roll. A rotation of the yaw angle is unrelated to a change in the weight effect of the exoskeleton.

The location of the CoM for positions other than the home position is defined as a sequence of homogeneous transformations

$$CoM(\theta) = R_z(\theta_1) R_y(-\theta_2) R_x(\theta_3) R_z(\theta_4) CoM_0 . \tag{5.1}$$

The direction of the rotation axes is defined as follows:

- *x*-axis: along the arm (positive when distal from the shoulder)
- *y*-axis: line shoulder to shoulder
- *z*-axis: vertical (positive is up)

The angle vector, θ, defines each of the four degrees of freedom of BONES [*yaw*, *pitch*, *roll*, *elbow*]. Positive values of these angles are described for the right arm configuration as follows:

- (+) *yaw*: arm goes toward body
- (+) *pitch*: arm goes UP
- (+) *roll*: forearm goes UP
- (+) *elbow*: the elbow is extended

An average upper arm length, *LH*=288mm (11.34in), was used in the calculations (Clauser et al. 1969). Similarly, we used *LFA*=355mm (13.98in) as the average forearm+hand length.

The location of the CoM at the home position is listed in Table 5.1. CoM data was extracted from (Klapp et al.). The mass properties of the exoskeleton components were determined using the CAD software and solid modeler *SolidWorks*.

TABLE 5.1. MASS PROPERTIES AND COM OF THE EXOSKELETON AND THE ARM IN THE HOME POSITION. MASS [KG] COM [CM]

	Mass	CoM (x)	CoM (y)	CoM (z)
ExosUpperArm	3.46	15.31	-11.73	-0.17
ExosForearm	0.95	40.72	-3.68	-3.38
HumanUpperArm(1)	1.68	15.18	0.00	0.00
HumanForearm(2)	1.43	34.09	0.00	0.00

(1) from (Clauser et al. 1969), Table I, average of line 6 and 7
(2) (Clauser et al. 1969), Table I, average of line 8 and 9

5.4 Torques generated by the *CoM*.

The torques generated by the arm and the exoskeleton structure is dependent on the location of their center of mass. If we define a gravity vector as

$$gravity = [0 \quad 0 \quad -1]$$

Then the torque can be computed from the dot product of the *CoM* (Table 5.1) vector and the gravity vector

$$\tau_i = weight_i \cdot (CoM_i \times gravity) \quad (i = 1..4) \tag{5.2}$$

where τ_i represents the joint torque of the *i*-th component. If we apply (5.2) to *ExosUpperArm*, *ExosForearm*, *HumanUpperArm* and *HumanForearm,* then the total torque required to counter the effect of gravity on the arm will be the summation of the torques generated by the four previously described components.

Because the springs are located in the rear Diamond Structure and the structure is decoupled from the elbow flexion/extension motion, the springs have no effect on the elbow. Accordingly, the torque (τ) is a three-dimensional vector.

5.5 Converting torques into actuator/spring forces

The force needed to counter-balance BONES using 3 springs in parallel with the cylinders in the Diamond Structure is determined using the Jacobian matrix, J, which relates actuator velocities and joint angle velocities

$$\dot{C} = J\dot{\theta}, \tag{5.3}$$

where *C* represents the cylinder/spring lengths and θ is the joint angle vector defined in 5.3.

Because we are using 3 springs (in parallel with cylinders 1, 3 and 4), we can remove the 2rd row of the original 3x4 Jacobian matrix determined to relate pneumatic cylinder force and joint torques. The Jacobian that relates the spring forces and the joint torques, J_S, will be an invertible 3x3 matrix.

$$F = \left(J_S{}^T\right)^{-1} \cdot \tau \,, \tag{5.4}$$

where F represents the spring force vector and τ represents the joint torque vector.

5.6 Determining the spring constants

In order to determine the spring constant we need to correlate the forces needed and the displacement of the cylinder rod (in parallel with its corresponding spring). So far we have calculated the force required to balance the exoskeleton and the arm for any given position. Now we correlate these forces with the corresponding rod lengths.

The set of arm configurations chosen to linearize the behavior of the spring is a vertical drop of the arm from a 45 degree elevation (θ_2) to a -45 degree position with the elbow flexed 40 degrees (θ_4). The results are shown in Figure 5.1.

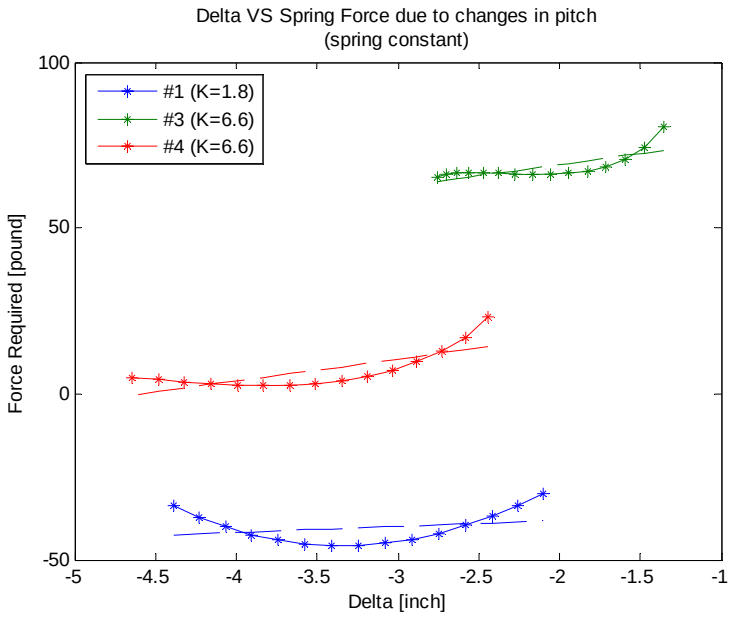

Figure 5.1. Spring constant linearization.

From the results of the initial simulations we observed that the spring placed in parallel with cylinder #1 was working in compression, while the other two were working in tension. In our first implementation of the gravity compensation mechanism, we used only the two tension springs. The mechanical design for this spring mechanism is shown in Figure 5.2. The preliminary experimental data collected from the balance prototype mechanism showed that the weight of the arm and the exoskeleton were greatly reduced for a region neighboring the home position, but the mechanism added high friction between the cables and the flexible cable housing, which reduced significantly the backdriveability of the exoskeleton.

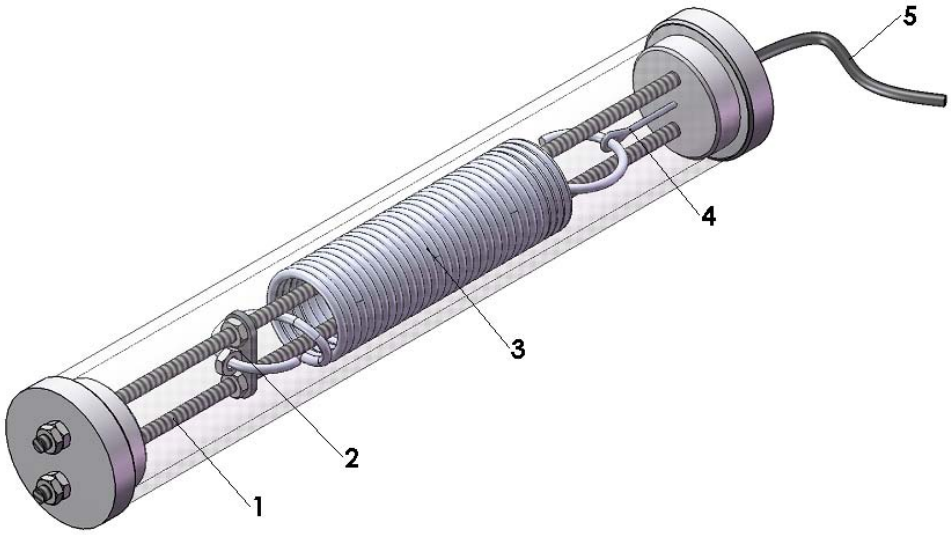

Figure 5.2. Spring compensation mechanism. (1) Threaded rod. (2) Spring tensioner anchor. (3) Spring. (4) Steel cable with thimble. (5) Cable housing with low friction nylon inner layer.

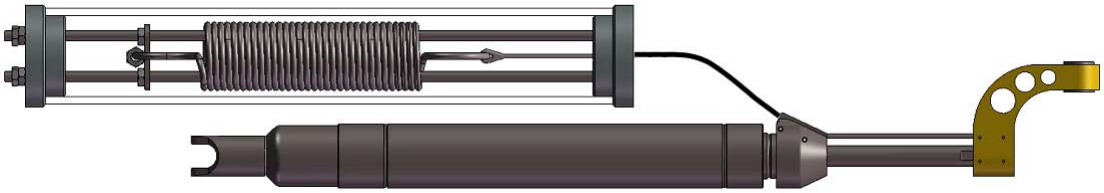

Figure 5.3. Full assembly of the spring compensation mechanism.

Our next goal was to reduce the friction by testing several material combinations of cable/housing. For the final solution, we modified the adapter at the rod end of the cylinder chamber in order to fit two brass inserts designed to eliminate any pinching point for the steel cable. The assembly of this low friction module is shown in Figure 5.4.

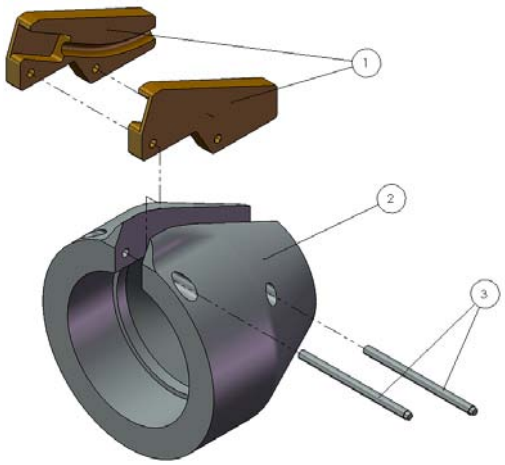

Figure 5.4. Low friction brass inserts. (1) Brass inserts. (2) Pneumatic cylinder adapter. (3) Press fit pins.

Despite our efforts to reduce friction with the brass inserts, drag created by the three spring modules was still offering undesirably high levels of friction. We decided to replace the existing support mechanism with a cable-free alternative. After analyzing the results from the previous solution with 3 springs, we tested several anchor points for a single spring-like element. The final design solution is shown in Figure 5.6. The overall length of the spring (Figure 5.5) was 12in, and its rate was 1.96 lb/inch. Elastomers were covered by a fabric sleeve serving a dual purpose: to prevent damage to the elastic filaments and to prevent injury in the case of filament rupture.

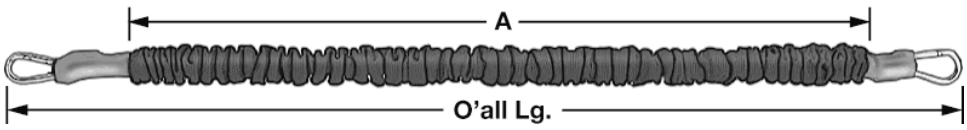

Figure 5.5. Extension spring used for the cable-free design.

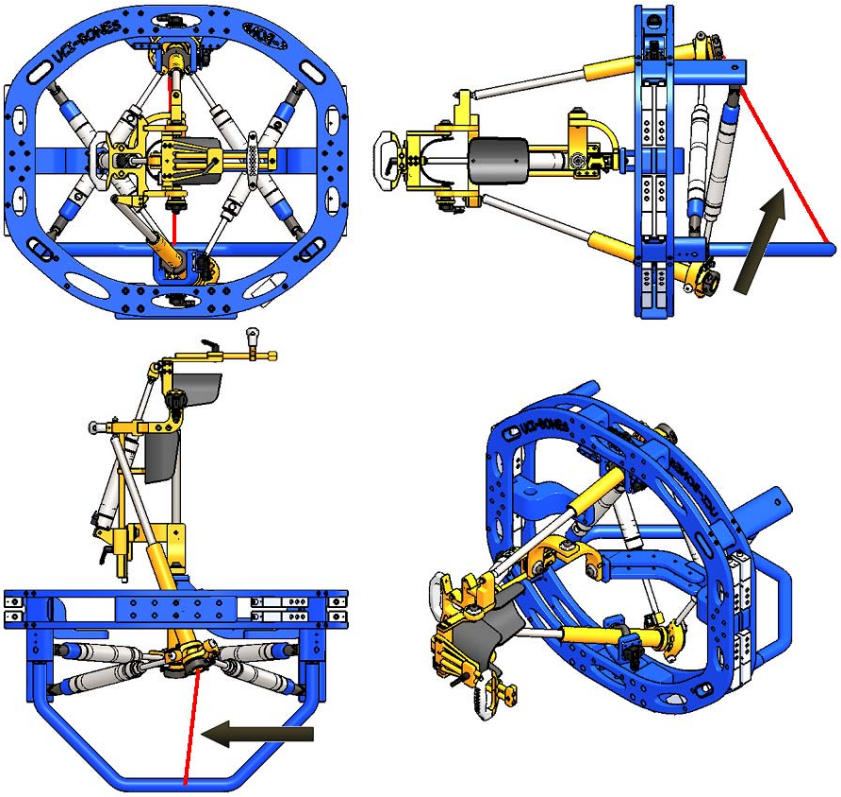

Figure 5.6. New mounted rear bar serves as an anchor point for a spring (marked with an arrow)

5.7 Conclusion

Testing of the counterbalancing mechanism validated the predicted results from Chapter 5.6: the robot remained in equilibrium for a wide range of arm configurations. The parallel springs successfully introduced static equilibrium to relieve the mass of the arm exoskeleton, adding the essential safety feature that prevented the robot from falling on the subject's lap in case of an emergency stop or power failure. Nevertheless, the cable-based parallel spring mechanism introduced large friction forces, reducing the smoothness of the non-balanced arm exoskeleton. Re-evaluation of the counter-balancing mechanism and simplification of compensation design minimized friction while preserving the safety of the robot.

Chapter 6 Learning a multi-joint movement with haptic guidance from BONES: part versus whole training

6.1 Introduction

In this chapter we describe a motor learning experiment intended to answer the question: is it better to learn a multi-joint motor task by performing all of its components synchronously as opposed to learning the single-joint subcomponents sequentially? If so, then multiple-joint devices like BONES and CRAMER are desirable for improving the functional outcome of robot-assisted movement training.

Chapter 4 described BONES, a 4 DOF upper-limb exoskeleton capable of assisting in naturalistic motions of the shoulder and elbow. One of the key motivations for developing BONES was to allow practice of more complex movements, closer to those used in everyday motor functions. Most previously developed robotic therapy devices have a reduced number of degrees of freedom compared to the human arm, and have found limited transfer of learning to functional tasks (Johnson 2006; Kwakkel et al. 2008). We hypothesize that practicing multi-

joint movements will improve transfer of learning to functional tasks, as most functional tasks require multi-joint synergies.

Taking advantage of the robot's compliance, large range of motion and high force capability, the experiment described in this section tested normal motor learning mechanisms during learning of a motor task that requires coordinated shoulder and elbow motions. Our goal was to understand whether learning several single-joint motions independently through haptic demonstration indeed has an inferior training effect compared to learning the same task by practicing with all the joints simultaneously, i.e. is it better to learn a complex arm motion by practicing the whole movement, rather than by learning the individual joint motions that compose it? If so, robotic devices aimed at functional rehabilitation should be capable of producing multi-joint complex motions (like BONES) in order to maximize the benefit of the rehabilitation process (or minimize its overall duration), assuming the rehabilitation process relies in large extent on normal motor learning mechanisms.

6.2 Overview

There have been several previous studies on what is called "part-whole transfer" in the motor learning literature (Brydges et al. 2007; Dubrowski et al. 2005; Hansen et al. 2005; Hommel et al. 2001; Klapp et al. 1987; Schmidt and Lee 1998; Swinnen et al. 1988; Wenderoth et al. 2003). Most of these studies have examined sequence learning, which refers to motor tasks that require the performance of a sequence of independent movements. Practicing parts of a sequence can improve performance on the whole task, but, practicing the whole sequence is typically more effective (Briggs and Brogden 1954; Kurtz and Lee 2003). However, when coordination between parts

is not a key element, part-practice training can sometimes have more beneficial results towards the whole task if compared to whole training (Mané 1984).

There has been less research examining part-whole transfer in tasks that require simultaneous coordination of multiple joints, also referred to as 'continuous tasks' (Schmidt and Lee 1998), which are the most common types of tasks used in rehabilitation. For a continuous task that requires coordination between its individual components (such as arm stroke, kicking and breathing involved in swimming), practicing this task by breaking it down into individual components will not be as effective as practicing this task as a whole due to the fact that, even if individual components are learned, the subject still must learn how to coordinate the individual components (Schmidt and Lee 1998). Other research suggests that the extent to which coordination is involved in a complex task (an extreme example being piloting a helicopter during liftoff, where 4 separate controls must be operated simultaneously) is directly related to the importance of training the task as a whole (Zavala et al. 1965). Nevertheless, practice of individual elements of a complex task can transfer to the overall task, even though practice of the complex task is usually more effective (Briggs and Waters 1958).

6.3 Experimental Method

6.3.1 Motor Task

The desired motion was a complex synergy of shoulder elevation, internal/external rotation, abduction/adduction and elbow flexion/extension. We define this synergetic movement as $S(t) = [\theta_1(t) \quad \theta_2(t) \quad \theta_3(t) \quad \theta_4(t)]$, with θ_1, θ_2,

θ_3 and θ_4 described in Figure 4.7. An example of the trajectory S is shown in Figure 6.1. The task assigned to the subject was to follow this trajectory using the 4 DOF of the upper limb. We decompose S into 4 single-joint components $C_1 = [\theta_1(t) \quad 0 \quad 0 \quad 0]$, $C_2 = [0 \quad \theta_2(t) \quad 0 \quad 0]$, $C_3 = \begin{bmatrix} 0 & 0 & \theta_3(t) & 0 \end{bmatrix}$, and $C_4 = \begin{bmatrix} 0 & 0 & 0 & \theta_4(t) \end{bmatrix}$. To present S and its components to the subject, subjects were comfortably seated and their arm strapped to the robot. BONES was programmed to compliantly assist the subject's arm in moving along the desired trajectory using a previously-developed adaptive controller (Wolbrecht 2007). The subject was instructed to try to follow along with the robot motion trying to predict the movement. In other words, the robot haptically guided the subject's arm through the desired trajectory during training. The subject was instructed to try to follow along with the robot during this haptic training, and also could watch the movement of their arm. During testing, the robot was put in backdrive mode, and provided no assistance for moving.

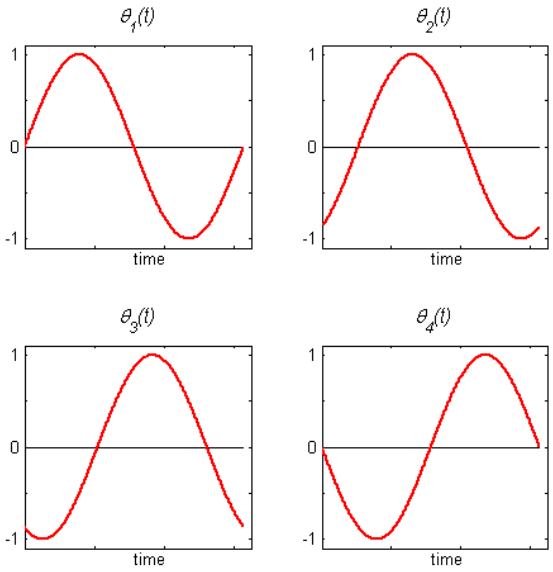

Figure 6.1. Example of multi-joint task. Each joint follows a sinusoidal wave with a different phase delay.

6.3.2 Hypothesis

When a whole motion or component was presented to a subject as a desired trajectory by the robot, the subject learned a corresponding force pattern u with his or her arm. This force pattern was later applied by the subject to move the robot in zero-force control mode, producing a tracking error e.

Our hypothesis was that "whole" training would be more effective in reducing the overall tracking error. Transfer of individual components into a synergistic motion is harder than learning the motion as whole, therefore, the part-whole learning transfer process is non-linear, and multiple-joint practice is better.

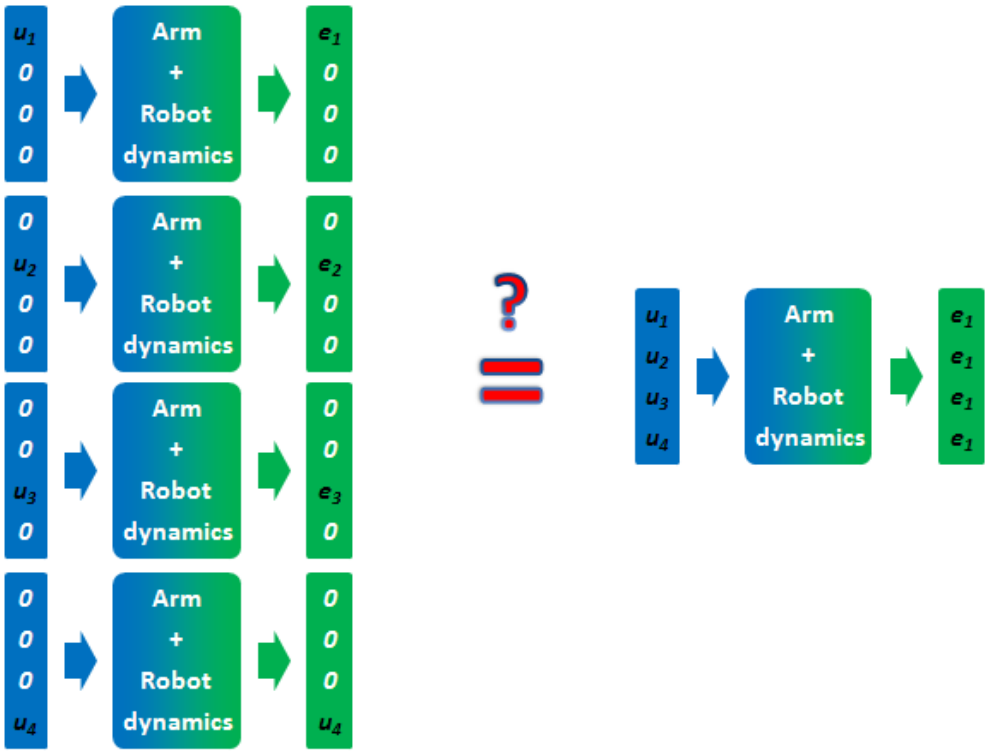

Figure 6.2. Part training VS Whole training. We hypothesized that learning to perform a task by training its individual joint components would not be as efficient as training the complex task using all the involved joints simultaneously.

6.3.3 Experimental Protocol

Four healthy adult volunteers performed two different motor tasks (S_1 and S_2) with BONES involving three degrees of freedom of shoulder movement and one degree of freedom of elbow movement. The four components of S_i are noted as $C_{i,1}, C_{i,2}, C_{i,3}$ and $C_{i,4}$ (for $i = 1, 2$), as described in Section 6.3.1. The actual values for the two motions used during the experiment, are shown in Figure 6.3.

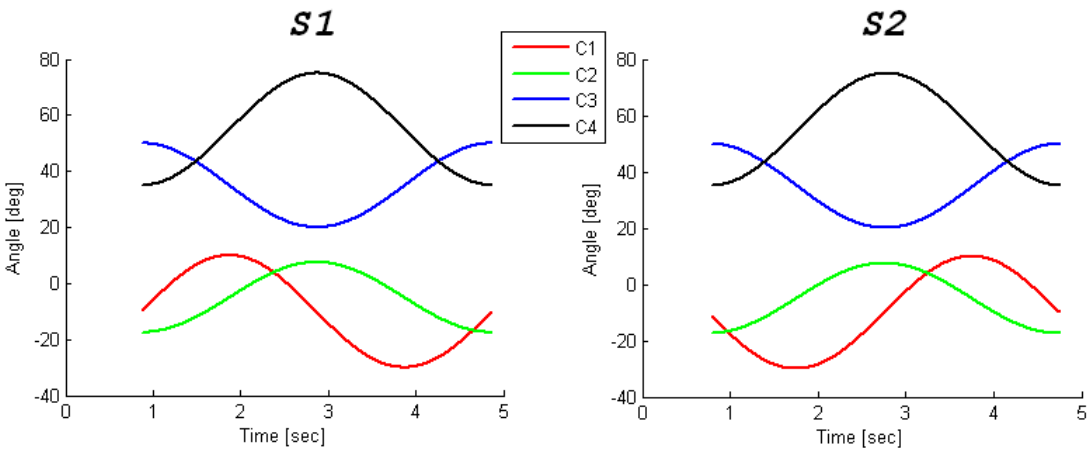

Figure 6.3. Components for motions S1 and S2, showing amplitude, delay, frequency and bias values used during experiment

During Phase I, each subject trained one of the two motions according to the "part" or "whole" approach. Later, in Phase II, subjects trained the remaining motion following the alternative strategy. For both strategies, an initial visual and acoustical cue was presented to the subjects so they could learn to synchronize their movements with respect to the starting signal. It has been shown that cues can help develop an implicit memory of action with a particular body part (Krakauer et al. 2006). No visual feedback was provided during assisted or unassisted motions. As suggested in the literature, reducing the proportion of trials for which information regarding results or performance is provided can result in more effective learning (Schmidt et al. 1990; Schmidt and Wulf 1997; Winstein and Schmidt 1990; Wulf and Shea 2002; Yao et al. 1994). More specifically, it has been suggested that providing performance summaries every fifth trial during a simulated batting exercise was more beneficial than providing performance summaries after every repetition (Schmidt and Wulf 1997). Furthermore, outcomes from the same study showed that delaying the

feedback for a few seconds was more effective learning than presenting immediate feedback. In this experiment, the only real-time feedback received by the subjects was the force pattern generated by the robot. A performance score was displayed after every non-assisted motion, but no information regarding performance was given to the subjects during the training trials (Winstein and Schmidt 1990; Wulf and Shea 2002). The measured outcome was the tracking error during the non-assisted repetitions. Subjects were instructed to focus on predicting the movements of the robot instead of focusing exclusively on their own body part movements. Some studies suggest that external-focus instructions enhance the effectiveness of practice sessions (Kelso 1995; Riley et al. 1999; Wulf et al. 1998; Wulf et al. 1999).

The order in which subjects trained "whole" or "part" and the motion used for each learning strategy were randomized: some subjects trained S_1 as "whole" and later trained S_2 as "part", other subjects trained S_2 as "whole" and then S_1 as "part".

The resulting training sequence in Phase I and Phase II for each subject is summarized in Table 6.1 and Table 6.2. In the tables we represent a movement set, characterized by 4 training repetitions followed by an assessment test. During each phase, subjects would repeat each set 15 times. When subjects trained a motion according to the "whole" approach, the robot would assist the whole motion 4 times. Afterwards, subjects would repeat the "whole" motion without assistance. This sequence would be repeated 15 times. In the case of "part" training, the robot would show each component sequentially (in randomized order) four times. After a total of 16 individual movements, the subjects would perform the "whole" unassisted strategy. The total number of movements for each joint was the same for each

training approach; consequently, the overall time of the "part" training was 4 times longer than that of the "whole" strategy.

TABLE 6.1. EXPERIMENTAL PROTOCOL: PHASE I

Subject	Training (repetitions)	Test
1	S_1 - whole (x4)	S_1 - whole
2	S_1 - part (x4)	S_1 - whole
3	S_2 - whole (x4)	S_2 - whole
4	S_2 - part (x4)	S_2 - whole

TABLE 6.2. EXPERIMENTAL PROTOCOL: PHASE II

Subject	Training (repetitions)	Test
1	S_2 - part (x4)	S_2 - whole
2	S_2 - whole (x4)	S_2 - whole
3	S_1 - part (x4)	S_1 - whole
4	S_1 - whole (x4)	S_1 - whole

After each phase, the subject's performance was characterized by a sequence of 15 scores, corresponding to the tracking error RMS for all four joint angles.

One week later, all subjects were asked to repeat the protocol in order to assess any learning retention.

6.3.4 Data Analysis

For each subject, we recorded their performance during each assessment trial (15 trials for each learning strategy). We calculated the RMS of the tracking error using the following equation

$$Score = \sqrt{\sum_{i=1}^{4}\left(\theta_i(t) - \hat{\theta}_i(t)\right)^2}\,, \tag{6.1}$$

where θ_i is the desired joint angle as a function of time, and $\hat{\theta}_i$ is the measured joint angle.

In order to value synchronization relative to each joint as opposed to synchronization with respect to time, we shifted each assessment trial. Using the maximal score as the cost function, the optimization of the phase delay can be expressed as

$$Score = \sqrt{\sum_{i=1}^{4}\left(\theta_i(t) - \hat{\theta}_i(t+d)\right)^2}\,, \tag{6.2}$$

where d is the phase delay for the measured joints. The delay was applied to all four components simultaneously. The increment step used for d was one millisecond, corresponding to the sampling period of our A/D acquisition hardware. A comparison between a subject's performance before and after applying the phase optimization is shown in Figure 6.4.

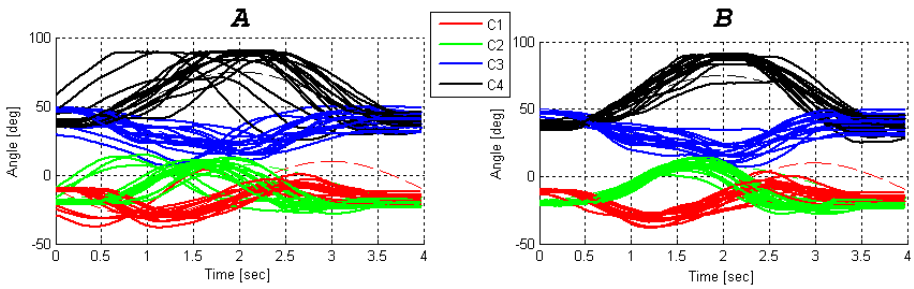

Figure 6.4. Original data (left), data after applying phase shifting optimization (right)

6.4 Results

An example of a subject's Phase I and Phase II results is shown in Figure 6.5.

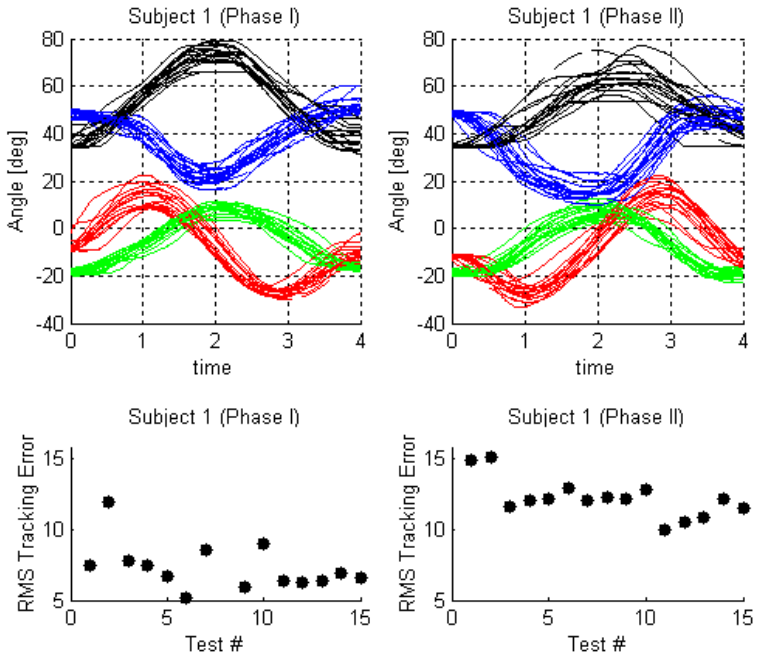

Figure 6.5. Data collection sample. Performance of a subject during Phase I (upper left) and Phase II (upper right). Score [deg] of each assessment trial during Phase I (lower left) and Phase II (lower right)

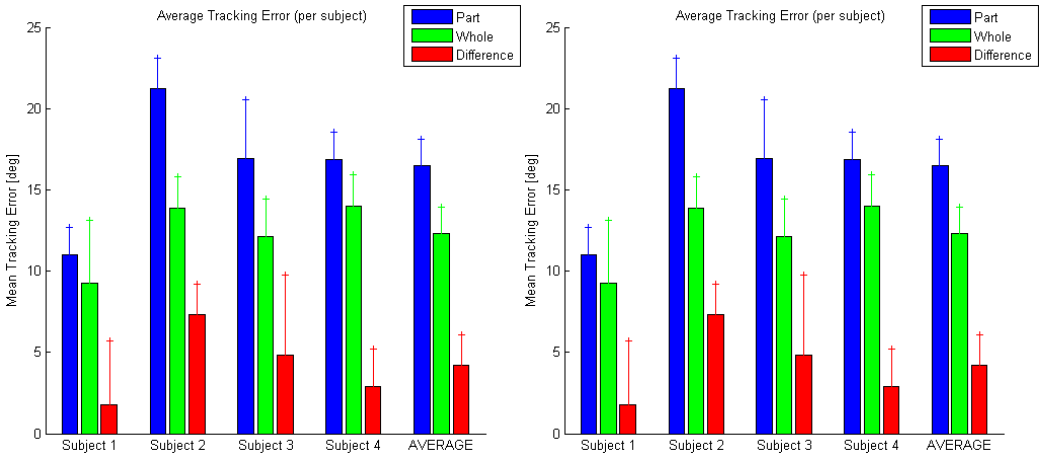

Figure 6.6. Overall performance (per subject) while training "part" and "whole" (left), and performance during assessment test, one week later (right)

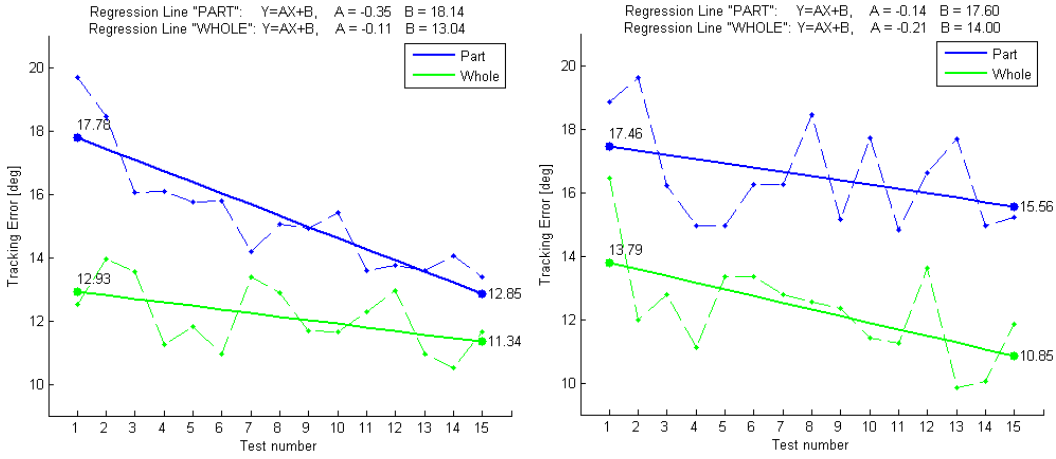

Figure 6.7. Regression lines of the overall scores as a function of test number (across tests, for all subjects) for each training strategy on the first training day (left) Regression lines for the retention test results, one week later (right)

The slope of the regression line (Figure 6.7) was negative in all cases, showing a significant learning rate. The difference between the two slopes was significantly different during the first day. One week later, during the retention test, slopes were not significantly different. Overall, "whole" training helped the participants to learn the trajectory significantly better than "part" training. The first score obtained by the

"whole" training subjects during the first day was significantly lower than the first "part" training score (t-test, $p = 0.04$). The last score with both learning strategies was not significantly different (t-test, $p = 0.26$). One week later, during the retention assessment, no significant differences were found for the first score (t-test, $p = 0.50$). Nevertheless, the last test was significantly better for "whole" compared to "part" (t-test, $p = 0.04$). A summary of the score values for both training strategies, and their differences can be found in Table 6.3, Table 6.4 and Table 6.5

TABLE 6.3. EXPERIMENTAL PROTOCOL RESULTS: SCORES [IN] (STANDARD DEVIATION)

	Day 1 (Std. Dev.)	One week later (Std. Dev.)
Overall Score (part)	15.3 (1.8)	16.5 (1.6)
Overall Score (whole)	12.1 (1.0)	12.3 (1.6)
First Score (part)	19.7 (4.2)	18.8 (4.3)
First Score (whole)	12.5 (3.8)	16.5 (3.3)
Last Score (part)	13.1 (1.4)	15.2 (3.9)
Last Score (whole)	11.6 (3.7)	11.8 (3.7)

TABLE 6.4. EXPERIMENTAL PROTOCOL RESULTS: SCORE DIFFERENCES [IN] (STANDARD DEVIATION)

	Day 1	One week later
Overall Score (difference)	3.2 (1.7)*	4.19 (1.9)*
First Score (difference)	7.2 (4.0)*	2.4 (6.3)
Last Score (difference)	1.7 (2.5)	3.3 (1.8)*

(*) significant with $p<0.05$. All differences are calculated as "part" – "whole"

TABLE 6.5. EXPERIMENTAL PROTOCOL RESULTS: REGRESSION LINES SLOPES [IN/TEST#]

	Day 1	One week later
Slope (part)	-0.35*	-0.13
Slope (whole)	-0.11	-0.21*
Slope (difference)	-0.23*	+0.17

(*) significant with $p<0.05$. All differences are calculated as "part" – "whole"

6.5 Summary

To our surprise and despite the complexity of the motor task, subjects were able to learn by training individual parts and later summing their effects into a synchronous motion. Nevertheless, whole-trained subjects had lower error across all trials (performance in "part" training was always about 5 degrees worse than "whole" training). If we compare learning over time, instead of over test number, whole training was not only more effective in producing lower errors, but caused the subjects to progress faster: the slope was steeper and the last score was better (lower) than part training. Figure 6.8 shows this time transformation. If we compare scores over time statistically, the new slope of the "part" is not significantly different from the "whole" slope (unaltered by the time transformation). We observed that both slopes are similar, indicating a similar learning rate.

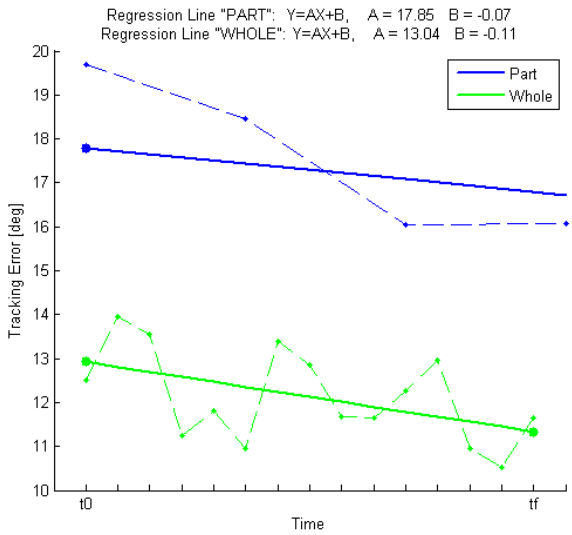

Figure 6.8. Regression lines of the overall scores as a function of time (across tests, for all subjects) for each training strategy

6.6 Conclusion

BONES proved to be an excellent tool for complex motion generation, which is desirable for providing a more efficient rehabilitation for impaired subjects who need to train the movements involved in the activities of daily living.

Subjects who trained by parts had to conceptually sum the individual trajectories for each single joint motion, while whole trained subjects didn't require this summation process solve the synergistic movement. Motion planning should be more effective if it is planned in terms of the overall intended outcome ("whole" motion), rather than in terms of the specific movement patterns (Prinz 1997). Nevertheless, "part" training provided information about the individual components in greater detail, such as range of motion for each movement. Because we were measuring overall tracking error accuracy, synchronization was a key factor in reducing the error. Information on motion components synchronization is transmitted more

effectively when subjects train the motion as a whole, yet individual motion detail may be learned more efficiently when training the motion as a part. This suggests that while whole training is the faster way for a person to conceptually grasp and begin to perform a complex movement, mixing some amount of part training into whole training may help people to more effectively tune the individual joint movements that comprise the whole.

Chapter 7 Summary of Contributions and Future Work

7.1 Summary of Contributions

This thesis describes the development and testing of three mechanisms that assist in the motion of the human arm. The primary contributions resulting from the development of these devices are described in the following sections.

7.1.1 Dynamic arm rest to assist in driving

We developed a spring-loaded, passive arm rest that moves up and down with the driver's forearm, allowing the driver to grasp the steering wheel in the recommended location while still receiving weight support for the arm. Using a driving simulator that mimicked driving on highways, we found that young adult drivers significantly reduced their hand grasp pressure by about 30% and their steering error by about 5~10%. These results demonstrated that incorporation of a dynamic arm rest into an automobile might improve driving ergonomics and safety.

During testing we observed some practical problems with the dynamic arm rest design. The clearance between the arm-machine contact surface and the lowest

element of the supporting structure needs to be optimized in order to reduce the interference with the driver's leg. Another issue is that if the driver executes a large turn (e.g. hand-over-hand turn), the arm may lose contact with the arm rest, which can then freely rotate to either side. This issue might be ameliorated by replacing the manually adjustable pre-load of the inner elastic element with a controlled motor that automatically retracts the arm rest into a standard arm rest position if the driver's arm loses contact with it. Such a mechatronic feature could also be used to automatically configure the weight support level for each driver.

7.1.2 CRAMER

We developed a novel, low-cost forearm and wrist rehabilitation mechanism that accommodates much of the natural range of motion of the three degrees of freedom of the human wrist and forearm. This Closed-chain Robot for Assisting in Manual Exercise and Rehabilitation (CRAMER) is a lightweight 3 DOF parallel mechanism actuated by 4 small, yet powerful, servomotors. The inspiration for the design of CRAMER was the motion of the Ulna and the Radius bones while prescribing the unique and complex motion of forearm pro/supination. A colleague integrated a Nintendo Wii remote into CRAMER in order to allow patients to play the motion-based games developed for the Wii, demonstrated the potential utility of this device for distal extremity rehabilitation.

7.1.3 BONES

The third mechanism presented in this dissertation was BONES (Biomimetic Orthosis for the Neurorehabilitation of the Elbow and Shoulder). We presented the

design and kinematic analysis of this novel 4 DOF pneumatically-actuated upper-limb rehabilitation robot. The device was able to assist the human arm in a wide range of motion, while also achieving low inertia and direct-drive force generation capability at the shoulder. A key accomplishment of this design was the ability to generate arm internal/external rotation without any circular bearing element such as a ring, a design feature again inspired by the biomechanics of the human forearm.

We also introduced a spring-based counterbalancing mechanism that introduced static equilibrium to relieve the mass of the arm exoskeleton, adding the essential safety feature that prevented the robot from falling onto the subject's lap in case of an emergency stop or power failure. However, the initial cable-based counterbalancing solution introduced large friction forces, reducing the smoothness of the non-balanced arm exoskeleton. Re-evaluation of the counter-balancing mechanism and simplification of compensation design minimized the friction while preserving the safety of the robot.

Important design goals for BONES were that it be capable of quantifying recovery of human movement ability of the four main joints of the human arm following rehabilitation exercise, and that it maximize motor learning during rehabilitation exercise by allowing functional movement practice. To validate these goals, we designed and implemented a motor learning experiment with healthy subjects. In this experiment we used BONES to assess whether motor learning of functional movement is improved by allowing practice of more functional movement. The hypothesis was that practicing an integrated, multi-joint movement improved movement ability more than practicing a matched amount of the isolated components

of the integrated movement. The results of this experiment proved BONES to be an excellent tool for complex motion generation, and showed that training of complex movements is more efficient when training the whole motion rather than the parts. However, unexpectedly, people can begin to learn a complex movement by experiencing only its parts.

7.2 Future Work

Important directions for future work are as follows.

7.2.1 Dynamic arm rest to assist in driving

The design of the arm support can be improved in order to reduce potential collision with driver's body. Safety features such as an emergency locking device could be implemented and synchronized to the airbag triggering signal in order to fold the arm rest during a collision, thus preventing potential injury caused by the device.

It is unclear how the dynamic arm rest would affect city-type driving, in which right angle turns are frequently made, and these driving conditions should be studied. Additionally, we only tested driving with one hand, therefore future research should examine how driving with two hands and two arm rests compares to driving with two hands and no arm rest, or driving with one hand.

7.2.2 CRAMER

Future work on CRAMER should be focused on the possibility of making the device wearable, and on incorporating alternative actuators in order to generate higher torques, so the device is strong enough to assist patients with abnormal,

elevated tone. Implementation of force control on CRAMER would improve the device's backdriveability.

7.2.3 BONES

The design of BONES can be improved in order to reduce the overall weight of the exoskeletal structure. Feedback from therapists has indicated the need for a simpler and faster mechanism to adjust arm length.

To use the mechanical capabilities of BONES at its maximum potential, a graphical user interface needs to be implemented. Such software should include engaging games for stroke patients that also make use of the wide range of motion of the robot.

A follow-up on motor learning experiments with a larger sample size is needed to assess the significance of our study. According to our results, learning a complex task as a "whole" was more efficient than training its individual movements. Nevertheless, subjects were able to sum the individual effects of the motion subcomponents into one synchronous movement. Future experiments should include testing of a combination of "part" and "whole". A combination of both training techniques might be the most effective way of learning, with whole training useful for quickly giving the trainee the overall concept of the movement, but part training useful for working on appropriate range of motion for individual joints, when the trainee persists in making systematic errors during the whole trajectory.

BONES provides the ability to implement a wide variety of force assistance algorithms for rehabilitation training after stroke, such as assisting, resisting, and perturbing naturalistic arm movements. Clinical testing with BONES should evaluate

whether these modes are differentially beneficial for provoking neuroplasticity after stroke. BONES will also allow a rigorous test of whether functional transfer of robotic therapy is improved by practicing more naturalistic movements.

BIBLIOGRAPHY

Adelstein BD. Three degree of freedom parallel mechanical linkage. USA: The United States of America as represented by the Administrator of the, 1998.

Anstey KJ, Wood J, Lord S, and Walker JG. Cognitive, sensory and physical factors enabling driving safety in older adults. *Clinical Psychology Review* 25: 45-65, 2005.

Ball SJ, Brown IE, and Scott SH. A planar 3DOF robotic exoskeleton for rehabilitation and assessment. In: *Engineering in Medicine and Biology Society, 2007 EMBS 2007 29th Annual International Conference of the IEEE*2007, p. 4024-4027.

Bergamasco M, Allotta B, Bosio L, Ferretti L, Parrini G, Prisco GM, Salsedo F, and Sartini G. An arm exoskeleton system for teleoperation and virtual environments applications. In: *Robotics and Automation, 1994 Proceedings, 1994 IEEE International Conference on*1994, p. 1449-1454 vol.1442.

Brenneman SK. Use of the Stroke Recovery of Activities of Daily Living and Mobility (RAM) Index for prediction of outcome. Philadelphia: University of Pennsylvania, 2000.

Brewer B, McDowell SK, and Worther-Chaudhari LC. Poststroke Upper Extremity Rehabilitation: A Review of Robotic Systems and Clinical Results. *Topics in Stroke Rehabilitation* 14: 22-44, 2007.

Briggs GE, and Brogden WJ. The effect of component practice on performance of a lever-positioning skill. *Journal of Experimental Psychology* 48: 375-380, 1954.

Briggs GE, and Waters LK. Training and transfer as a function of component interaction. *Journal of Experimental Psychology* 56: 492-500, 1958.

Brown J, and Huffman W. Psychophysiological measures of drivers under actual driving conditions. *Journal of Safety Research* 4: 172-178, 1972.

Bryan J, and Luszcz MA. Measurement of Executive Function: Considerations for Detecting Adult Age Differences. *Journal of Clinical and Experimental Neuropsychology (Neuropsychology, Developm* 22: 40-55, 2000.

Brydges R, Carnahan H, Backstein D, and Dubrowski A. Application of motor learning principles to complex surgical tasks: searching for the optimal practice schedule. *Journal of Motor Behavior* 39: 40-48, 2007.

Burgar CG, Lum PS, Shor PC, and Machiel Van der Loos HF. Development of robots for rehabilitation therapy: the Palo Alto VA/Stanford experience. *Journal of Rehabilitation Research & Development* 37: 663-736, 2000.

Carignan C, Liszka M, and Roderick S. Design of an arm exoskeleton with scapula motion for shoulder rehabilitation. In: *Advanced Robotics, 2005 ICAR '05 Proceedings, 12th International Conference on*2005, p. 524-531.

Chakrabarti A, and Abel C. The mobile arm support project: a test-bed for design research at the Cambridge Engineering Design Centre. In: *Engineering in Medicine*

*and Biology Society, 1994 Engineering Advances: New Opportunities for Biomedical Engineers Proceedings of the 16th Annual International Conference of the IEEE*1994, p. 486-487 vol.481.

Charles SK, Krebs HI, Volpe BT, Lynch D, and Hogan N. Wrist rehabilitation following stroke: initial clinical results. In: *Rehabilitation Robotics, 2005 ICORR 2005 9th International Conference on*2005, p. 13-16.

Chiou I-IL, and Burnett CN. Values of Activities of Daily Living: A Survey of Stroke Patients and Their Home Therapists. *Physical Therapy* 65: 901-906, 1985.

Clauser CE, McConville JT, and Young JW. Weight, volume, and center of mass of segments of the human body. edited by Air Force Systems Command. Wright-Patterson Air Force Base, Ohio: 1969.

Coote S, Stokes EK, Murphy BT, and Harwin WS. The effect of GENTLE/s robot mediated therapy on upper extremity function post stroke. In: *Proceedings International Conference on Rehabilitation Robotics* Korea: 2003, p. 59-61.

Denève A, Moughamir S, Afilal L, and Zaytoon J. Control system design of a 3-DOF upper limbs rehabilitation robot. *The 6th IFAC Symposium on Modelling and Control in Biomedical Systems* 89: 202-214, 2008.

Dewald JPA, and Beer RF. Abnormal joint torque patterns in the paretic upper limb of subjects with hemiparesis. *Muscle & Nerve* 24: 273-283, 2001.

Dubrowski A, Backstein D, Abughaduma R, Leidl D, and Carnahan H. The influence of practice schedules in the learning of a complex bone-plating surgical task. *American Journal of Surgery* 190: 359-363, 2005.

Emken JL, Benitez R, Sideris A, Bobrow JE, and Reinkensmeyer DJ. Motor Adaptation as a Greedy Optimization of Error and Effort. *Journal of Neurophysiology* 97: 3997-4006, 2007.

Frisoli A, Borelli L, Montagner A, Marcheschi S, Procopio C, Salsedo F, Bergamasco M, Carboncini MC, Tolaini M, and Rossi B. Arm rehabilitation with a robotic exoskeleleton in Virtual Reality. In: *Rehabilitation Robotics, 2007 ICORR 2007 IEEE 10th International Conference on*2007, p. 631-642.

Frisoli A, Rocchi F, Marcheschi S, Dettori A, Salsedo F, and Bergamasco M. A new force-feedback arm exoskeleton for haptic interaction in virtual environments. In: *Eurohaptics Conference, 2005 and Symposium on Haptic Interfaces for Virtual Environment and Teleoperator Systems, 2005 World Haptics 2005 First Joint*2005, p. 195-201.

Fugl-Meyer A, Jääsko L, Leyman I, Olsson S, and Steglind S. The post-stroke hemiplegic patient. 1: a method for evaluation of physical performance. *Scand J Rehabil Med* 7: 13-31, 1975.

Giszter SF. Spinal Cord Injury: Present and Future Therapeutic Devices and Prostheses. *Neurotherapeutics* 5: 147-162, 2008.

Gopura RARC, and Kiguchi K. Development of an exoskeleton robot for human wrist and forearm motion assist. In: *Industrial and Information Systems, 2007 ICIIS 2007 International Conference on*2007, p. 535-540.

Gosman-Hedström G, Claesson L, and Blomstrand C. Consequences of severity at stroke onset for health-related quality of life (HRQL) and informal care: A 1-year follow-up in elderly stroke survivors. *Archives of Gerontology and Geriatrics* 47: 79-91, 2008.

Greenshields B, and Plat F. Developement of a method of predicting high accident and high violation drivers. *Journal of Applied Psychology* 55: 205-210, 1967.

Grinstead J. Driving School Presentation. edited by Northern California Racing2007.

Gupta A, and O'Malley MK. Design of a haptic arm exoskeleton for training and rehabilitation. In: *Mechatronics, IEEE/ASME Transactions on*2006, p. 280-289.

Hansen S, Tremblay L, and Elliott D. Part and Whole Practice: Chunking and Online Control in the Acquisition of a Serial Motor Task. *Research Quarterly for Exercise and Sport* 76: 60-66, 2005.

Harris CM, and Wolpert DM. Signal-dependent noise determines motor planning. *Nature* 394: 780-784, 1998.

He J, Koeneman EJ, Schultz RS, Herring DE, Wanberg J, Huang H, Sugar T, Herman R, and Koeneman JB. RUPERT: a Device for Robotic Upper Extremity Repetitive Therapy. In: *Engineering in Medicine and Biology Society, 2005 IEEE-EMBS 2005 27th Annual International Conference of the*, edited by Koeneman EJ2005, p. 6844-6847.

Herder JL. Development of a statically balanced arm support: ARMON. In: *Rehabilitation Robotics, 2005 ICORR 2005 9th International Conference on*2005, p. 281-286.

Herder JL, Vrijlandt N, Antonides T, Cloosterman M, and Mastenbroek PL. Principle and design of a mobile arm support for people with muscular weakness. *Journal of Rehabilitation Research & Development* 43: 591-604, 2006.

Hesse S, Schulte-Tigges G, Konrad M, Bardeleben A, and Werner C. Robot-assisted arm trainer for the passive and active practice of bilateral forearm and wrist movements in hemiparetic subjects. *Archives of Physical Medicine and Rehabilitation* 84: 915-920, 2003.

Hesse S, Werner C, Pohl M, Rueckriem S, Mehrholz J, and Lingnau ML. Computerized Arm Training Improves the Motor Control of the Severely Affected Arm After Stroke: A Single-Blinded Randomized Trial in Two Centers. *Stroke* 36: 1960-1966, 2005.

Hogan N, Krebs H, Sharon A, and Charnnarong J. Interactive Robot Therapist. Massachusetts Institute of Technology, 1995.

Hommel B, Müsseler J, Aschersleben G, and Prinz W. The Theory of Event Coding (TEC): A framework for perception and action planning. *Behavioral and Brain Sciences* 5: 849-878, 2001.

Housman SJ, Le V, Rahman T, Sanchez RJ, and Reinkensmeyer DJ. Arm-Training with T-WREX After Chronic Stroke: Preliminary Results of a Randomized Controlled Trial. In: *Rehabilitation Robotics, 2007 ICORR 2007 IEEE 10th International Conference on*2007, p. 562-568.

Hu XL, Tong KY, Song R, Zheng XJ, Lui KH, Leung WWF, Ng S, and Au-Yeung SSY. Quantitative evaluation of motor functional recovery process in chronic stroke patients during robot-assisted wrist training. *Journal of Electromyography and Kinesiology* In Press, Corrected Proof.

Hurmuzlu Y, Ephanov A, and Stoianovici D. Effect of a Pneumatically Driven Haptic Interface on the Perceptional Capabilities of Human Operators. *Presence: Teleoperators & Virtual Environments* 7: 290-307, 1998.

Jackson A, Culmer P, Makower S, Levesley M, Richardson R, Cozens A, Williams MM, and Bhakta B. Initial patient testing of iPAM - a robotic system for Stroke rehabilitation. In: *Rehabilitation Robotics, 2007 ICORR 2007 IEEE 10th International Conference on*, edited by Culmer P2007, p. 250-256.

JAECO. Wilmington Robotic Exoskeleton. edited by Orthopedic J2007.

Jan Nijhof E, and Gabriel DA. Maximum isometric arm forces in the horizontal plane. *Journal of Biomechanics* 39: 708-716, 2006.

Jiping H, Koeneman EJ, Schultz RS, Huang H, Wanberg J, Herring DE, Sugar T, Herman R, and Koeneman JB. Design of a robotic upper extremity repetitive therapy device. In: *Rehabilitation Robotics, 2005 ICORR 2005 9th International Conference on*2005, p. 95-98.

Johnson M. Recent trends in robot-assisted therapy environments to improve real-life functional performance after stroke. *Journal of NeuroEngineering and Rehabilitation* 3: 29, 2006.

Kahn L, Zygman M, Rymer WZ, and Reinkensmeyer D. Robot-assisted reaching exercise promotes arm movement recovery in chronic hemiparetic stroke: a randomized controlled pilot study. *Journal of NeuroEngineering and Rehabilitation* 3: 12, 2006.

Kang T, He J, and Tillery S. Determining natural arm configuration along a reaching trajectory. *Experimental Brain Research* 167: 352-361, 2005.

Kecskeméthy A, and Weinberg A. An Improved Elasto-Kinematic Model of the Human Forearm for Biofidelic Medical Diagnosis. *Multibody System Dynamics* 14: 1-21, 2005.

Kelso JAS. *Dynamic patterns : the self-organization of brain and behavior*. Cambridge, Mass.: MIT Press,, 1995, p. 334.

Kikuchi T, Furusho J, Oda K, Ying J, Chengqiu L, Morita T, Shichi N, Ohyama Y, and Inoue A. Development of a 6-DOF Rehabilitation Robot and its Software for

Clinical Evaluation Based on Virtual Reality. In: *Complex Medical Engineering, 2007 CME 2007 IEEE/ICME International Conference on*2007, p. 1285-1288.

Klapp ST, Martin ZE, McMillan GG, and Brock DT. Whole-task and part-task training in dual motor tasks. In: *Ergonomics and Human Factors*, edited by L. S. Mark JSWRLH. New York: Springer-Verlag, 1987, p. 125-130.

Koeneman EJ, Schultz RS, Wolf SL, Herring DE, and Koeneman JB. A pneumatic muscle hand therapy device. In: *Engineering in Medicine and Biology Society, 2004 IEMBS '04 26th Annual International Conference of the IEEE*2004, p. 2711-2713 Vol.2714.

Krakauer JW, Mazzoni P, Ghazizadeh A, Ravindran R, and Shadmehr R. Generalization of Motor Learning Depends on the History of Prior Action. *PLoS Biology* 4: e316, 2006.

Kramer G, Romer GRB, and Stuyt HJA. Design of a Dynamic Arm Support (DAS) for gravity compensation. In: *Rehabilitation Robotics, 2007 ICORR 2007 IEEE 10th International Conference on*2007, p. 1042-1048.

Krebs HI, Hogan N, Aisen ML, and Volpe BT. Robot-aided neurorehabilitation. *Rehabilitation Engineering, IEEE Transactions on [see also IEEE Trans on Neural Systems and Rehabilitation]* 6: 75-87, 1998.

Krebs HI, Volpe BT, Williams D, Celestino J, Charles SK, Lynch D, and Hogan N. Robot-Aided Neurorehabilitation: A Robot for Wrist Rehabilitation. *Neural Systems and Rehabilitation Engineering, IEEE Transactions on* 15: 327-335, 2007.

Kurtz S, and Lee TD. Part and whole perceptual-motor practice of a polyrhythm. *Neuroscience Letters* 338: 205-208, 2003.

Kwakkel G, Kollen BJ, and Krebs HI. Effects of Robot-Assisted Therapy on Upper Limb Recovery After Stroke: A Systematic Review. *Neurorehabilitation and Neural Repair* 22: 111-121, 2008.

Kwakkel G, van Peppen R, Wagenaar RC, Wood Dauphinee S, Richards C, Ashburn A, Miller K, Lincoln N, Partridge C, Wellwood I, and Langhorne P. Effects of Augmented Exercise Therapy Time After Stroke: A Meta-Analysis. *Stroke* 35: 2529-2539, 2004.

Land Transport Safety Authority. Motor Vehicle Crashes in New Zealand. edited by New Zealand Ministry of Transport2005.

Lehrer J. Drive this way. In: *American Automobile Association - Westways*2007.

Li-Qun Z, Hyung-Soon P, and Yupeng R. Developing an Intelligent Robotic Arm for Stroke Rehabilitation. In: *Rehabilitation Robotics, 2007 ICORR 2007 IEEE 10th International Conference on*2007, p. 984-993.

Llaneras RE, Swezey RW, Brock JF, Rogers WC, and Van Cott HP. Enhancing the safe driving performance of older commercial vehicle drivers. *International Journal of Industrial Ergonomics* 22: 217-245, 1998.

Long D. Hands on the steering wheel: 10 and 2 oclock is not the rule. Wisconsin Department of Transportation, 2004, p. 7.

Lord SR, Sherrington C, and Menz HB. *Ageing and society*. Cambridge: Cambridge University Press, 2007, p. 249.

Loureiro R, Amirabdollahian F, Topping M, Driessen B, and Harwin W. Upper Limb Robot Mediated Stroke Therapy—GENTLE/s Approach. *Autonomous Robots* 15: 35-51, 2003.

Lum PS, Burgar CG, Shor PC, Majmundar M, and Van der Loos M. Robot-assisted movement training compared with conventional therapy techniques for the rehabilitation of upper-limb motor function after stroke. *Archives of Physical Medicine and Rehabilitation* 83: 952-959, 2002.

Lum PS, Burgar CG, Van der Loos M, Shor PC, Majmundar M, and Yap R. The MIME robotic system for upper-limb neuro-rehabilitation: results from a clinical trial in subacute stroke. In: *Rehabilitation Robotics, 2005 ICORR 2005 9th International Conference on*2005, p. 511-514.

Mané AM. Acquisition of perceptual motor skill. In: *Human Factors Society 28th Annual Meeting*. Santa Monica, CA: Human Factors Society, 1984, p. 522-526.

Manitoba Public Insurance. Proper hand position on the steering wheel. 2007.

Mastenbroek B, de Haan E, van den Berg M, and Herder JL. Development of a Mobile Arm Support (Armon): Design Evolution and Preliminary User Experience. In: *Rehabilitation Robotics, 2007 ICORR 2007 IEEE 10th International Conference on*2007, p. 1114-1120.

Mayr A, Kofler M, and Saltuari L. ARMOR: An Electromechanical Robot for Upper Limb Training Following Stroke. A Prospective Randomised Controlled Pilot Study. *Handchir Mikrochir Plast Chir* 40: 66-73, 2008.

Merlet JP. Jacobian, Manipulability, Condition Number, and Accuracy of Parallel Robots. *Journal of mechanical design* 128: 199-206, 2006.

Mihelj M, Nef T, and Riener R. ARMin - Toward a six DoF upper limb rehabilitation robot. In: *Biomedical Robotics and Biomechatronics, 2006 BioRob 2006 The First IEEE/RAS-EMBS International Conference on*, edited by Nef T2006, p. 1154-1159.

Mihelj M, Nef T, and Riener R. ARMin II - 7 DoF rehabilitation robot: mechanics and kinematics. In: *Robotics and Automation, 2007 IEEE International Conference on*2007, p. 4120-4125.

Minnesota Department of Public Safety. Minnesota Drivers Manual. edited by Minnesota Department of Public Safety Driver and Vehicle Services2007.

Mistry M, Mohajerian P, and Schaal S. An exoskeleton robot for human arm movement study. In: *Intelligent Robots and Systems, 2005 (IROS 2005) 2005 IEEE/RSJ International Conference on*, edited by Mohajerian P2005, p. 4071-4076.

Murray R, Li Z, and Sastry S. *A Mathematical Introduction to Robotic Manipulation*. Boca Raton, FL.: CRC Press, 1994, p. 456.

Nagai K, Nakanishi I, Hanafusa H, Kawamura S, Makikawa M, and Tejima N. Development of an 8 DOF robotic orthosis for assisting human upper limb motion. In: *Robotics and Automation, 1998 Proceedings 1998 IEEE International Conference on*1998, p. 3486-3491 vol.3484.

National Aeronautics and Space Administration. Man-Systems Integration Standards, Revision B. Washington, DC: 1995.

National Institute of Neurological Disorders and Stroke. Post-Stroke Rehabilitation Fact Sheet. Bethesda, MD: NINDS and NIH, 2008.

Nef T, Mihelj M, Colombo G, and Riener R. ARMin - robot for rehabilitation of the upper extremities. In: *Robotics and Automation, 2006 ICRA 2006 Proceedings 2006 IEEE International Conference on*2006, p. 3152-3157.

Nef T, Mihelj M, Kiefer G, Perndl C, Muller R, and Riener R. ARMin - Exoskeleton for Arm Therapy in Stroke Patients. In: *Rehabilitation Robotics, 2007 ICORR 2007 IEEE 10th International Conference on*, edited by Mihelj M2007a, p. 68-74.

Nef T, Mihelj M, and Riener R. ARMin: a robot for patient-cooperative arm therapy. *Medical and Biological Engineering and Computing* 45: 887-900, 2007b.

Odell D, Barr A, Goldberg R, Chung J, and Rempel D. Evaluation of a dynamic arm support for seated and standing tasks: a laboratory study of electromyography and subjective feedback. *Ergonomics* 50: 520-535, 2007.

Pennsylvania Department of Transportation. Pennsylvania Driver's Manual. 2007.

Perry JC, Rosen J, and Burns S. Upper-Limb Powered Exoskeleton Design. *Mechatronics, IEEE/ASME Transactions on* 12: 408-417, 2007.

Prange GB, Stienen AHA, Jannink MJA, van der Kooij H, Ijzerman MJ, and Hermens HJ. Increased range of motion and decreased muscle activity during maximal reach with gravity compensation in stroke patients. In: *Rehabilitation Robotics, 2007 ICORR 2007 IEEE 10th International Conference on*2007, p. 467-471.

Prinz W. Perception and Action Planning. *The European Journal of Cognitive Psychology* 9: 129-154, 1997.

Radomski MV, and Trombly Latham CT. *Occupational therapy for physical dysfunction*. Philadelphia: Lippincott Williams & Wilkins, 2008, p. 1432.

Rahman T, Ramanathan R, Seliktar R, and Harwin W. A simple technique to passively gravity-balance articulated mechanisms. *Journal of mechanical design* 117: 655-658, 1995.

Rahman T, Sample W, and Seliktar R. Design and Testing of WREX. In: *Advances in Rehabilitation Robotics*2004, p. 243-250.

Rahman T, Sample W, Seliktar R, Alexander M, and Scavina M. A body-powered functional upper limb orthosis. *Journal of Rehabilitation Research and Developement* 37: 675-680, 2000.

Reinkensmeyer DJ, Kahn LE, Averbuch M, McKenna-Cole A, Schmit BD, and Rymer WZ. Understanding and treating arm movement impairment after chronic brain injury: progress with the ARM guide. *Journal of Rehabilitation Research & Development* 37: 653-662, 2000.

Reinkensmeyer DJ, Pang CT, Nessler JA, and Painter CC. Web-based telerehabilitation for the upper extremity after stroke. *Neural Systems and Rehabilitation Engineering, IEEE Transactions on [see also IEEE Trans on Rehabilitation Engineering]* 10: 102-108, 2002.

Riener R, Nef T, and Colombo G. Robot-aided neurorehabilitation of the upper extremities. *Medical & biological engineering & computing* 43: 2-10, 2005.

Riley MA, Stoffregen TA, Grocki MJ, and Turvey MT. Postural stabilization for the control of touching. *Human Movement Science* 18: 795-817, 1999.

Rodriguez PL. Arm rest and support. USA: 1972.

Rosamond W, Flegal K, Furie K, Go A, Greenlund K, Haase N, Hailpern SM, Ho M, Howard V, Kissela B, Kittner S, Lloyd-Jones D, McDermott M, Meigs J, Moy C, Nichol G, O'Donnell C, Roger V, Sorlie P, Steinberger J, Thom T, Wilson M, Hong Y, for the American Heart Association Statistics C, and Stroke Statistics S. Heart Disease and Stroke Statistics--2008 Update: A Report From the American Heart Association Statistics Committee and Stroke Statistics Subcommittee. *Circulation* 117: e25-146, 2008.

Rosati G, Gallina P, and Masiero S. Design, Implementation and Clinical Tests of a Wire-Based Robot for Neurorehabilitation. In: *Neural Systems and Rehabilitation Engineering, IEEE Transactions on [see also IEEE Trans on Rehabilitation Engineering]*2007, p. 560-569.

Rosen J, Perry JC, Manning N, Burns S, and Hannaford B. The human arm kinematics and dynamics during daily activities - toward a 7 DOF upper limb powered exoskeleton. In: *Advanced Robotics, 2005 ICAR '05 Proceedings, 12th International Conference on*, edited by Perry JC2005, p. 532-539.

Saad Y. Numerical Solution of Large Nonsymmetric Eigenvalue Problems. *Comput Phys Comm* 53: 71-90, 1989.

Sadowsky C, Volshteyn O, Schultz L, and McDonald JW. Spinal cord injury. *Disability and Rehabilitation* 24: 680-687, 2002.

Sanchez RJ, Liu J, Rao S, Shah P, Smith R, Rahman T, Cramer SC, Bobrow JE, and Reinkensmeyer DJ. Automating Arm Movement Training Following Severe Stroke: Functional Exercises With Quantitative Feedback in a Gravity-Reduced Environment. In: *Neural Systems and Rehabilitation Engineering, IEEE Transactions on [see also IEEE Trans on Rehabilitation Engineering]*, edited by Liu J2006, p. 378-389.

Sanchez RJ, Wolbrecht ET, Smith R, Liu J, Rao S, Cramer S, Rahman T, Bobrow JE, and Reinkensmeyer DJ. A pneumatic robot for re-training arm movement after stroke: rationale and mechanical design. In: *Rehabilitation Robotics, 2005 ICORR 2005 9th International Conference on*, edited by Wolbrecht E2005, p. 500-504.

Scheidt R, Reinkensmeyer D, Conditt M, Rymer W, and Mussa-Ivaldi F. Persistence of motor adaptation during constrained, multi-joint arm movements. *Journal of Neurophysiology* 84: 853-862, 2000.

Schiele A, and van der Helm FCT. Kinematic Design to Improve Ergonomics in Human Machine Interaction. In: *Neural Systems and Rehabilitation Engineering, IEEE Transactions on [see also IEEE Trans on Rehabilitation Engineering]*, edited by van der Helm FCT2006, p. 456-469.

Schmidt H, Hesse S, Werner C, and Bardeleben A. Upper and lower extremity robotic devices to promote motor recovery after stroke -recent developments. In: *Engineering in Medicine and Biology Society, 2004 IEMBS '04 26th Annual International Conference of the IEEE*2004, p. 4825-4828.

Schmidt RA, Lange C, and Young DE. Optimizing summary knowledge of results for skill learning. *Human Movement Science* 9: 325-348, 1990.

Schmidt RA, and Lee TD. *Motor Control and Learning: A Behavioral Emphasis*. Champaign, Illinois: Human Kinetics Publishers, 1998, p. 495.

Schmidt RA, and Wulf G. Continuous Concurrent Feedback Degrades Skill Learning: Implications for Training and Simulation. *Human Factors: The Journal of the Human Factors and Ergonomics Society* 39: 509-525, 1997.

Schmidt SM, Guo L, and Scheer SJ. Changes in the status of hospitalized stroke patients since inception of the prospective payment system in 1983. *Archives of Physical Medicine and Rehabilitation* 83: 894-898, 2002.

Schulte HF. The characteristics of the McKibben artificial muscle. In: *The application of external power in prosthetics and orthotics* Washington, DC: National Academy of Science, 1962, p. 94-115.

Seeley PR, Stephens TD, and Tate P. *Anatomy & Phisiology*. Boston, Mass.: McGraw-Hill College, 2003.

Seligman ME, and Maier SF. Failure to escape traumatic shock. *Experimental Psychology* 74: 1-9, 1967.

Šenk M, and Chèze L. Rotation sequence as an important factor in shoulder kinematics. *Proceedings of the 5th Meeting of the International Shoulder Group* 21: S3-S8, 2006.

Siciliano B, and Khatib O. *Springer Handbook of Robotics*. Berlin, Germany: Springer, 2008, p. 1611.

Sledd A, and O'Malley MK. Performance Enhancement of a Haptic Arm Exoskeleton. In: *Haptic Interfaces for Virtual Environment and Teleoperator Systems, 2006 14th Symposium on*, edited by O'Malley MK2006, p. 375-381.

Spencer SJ. Robotic Wrist Wiihab: A Low Cost Parallel Robot and Trajectory Optimization Method for Wrist Rehabilitation Using the Wii. In: *Mechanical and Aerospace Engineering*. Irvine: University of California, Irvine, 2008, p. 125.

Spencer SJ, Klein J, Minakata K, Le V, Bobrow JE, and Reinkensmeyer DJ. A Low Cost Parallel Robot and Trajectory Optimization Method for Wrist and Forearm Rehabilitation using the Wii. In: *IEEE Conference on Biomedical Robotics and Biomechatronics*. Scottsdale, AZ, USA: 2008, p. 869-874.

State Compensation Insurance Fund. Driving Comfort Tips http://www.scif.com. [3/9/2008, 2008].

Stewart D. A platform with six degrees of freedom. *Proc Inst Mech Eng* 180: 371-386, 1965.

Sugar TG, Jiping H, Koeneman EJ, Koeneman JB, Herman R, Huang H, Schultz RS, Herring DE, Wanberg J, Balasubramanian S, Swenson P, and Ward JA. Design and Control of RUPERT: A Device for Robotic Upper Extremity Repetitive Therapy. In: *Neural Systems and Rehabilitation Engineering, IEEE Transactions on [see also IEEE Trans on Rehabilitation Engineering]*, edited by Jiping H2007, p. 336-346.

Swinnen S, Walter CB, and Shapiro DC. The coordination of limb movements with different kinematic patterns. *Brain and Cognition* 8: 326-373, 1988.

Takahashi CD, Der-Yeghiaian L, Le VH, and Cramer SC. A robotic device for hand motor therapy after stroke. In: *Rehabilitation Robotics, 2005 ICORR 2005 9th International Conference on*, edited by Der-Yeghiaian L2005, p. 17-20.

Takaiwa M, and Noritsugu T. Development of Wrist Rehabilitation Equipment Using Pneumatic Parallel Manipulator. In: *Robotics and Automation, 2005 ICRA 2005 Proceedings of the 2005 IEEE International Conference on*2005, p. 2302-2307.

Toth A, Fazekas G, Arz G, Jurak M, and Horvath M. Passive robotic movement therapy of the spastic hemiparetic arm with REHAROB: report of the first clinical test and the follow-up system improvement. In: *Rehabilitation Robotics, 2005 ICORR 2005 9th International Conference on*2005, p. 127-130.

Walton D, and Thomas JA. Naturalistic observations of driver hand positions. *Transportation Research Part F: Traffic Psychology and Behaviour* 8: 229-238, 2005.

Wenderoth N, Puttemans V, Vangheluwe S, and Swinnen SP. Bimanual training reduces spatial interference. *Journal of Motor Behavior* 35: 296-308, 2003.

Williams DJ, Krebs HI, and Hogan N. A robot for wrist rehabilitation. In: *Engineering in Medicine and Biology Society, 2001 Proceedings of the 23rd Annual International Conference of the IEEE*2001, p. 1336-1339 vol.1332.

Winstein CJ, and Schmidt RA. Reduced frequency of knowledge of results enhances motor skill learning. *Journal of Experimental Psychology: Learning, Memory, and Cognition* 16: 677-691, 1990.

Wolbrecht E. Adaptive, Assist-as-Needed Control of a Pneumatic Orthosis for Optimizing Robotic Movement Therapy Following Stroke. In: *Mechanical And Aerospace Engineering*. Irvine: University of California Irvine, 2007, p. 144.

Wolbrecht ET, Leavitt J, Reinkensmeyer DJ, and Bobrow JE. Control of a Pneumatic Orthosis for Upper Extremity Stroke Rehabilitation. In: *Engineering in Medicine and Biology Society, 2006 EMBS '06 28th Annual International Conference of the IEEE*, edited by Leavitt J2006, p. 2687-2693.

Wolf SL, Lecraw DE, Barton LA, and Jann BB. Forced use of hemiplegic upper extremities to reverse the effect of learned nonuse among chronic stroke and head-injured patients. *Experimental Neurology* 104: 125-132, 1989.

Woodson WE, Tillman P, and Tillman B. *Human Factors Design Handbook*. McGraw-Hill Professional, 1992, p. 1056.

Wu G, van der Helm FCT, Veeger HEJ, Makhsous M, Van Roy P, Anglin C, Nagels J, Karduna AR, McQuade K, Wang X, Werner FW, and Buchholz B. ISB recommendation on definitions of joint coordinate systems of various joints for the reporting of human joint motion—Part II: shoulder, elbow, wrist and hand. *Journal of Biomechanics* 38: 981-992, 2005.

Wulf G, Höß M, and Prinz W. Instructions for motor learning: Differential effects of internal vs external focus of attention. *Journal of Motor Behavior* 30: 169-179, 1998.

Wulf G, Lauterbach B, and Toole T. The learning advantages of an external focus of attention in golf. *Research quarterly for exercise and sport* 70: 120-126, 1999.

Wulf G, and Shea CH. Principles derived from the study of simple skills do not generalize to complex skill learning. *Psychonomic Bulletin & Review* 9: 185-211, 2002.

Yao WX, Fischman MG, and Wang YT. Motor skill acquisition and retention as a function of average feedback, summary feedback, and performance variability. *Journal of Motor Behavior* 26: 273-282, 1994.

Zavala A, Locke EA, Van Cott HP, and Fleishman EA. The analysis of helicopter pilot performance (Tech. Rep. AIR-E-29-6/65). edited by American Institutes for Research. Washington D.C.: 1965.

Zhang LQ, Park HS, and Ren Y. Developing an Intelligent Robotic Arm for Stroke Rehabilitation. In: *Rehabilitation Robotics, 2007 ICORR 2007 IEEE 10th International Conference on*, edited by Park H-S2007, p. 984-993.

Appendix A Jacobian Matrix Derivations

A.1 Jacobian Matrix for CRAMER

Following, we summarize the derivation of the time-derivative leading to the Jacobian matrix for CRAMER (Chapter 3).

For simplicity, (3.8) is broken up into

$$q(\theta) = g\left(B(\theta), D(\theta)\right), \tag{A.1}$$

which leads to

$$\dot{q} = \frac{dq}{dt} = \left(\frac{\partial g}{\partial B}\frac{\partial B}{\partial \theta} + \frac{\partial g}{\partial D}\frac{\partial D}{\partial \theta}\right)\dot{\theta} = J(\theta)\dot{\theta}. \tag{A.2}$$

Due to the length of the equations, each matrix component will be described separately, according to the following notation

$$\frac{\partial g}{\partial B}=\begin{bmatrix} \frac{\partial g}{\partial B_{11}} & \frac{\partial g}{\partial B_{12}} & \frac{\partial g}{\partial B_{13}} & \frac{\partial g}{\partial B_{14}} \\ \frac{\partial g}{\partial B_{21}} & \frac{\partial g}{\partial B_{22}} & \frac{\partial g}{\partial B_{23}} & \frac{\partial g}{\partial B_{24}} \\ \frac{\partial g}{\partial B_{31}} & \frac{\partial g}{\partial B_{32}} & \frac{\partial g}{\partial B_{33}} & \frac{\partial g}{\partial B_{34}} \\ \frac{\partial g}{\partial B_{41}} & \frac{\partial g}{\partial B_{42}} & \frac{\partial g}{\partial B_{43}} & \frac{\partial g}{\partial B_{44}} \end{bmatrix}. \tag{A.3}$$

The components of (A.3) are

$$\left[\frac{\partial g}{\partial B}\right]_{11}=\frac{\left(B_z(\theta)-A_z\right)}{\left(B_x(\theta)-A_x\right)^2+\left(B_z(\theta)-A_z\right)^2},$$

$$\left[\frac{\partial g}{\partial B}\right]_{12}=0,$$

$$\left[\frac{\partial g}{\partial B}\right]_{13}=-\frac{\left(B_x(\theta)-A_x\right)}{\left(B_x(\theta)-A_x\right)^2+\left(B_z(\theta)-A_z\right)^2},$$

$$\left[\frac{\partial g}{\partial B}\right]_{21}=-\frac{\left(B_x(\theta)-A_x\right)\left(B_y(\theta)-A_y\right)}{\left\|B(\theta)-A\right\|^2\sqrt{\left(B_x(\theta)-A_x\right)^2+\left(B_z(\theta)-A_z\right)^2}},$$

$$\left[\frac{\partial g}{\partial B}\right]_{22}=\frac{\sqrt{\left(B_x(\theta)-A_x\right)^2+\left(B_z(\theta)-A_z\right)^2}}{\left\|B(\theta)-A\right\|^2},$$

$$\left[\frac{\partial g}{\partial B}\right]_{23}=-\frac{\left(B_y(\theta)-A_y\right)\left(B_z(\theta)-A_z\right)}{\left\|B(\theta)-A\right\|^2\sqrt{\left(B_x(\theta)-A_x\right)^2+\left(B_z(\theta)-A_z\right)^2}},$$

and

$$\left[\frac{\partial g}{\partial B}\right]_{31}=\left[\frac{\partial g}{\partial B}\right]_{32}=\left[\frac{\partial g}{\partial B}\right]_{33}=\left[\frac{\partial g}{\partial B}\right]_{41}=\left[\frac{\partial g}{\partial B}\right]_{42}=\left[\frac{\partial g}{\partial B}\right]_{43}=0$$

Accordingly, we repeat the process for $\frac{\partial g}{\partial D}$, obtaining

$$\left[\frac{\partial g}{\partial D}\right]_{31}=\frac{\left(D_z(\theta)-C_z\right)}{\left(D_x(\theta)-C_x\right)^2+\left(D_z(\theta)-C_z\right)^2},$$

$$\left[\frac{\partial g}{\partial D}\right]_{32}=0,$$

$$\left[\frac{\partial g}{\partial D}\right]_{33}=-\frac{\left(D_x(\theta)-C_x\right)}{\left(D_x(\theta)-C_x\right)^2+\left(D_z(\theta)-C_z\right)^2},$$

$$\left[\frac{\partial g}{\partial D}\right]_{41}=-\frac{\left(D_x(\theta)-C_x\right)\left(D_y(\theta)-C_y\right)}{\left\|D(\theta)-C\right\|^2\sqrt{\left(D_x(\theta)-C_x\right)^2+\left(D_z(\theta)-C_z\right)^2}},$$

$$\left[\frac{\partial g}{\partial D}\right]_{42}=\frac{\sqrt{\left(D_x(\theta)-C_x\right)^2+\left(D_z(\theta)-C_z\right)^2}}{\left\|D(\theta)-C\right\|^2},$$

and

$$\left[\frac{\partial g}{\partial D}\right]_{43}=-\frac{\left(D_y(\theta)-C_y\right)\left(D_z(\theta)-C_z\right)}{\left\|D(\theta)-C\right\|^2\sqrt{\left(D_x(\theta)-C_x\right)^2+\left(D_z(\theta)-C_z\right)^2}}.$$

The remaining components of $\frac{\partial g}{\partial D}$ are

$$\left[\frac{\partial g}{\partial D}\right]_{11} = \left[\frac{\partial g}{\partial D}\right]_{12} = \left[\frac{\partial g}{\partial D}\right]_{13} = \left[\frac{\partial g}{\partial D}\right]_{21} = \left[\frac{\partial g}{\partial D}\right]_{22} = \left[\frac{\partial g}{\partial D}\right]_{23} = 0 .$$

A.2 Jacobian Matrix for BONES

In this section we present the detailed derivation of the time-derivative leading to the Jacobian matrix for BONES, previously introduced in 4.5.1. For simplicity purposes, we will use the following abbreviations

$$\begin{array}{lll} c_y = \cos(\theta_1) & & s_y = \sin(\theta_1) \\ c_p = \cos(\theta_2) & \text{and} & s_p = \sin(\theta_2), \\ c_r = \cos(\theta_3) & & s_r = \sin(\theta_3) \\ c_e = \cos(\theta_4) & & s_e = \sin(\theta_4) \end{array}$$

where the angle vector θ follows the notation defined in Figure 4.7 . As stated in 4.5.1, we divide the overall Jacobian relating the actuator to the end-effector into several intermediate steps (Figure 4.13). For simplicity purposes, we will describe the first 3 steps in reverse order: starting with the shoulder angles in order to locate TEC and BEC , then progressing to TTV and BTV , and finalizing at cylinders the rear diamond structure.

Starting with step 3, we relate the arm angles the location of TEC, BEC (Figure 4.9) and the arm angles θ. We expand (4.1) and (4.2) to their expanded symbolic form:

$$TEC = \begin{bmatrix} c_y c_p LH + \left(s_y s_r + c_y s_p c_r\right) LE \\ s_y c_p LH + \left(-c_y s_r + s_y s_p c_r\right) LE \\ s_p LH + c_p c_r LE \end{bmatrix}, \tag{A.4}$$

$$BEC = \begin{bmatrix} c_y c_p LH - \left(s_y s_r + c_y s_p c_r\right) LE \\ s_y c_p LH - \left(-c_y s_r + s_y s_p c_r\right) LE \\ -s_p LH - c_p c_r LE \end{bmatrix}. \tag{A.5}$$

Similarly, we expand (4.3) and (4.4), to obtain

$$BTV = \begin{bmatrix} \dfrac{LS \cdot F_{1,1}}{\sqrt{F_{1,1}{}^2 + F_{2,1}{}^2 + F_{3,1}{}^2}} + YB_x \\ \dfrac{LS \cdot F_{2,1}}{\sqrt{F_{1,1}{}^2 + F_{2,1}{}^2 + F_{3,1}{}^2}} + YB_y \\ \dfrac{LS \cdot F_{3,1}}{\sqrt{F_{1,1}{}^2 + F_{2,1}{}^2 + F_{3,1}{}^2}} + YB_z \end{bmatrix}, \tag{A.6}$$

where YB and LS are defined in Figure 4.9, and

$$\begin{aligned} F_{1,1} &= YB_x - c_y c_p LH + \left(-s_y s_r + c_y s_p c_r\right) LE \\ F_{2,1} &= YB_y - s_y c_p LH + \left(-c_y s_r + s_y s_p c_r\right) LE \\ F_{3,1} &= YB_z + s_p LH + c_p c_r LE \end{aligned}$$

and

$$TTV = \begin{bmatrix} \dfrac{LS \cdot F_{1,2}}{\sqrt{F_{1,2}{}^2 + F_{2,2}{}^2 + F_{3,2}{}^2}} + YT_x \\ \dfrac{LS \cdot F_{2,2}}{\sqrt{F_{1,2}{}^2 + F_{2,2}{}^2 + F_{3,2}{}^2}} + YT_y \\ \dfrac{LS \cdot F_{3,2}}{\sqrt{F_{1,2}{}^2 + F_{2,2}{}^2 + F_{3,2}{}^2}} + YT_z \end{bmatrix}, \qquad \text{(A.7)}$$

with

$$\begin{aligned} F_{1,2} &= YT_x - c_y c_p LH - \left(s_y s_r \; + \; c_y s_p c_r\right) LE \\ F_{2,2} &= YT_y - s_y c_p LH - \left(-c_y s_r \; + \; s_y s_p c_r\right) LE \\ F_{3,2} &= YT_z + s_p LH - c_p c_r LE \end{aligned}$$

We differentiate (A.4) and (A.5) with respect to θ,

$$\frac{\partial TEC}{\partial \theta} = \begin{bmatrix} -c_y\left(s_p LH - c_{\,p} c_r LE\right) & -s_y c_p LH + \left(c_y s_r - s_y s_p c_r\right) LE & -\left(-s_y c_r + c_y s_p s_r\right) LE \\ -s_y\left(s_p LH - c_p c_r LE\right) & c_y c_p LH + \left(s_y s_r + c_y s_p c_r\right) LE & -\left(c_y c_r + s_y s_p s_r\right) LE \\ -c_p LH - s_p c_r LE & 0 & -c_p s_r LE \end{bmatrix}$$

(B.8)

$$\frac{\partial BEC}{\partial \theta} = \begin{bmatrix} -c_y\left(s_p LH + c_{\,p} c_r LE\right) & -s_y c_p LH - \left(c_y s_r - s_y s_p c_r\right) LE & \left(-s_y c_r + c_y s_p s_r\right) LE \\ -s_y\left(s_p LH + c_p c_r LE\right) & c_y c_p LH - \left(s_y s_r + c_y s_p c_r\right) LE & \left(c_y c_r + s_y s_p s_r\right) LE \\ -c_p LH + s_p c_r LE & 0 & c_p s_r LE \end{bmatrix}$$

(B.9)

We define J_{thEC}, an intermediate Jacobian matrix relating the shoulder angles to TEC, BEC. Using (B.8) and (B.9), we obtain J_{thEC}.

$$J_{thEC} = \begin{bmatrix} \dfrac{\partial TEC}{\partial \theta} \\ \dfrac{\partial BEC}{\partial \theta} \end{bmatrix} \tag{A.10}$$

In step 2, we repeat the previous process applied to (A.6) and (A.7), which leads to

$$\frac{\partial TTV}{\partial \theta} = -LS_1 \cdot \left(\frac{I_3}{|TEC - YT|} - \frac{(TEC - YT)^2}{|TEC - YT|^3} \right) = \begin{bmatrix} Column_1 & Column_2 & Column_3 \end{bmatrix}, \tag{A.11}$$

with

$$Column_1 = LS_1 \begin{bmatrix} \dfrac{1}{\sqrt{F_{1,3}{}^2 + F_{2,3}{}^2 + F_{3,3}{}^2}} - \dfrac{F_{1,3}{}^2}{\left(F_{1,3}{}^2 + F_{2,3}{}^2 + F_{3,3}{}^2\right)^{3/2}} \\ -\dfrac{F_{1,3}F_{2,3}}{\left(F_{1,3}{}^2 + F_{2,3}{}^2 + F_{3,3}{}^2\right)^{3/2}} \\ -\dfrac{F_{1,3}F_{3,3}}{\left(F_{1,3}{}^2 + F_{2,3}{}^2 + F_{3,3}{}^2\right)^{3/2}} \end{bmatrix}$$

$$Column_2 = LS_1 \begin{bmatrix} -\dfrac{F_{1,3}F_{2,3}}{\left(F_{1,3}{}^2 + F_{2,3}{}^2 + F_{3,3}{}^2\right)^{3/2}} \\ \dfrac{1}{\sqrt{F_{1,3}{}^2 + F_{2,3}{}^2 + F_{3,3}{}^2}} - \dfrac{F_{2,3}{}^2}{\left(F_{1,3}{}^2 + F_{2,3}{}^2 + F_{3,3}{}^2\right)^{3/2}} \\ -\dfrac{F_{2,3}F_{3,3}}{\left(F_{1,3}{}^2 + F_{2,3}{}^2 + F_{3,3}{}^2\right)^{3/2}} \end{bmatrix}$$

$$Column_3 = LS_1 \begin{bmatrix} -\dfrac{F_{1,3}F_{3,3}}{\left(F_{1,3}{}^2 + F_{2,3}{}^2 + F_{3,3}{}^2\right)^{3/2}} \\ -\dfrac{F_{1,3}F_{3,3}}{\left(F_{1,3}{}^2 + F_{2,3}{}^2 + F_{3,3}{}^2\right)^{3/2}} \\ \dfrac{1}{\sqrt{F_{1,3}{}^2 + F_{2,3}{}^2 + F_{3,3}{}^2}} - \dfrac{F_{3,3}{}^2}{\left(F_{1,3}{}^2 + F_{2,3}{}^2 + F_{3,3}{}^2\right)^{3/2}} \end{bmatrix}$$

$$\begin{aligned} F_{1,3} &= YT_x - c_y c_p LH - \left(s_y s_r + c_y s_p c_r\right) LE \\ F_{2,3} &= YT_y - s_y c_p LH - \left(-c_y s_r + s_y s_p c_r\right) LE \\ F_{3,3} &= YT_z + s_p LH - c_p c_r LE \end{aligned}$$

Similarly for BTV, we obtain

$$\frac{\partial BTV}{\partial \theta} = -LS_2 \cdot \left(\frac{I_3}{|BEC - YB|} - \frac{(BEC - YB)^2}{|BEC - YB|^3} \right) = \begin{bmatrix} Column_1 & Column_2 & Column_3 \end{bmatrix}, \quad \text{(A.12)}$$

with

$$Column_1 = LS_2 \begin{bmatrix} \dfrac{1}{\sqrt{F_{1,4}{}^2 + F_{2,4}{}^2 + F_{3,4}{}^2}} - \dfrac{F_{1,4}{}^2}{\left(F_{1,4}{}^2 + F_{2,4}{}^2 + F_{3,4}{}^2\right)^{3/2}} \\ -\dfrac{F_{1,4}F_{2,4}}{\left(F_{1,4}{}^2 + F_{2,4}{}^2 + F_{3,4}{}^2\right)^{3/2}} \\ -\dfrac{F_{1,4}F_{3,4}}{\left(F_{1,4}{}^2 + F_{2,4}{}^2 + F_{3,4}{}^2\right)^{3/2}} \end{bmatrix}$$

$$Column_2 = LS_2 \begin{bmatrix} -\dfrac{F_{1,4}F_{2,4}}{\left(F_{1,4}{}^2 + F_{2,4}{}^2 + F_{3,4}{}^2\right)^{3/2}} \\ \dfrac{1}{\sqrt{F_{1,4}{}^2 + F_{2,4}{}^2 + F_{3,4}{}^2}} - \dfrac{F_{1,4}{}^2}{\left(F_{1,4}{}^2 + F_{2,4}{}^2 + F_{3,4}{}^2\right)^{3/2}} \\ -\dfrac{F_{2,4}F_{3,4}}{\left(F_{1,4}{}^2 + F_{2,4}{}^2 + F_{3,4}{}^2\right)^{3/2}} \end{bmatrix}$$

$$Column_3 = LS_2 \begin{bmatrix} -\dfrac{F_{1,4}F_{3,4}}{\left(F_{1,4}{}^2 + F_{2,4}{}^2 + F_{3,4}{}^2\right)^{3/2}} \\ -\dfrac{F_{2,4}F_{3,4}}{\left(F_{1,4}{}^2 + F_{2,4}{}^2 + F_{3,4}{}^2\right)^{3/2}} \\ \dfrac{1}{\sqrt{F_{1,4}{}^2 + F_{2,4}{}^2 + F_{3,4}{}^2}} - \dfrac{F_{1,4}{}^2}{\left(F_{1,4}{}^2 + F_{2,4}{}^2 + F_{3,4}{}^2\right)^{3/2}} \end{bmatrix}$$

$$\begin{aligned} F_{1,4} &= YB_x - c_y c_p LH + \left(s_y s_r + c_y s_p c_r\right) LE \\ F_{2,4} &= YB_y - s_y c_p LH + \left(-c_y s_r + s_y s_p c_r\right) LE \\ F_{3,4} &= YB_z + s_p LH + c_p c_r LE \end{aligned}$$

Summarizing step 2, we define J_{ECTV}, the Jacobian matrix relating TEC, BEC and TTV, BTV.

$$J_{ECTV} = \begin{bmatrix} \dfrac{\partial TTV}{\partial \theta} & 0_{3x3} \\ 0_{3x3} & \dfrac{\partial BTV}{\partial \theta} \end{bmatrix} \tag{A.13}$$

Progressing to step 1, we calculate the differentials for the rear diamond cylinders lengths $[q_1, q_2, q_3, q_4]$, expressed as

$$\frac{\partial q_1}{\partial \theta} = \left[\frac{F_{4,5}}{\sqrt{{F_{4,5}}^2 + {F_{5,5}}^2 + {F_{6,5}}^2}} \quad \frac{F_{5,5}}{\sqrt{{F_{4,5}}^2 + {F_{5,5}}^2 + {F_{6,5}}^2}} \quad \frac{F_{6,5}}{\sqrt{{F_{4,5}}^2 + {F_{5,5}}^2 + {F_{6,5}}^2}} \right], \quad \text{(A.14)}$$

$$F_{1,5} = YT_x - c_y c_p LH - \left(s_y s_r + c_y s_p c_r \right) LE$$
$$F_{2,5} = YT_y - s_y c_p LH - \left(-c_y s_r + s_y s_p c_r \right) LE$$
$$F_{3,5} = YT_z + s_p LH - c_p c_r LE$$
$$F_{4,5} = LS \frac{F_{1,5}}{\sqrt{{F_{1,5}}^2 + {F_{2,5}}^2 + {F_{3,5}}^2}} + YB_x - CBR0_x$$
$$F_{5,5} = LS \frac{F_{2,5}}{\sqrt{{F_{1,5}}^2 + {F_{2,5}}^2 + {F_{3,5}}^2}} + YB_y - CBR0_y$$
$$F_{6,5} = LS \frac{F_{3,7}}{\sqrt{{F_{1,5}}^2 + {F_{2,5}}^2 + {F_{3,5}}^2}} + YB_z - CBR0_z$$

$$\frac{\partial q_2}{\partial \theta} = \left[\frac{F_{4,6}}{\sqrt{{F_{4,6}}^2 + {F_{5,6}}^2 + {F_{6,6}}^2}} \quad \frac{F_{5,6}}{\sqrt{{F_{4,6}}^2 + {F_{5,6}}^2 + {F_{6,6}}^2}} \quad \frac{F_{6,6}}{\sqrt{{F_{4,6}}^2 + {F_{5,6}}^2 + {F_{6,6}}^2}} \right], \quad \text{(A.15)}$$

$$F_{1,6} = YT_x - c_y c_p LH - \left(s_y s_r + c_y s_p c_r \right) LE$$
$$F_{2,6} = YT_y - s_y c_p LH - \left(-c_y s_r + s_y s_p c_r \right) LE$$
$$F_{3,6} = YT_z + s_p LH - c_p c_r LE$$
$$F_{4,6} = LS \frac{F_{1,5}}{\sqrt{{F_{1,6}}^2 + {F_{2,6}}^2 + {F_{3,6}}^2}} + YB_x - CBL0_x$$
$$F_{5,6} = LS \frac{F_{2,5}}{\sqrt{{F_{1,6}}^2 + {F_{2,6}}^2 + {F_{3,6}}^2}} + YB_y - CBL0_y$$
$$F_{6,6} = LS \frac{F_{3,7}}{\sqrt{{F_{1,6}}^2 + {F_{2,6}}^2 + {F_{3,6}}^2}} + YB_z - CBL0_z$$

$$\frac{\partial q_3}{\partial \theta} = \left[\frac{F_{4,7}}{\sqrt{F_{4,7}{}^2 + F_{5,7}{}^2 + F_{6,7}{}^2}} \quad \frac{F_{5,7}}{\sqrt{F_{4,7}{}^2 + F_{5,7}{}^2 + F_{6,7}{}^2}} \quad \frac{F_{6,7}}{\sqrt{F_{4,7}{}^2 + F_{5,7}{}^2 + F_{6,7}{}^2}} \right], \quad \text{(A.16)}$$

$$\begin{aligned}
F_{1,7} &= YT_x - c_y c_p LH - \left(s_y s_r + c_y s_p c_r \right) LE \\
F_{2,7} &= YT_y - s_y c_p LH - \left(-c_y s_r + s_y s_p c_r \right) LE \\
F_{3,7} &= YT_z + s_p LH - c_p c_r LE \\
F_{4,7} &= LS \frac{F_{1,5}}{\sqrt{F_{1,7}{}^2 + F_{2,7}{}^2 + F_{3,7}{}^2}} + YT_x - CTL0_x \\
F_{5,7} &= LS \frac{F_{2,5}}{\sqrt{F_{1,7}{}^2 + F_{2,7}{}^2 + F_{3,7}{}^2}} + YT_y - CTL0_y \\
F_{6,7} &= LS \frac{F_{3,7}}{\sqrt{F_{1,7}{}^2 + F_{2,7}{}^2 + F_{3,7}{}^2}} + YT_z - CTL0_z
\end{aligned}$$

$$\frac{\partial q_4}{\partial \theta} = \left[\frac{F_{4,8}}{\sqrt{F_{4,8}{}^2 + F_{5,8}{}^2 + F_{6,8}{}^2}} \quad \frac{F_{5,8}}{\sqrt{F_{4,8}{}^2 + F_{5,8}{}^2 + F_{6,8}{}^2}} \quad \frac{F_{6,8}}{\sqrt{F_{4,8}{}^2 + F_{5,8}{}^2 + F_{6,8}{}^2}} \right], \quad \text{(A.17)}$$

$$\begin{aligned}
F_{1,8} &= YT_x - c_y c_p LH - \left(s_y s_r + c_y s_p c_r \right) LE \\
F_{2,8} &= YT_y - s_y c_p LH - \left(-c_y s_r + s_y s_p c_r \right) LE \\
F_{3,8} &= YT_z + s_p LH - c_p c_r LE \\
F_{4,8} &= LS \frac{F_{1,5}}{\sqrt{F_{1,8}{}^2 + F_{2,8}{}^2 + F_{3,8}{}^2}} + YT_x - CTR0_x \\
F_{5,8} &= LS \frac{F_{2,5}}{\sqrt{F_{1,8}{}^2 + F_{2,8}{}^2 + F_{3,8}{}^2}} + YT_y - CTR0_y \\
F_{6,8} &= LS \frac{F_{3,5}}{\sqrt{F_{1,8}{}^2 + F_{2,8}{}^2 + F_{3,8}{}^2}} + YT_z - CTR0_z
\end{aligned}$$

Concluding step 1, we introduce J_{TVc}, the Jacobian matrix relating TTV, BTV and the cylinder lengths at the rear diamond structure.

$$J_{TVc} = \begin{bmatrix} \frac{\partial q_3}{\partial \theta} & 0_{1x3} \\ \frac{\partial q_4}{\partial \theta} & 0_{1x3} \\ 0_{1x3} & \frac{\partial q_2}{\partial \theta} \\ 0_{1x3} & \frac{\partial q_1}{\partial \theta} \end{bmatrix} \tag{A.18}$$

Finally, the Jacobian matrix that relates the rear diamond pneumatic actuator's velocity and the elbow motion (steps 1~3) is

$$J_{thC} = J_{TVc} J_{ECTV} J_{thEC}, \tag{A.19}$$

So far, we have determined the relation between the 4 pneumatic cylinders in the diamond structure and the elbow orientation. Now we will introduce the decoupled action of the elbow cylinder (step 4).

Recall (4.11), which related q_5 (the elbow cylinder) and θ_4 (the elbow angle). If we differentiate the equation with respect to θ_4, we obtain

$$\frac{\partial q_5}{\partial \theta_4} = \frac{-b \cdot c \cdot sin\left(\theta_4 - \beta_1 - \beta_2\right)}{\sqrt{b^2 + c^2 - 2 \cdot b \cdot c \cdot cos\left(\theta_4 - \beta_1 - \beta_2\right)}} \tag{A.20}$$

Let us define $J_{thXYZS} = \frac{\partial q_5}{\partial \theta_4}$, then the overall Jacobian matrix relating the 5 pneumatic actuators and the 4 arm angles, defined in (4.15), is

$$J = \begin{bmatrix} J_{thc} & 0 \\ 0 & J_{thXYZS} \end{bmatrix} \tag{A.21}$$